

Strong Optical Injection Locking of Edge-Emitting Lasers and Its Applications

Hyuk-Kee Sung

Electrical Engineering and Computer Sciences
University of California at Berkeley

Technical Report No. UCB/EECS-2006-107

<http://www.eecs.berkeley.edu/Pubs/TechRpts/2006/EECS-2006-107.html>

August 18, 2006



Copyright © 2006, by the author(s).
All rights reserved.

Permission to make digital or hard copies of all or part of this work for personal or classroom use is granted without fee provided that copies are not made or distributed for profit or commercial advantage and that copies bear this notice and the full citation on the first page. To copy otherwise, to republish, to post on servers or to redistribute to lists, requires prior specific permission.

Strong Optical Injection Locking of Edge-Emitting Lasers and Its Applications

by

Hyuk-Kee Sung

B.S. (Yonsei University, Korea) 1999

M.S. (Yonsei University, Korea) 2001

A dissertation submitted in partial satisfaction of the requirements for the degree of

Doctor of Philosophy in

Engineering - Electrical Engineering and Computer Sciences

in the

Graduate Division

of the

University of California, Berkeley

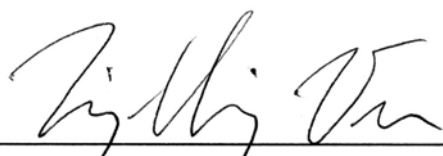
Committee in charge: Professor Ming C. Wu, Chair

Professor Constance Chang-Hasnain

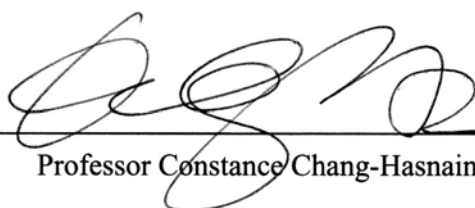
Professor Costas P. Grigoropoulos

Fall 2006

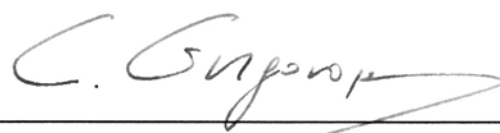
The dissertation of Hyuk-Kee Sung is approved.



Professor Ming C. Wu Chair 8/14/2006
Date



Professor Constance Chang-Hasnain 8/15/06
Date



Professor Costas P. Grigoropoulos 8/14/2006
Date

University of California, Berkeley

Fall 2006

Strong Optical Injection Locking of Edge-Emitting Lasers and Its Applications

© 2006

by Hyuk-Kee Sung

ABSTRACT

Strong Optical Injection Locking of Edge-Emitting Lasers and Its Applications

by

Hyuk-Kee Sung

Doctor of Philosophy in Engineering - Electrical Engineering and Computer Sciences

University of California, Berkeley

Professor Ming C. Wu, Chair

Semiconductor lasers are essential components that enable high-speed long-haul communication and have been widely used for various applications in photonics technology. Semiconductor lasers under optical injection locking exhibit superior performance over free-running lasers and provide useful applications not achievable through the free-running lasers. The performance of injection-locked lasers has been found to be significantly improved with stronger injection.

In this dissertation, the characteristics and applications of semiconductor lasers under strong optical injection locking are presented and analyzed in various aspects. First, ultra-strong (injection ratio $R \sim 10$ dB) optical injection locking properties are investigated experimentally and theoretically. Direct modulation responses of ultra-strong optical injection-locked distributed feedback (DFB) lasers show three distinctive modulation characteristics depending on frequency detuning values. These different optical properties and electric modulation characteristics can be utilized in various

applications such as analog fiber optic link, broadband digital communications, RF photonics and opto-electronic oscillators (OEOs). Using the strong injection-locked lasers, a novel single sideband generation has been demonstrated. A modulation sideband on the longer wavelength side is enhanced due to the resonant amplification by the slave laser's cavity mode, resulting in a 12-dB asymmetry at 20-GHz RF modulation. The dispersion-limited RF bandwidth has been greatly increased by maintaining the variation of fiber transmission response within 7 dB up to 20-GHz RF carrier frequency over 80-km fiber transmission.

Second, to improve fiber optic link performances, gain-lever distributed Bragg reflector (DBR) lasers have been fabricated. With a gain-lever modulation, 9-dB increase of a link gain has been achieved compared with a standard modulation. By combining the gain-lever modulation with optical injection locking, nonlinear distortion reduction and modulation bandwidth enhancement have been achieved as well as maintaining the improved link gain.

Finally, we have proposed two-section DFB lasers for simple optical injection locking systems. The two-section DFB lasers show similar locking / unlocking phenomena as conventional injection locking systems using external master lasers. Electrically isolated gain sections in monolithic lasers can support independent lasing modes. The independent modes are mutually locked under certain current bias conditions. With a direct modulation of the monolithic lasers, we achieved resonance frequency enhancement, modulation bandwidth increase and chirp reduction. We have also demonstrated high optical extinction ratio and millimeter-wave generation using the monolithic lasers.

For future works, ultra-strong injection-locked lasers might enable broadband (> 40 Gb/s) digital signal transmission of directly-modulated lasers and be employed in high-frequency (> 60 GHz) OEOs. The integration of the two-section lasers with modulators will enable high optical extinction ratio (> 65 dB) with modulation bandwidth up to several GHz. The ultra-strong injection locking technique and monolithic injection-locked lasers can significantly extend the performance of directly-modulated lasers for high frequency applications.



Professor Ming C. Wu
Dissertation Committee Chair

To my family
for all the love, support and encouragement

TABLE OF CONTENTS

TABLE OF CONTENTS	ii
LIST OF FIGURES	v
LIST OF TABLES.....	xii
ACKNOWLEDGEMENTS.....	xiii
Chapter 1 Introduction	1
1.1 Fundamentals of Optical Injection Locking	2
1.1.1 History	2
1.1.2 Basic Operation	4
1.2 State of the Art of Optical Injection Locking	7
1.2.1 Modulation Bandwidth Enhancement	7
1.2.2 Link Linearity Improvement	7
1.2.3 Millimeter-Wave Generation.....	10
1.2.4 Optical Injection Phase-Locked Loop (OIPLL)	10
1.2.5 Injection Locking of Mode-Locked Lasers	12
1.2.6 Optical Signal Processing and Other Applications.....	13
1.3 Organization of the Dissertation.....	15
Chapter 2 Strong Optical Injection Locking	17
2.1 Limitations of Directly-Modulated Lasers	17
2.2 Motivation for Ultra-Strong Injection	19
2.3 Experimental Observations.....	23
2.2.1 Experimental Setup	23
2.2.2 Measured Optical Spectra and Modulation Responses	24
2.4 Theoretical Model.....	29
2.5 Broad 3-dB Bandwidth and High Resonance Frequency with Narrowband RF Gain	36

2.6 Summary.....	38
Chapter 3 Optical Single Sideband Generation Using Strong Optical Injection-Locked Semiconductor Lasers	
3.1 Asymmetric Modulation Sidebands in Strong Optical Injection-Locked Lasers.	40
3.2 Principles and Experimental Results	40
3.3 Fiber Chromatic Dispersion Effect on Modulation Sidebands.....	48
3.4 Fiber Transmission Measurements	51
3.5 Summary.....	53
Chapter 4 Optically Injection-Locked Gain-Lever Distributed Bragg Reflector (DBR) Lasers with Enhanced RF Performances.....	
4.1 Fiber-Optic Link Gain Improvement.....	54
4.2 Gain-Lever Modulation Combined with Optical Injection Locking	55
4.3 Device Fabrication: Gain-Lever DBR Lasers	57
4.4 Experimental Results	59
4.4.1 DC Performance of Gain-Lever DBR Lasers.....	59
4.4.2 Modulation Performance of Gain-lever DBR Lasers	61
4.4.3 Optical Injection Locking of Gain-Lever DBR Lasers	65
4.4.4 Ultra-Strong Injection-Locked Gain-Lever DBR Lasers	72
4.5 Summary	75
Chapter 5 Monolithic Injection Locking in Multi-Section Distributed Feedback (DFB) Lasers.....	
5.1 Introduction	77
5.2 Principles and Device Fabrication.....	79
5.3 Optimization of Multi-Section DFB Lasers for Mutual Locking Purpose	81
5.3.1 Introduction	81
5.3.2 Quarter-Wavelength Shifted DFB Lasers with Bent Waveguide	82
5.3.3 Device Yield	85
5.4 Experimental Results on Optical Properties	87
5.5 Modulation Responses and Nonlinear Distortion Reduction	90
5.6 Chirp Reduction and BER Performances	96

5.7 Summary.....	99
Chapter 6 Applications of Multi-Section Distributed Feedback (DFB) Lasers...	101
6.1 Optical Extinction Ratio Improvement Using Directly-Modulated Two-Section DFB Lasers.....	101
6.1.1 Link Requirements: Digital versus Analog Link.....	102
6.1.2 Measured Large-Signal Response of Directly-Modulated Lasers.....	105
6.1.3 Optical Extinction Ratio Improvement	107
6.2 Optical Generation of a Millimeter-Wave Signal Using Sideband Injection Locking in a Two-Section DFB Laser	114
6.2.1 Principles of Optical Millimeter-Wave Generation.....	114
6.2.2 Experimental Results.....	116
6.2.3 Summary	121
Chapter 7 Future Directions and Conclusions	122
7.1 Futures Directions.....	122
7.1.1 Opto-Electronic Oscillators Using Strong Optical Injection locking.....	122
7.1.2 Two-Section Laser Array Integrated with Electroabsorption Modulator	124
7.2 Conclusions	125
References.....	128

LIST OF FIGURES

Figure 1-1. Schematic of optical injection locking.....	4
Figure 1-2. Calculated slave laser intensity, which consists of amplified spontaneous emission and amplified injected field, versus the frequency detuning, after [40]...	5
Figure 1-3. Experimentally measured optical spectra for an unlocked (dotted line) and injection-locked (solid line) DFB laser.....	6
Figure 1-4. Experimentally measured optical spectra of a (a) free-running and (b) injection-locked F-P laser.	6
Figure 1-5. Measured frequency responses of an injection-locked DFB laser, after [35].....	8
Figure 1-6. Measured RF fundamental power and third-order intermodulation products for a free-running laser and injection-locked DFB laser, after [43].	9
Figure 1-7. Measured SFDR improvement versus injection ratio for an injection-locked VCSEL, after [44].	9
Figure 1-8. Schematic of optical injection phase-locked loop (OIPLL) for heterodyne systems. Synchronization is achieved by both optical injection locking and optical phase-locked loop, after [69].	11
Figure 1-9. Power error spectral densities for homodyne OPLL and OIPLL systems, after [69].	12
Figure 1-10. Conceptual architecture of coherent channelizer, after [70].	13
Figure 1-11. Schematic of optical waveform reshaping by injection locking, after [75].....	14
Figure 2-1. Schematics of fiber optic links using (a) external modulation (b) direct modulation.	18
Figure 2-2. Frequency responses of free-running and injection-locked VCSELs for various injection ratios, after [44].	21
Figure 2-3. Injection locking range of DFB lasers as a function of injection ratio, after [35].	22
Figure 2-4. Experimental setup for ultra-strong optical injection locking. The optical spectrum and the RF modulation responses are monitored simultaneously. (ECTL: external cavity tunable laser; EDFA: Erbium-doped fiber laser; Attn.: optical attenuator; Pol. cont.: polarization controller; OSA: optical spectrum	

analyzer; RF-SA: RF-spectrum analyzer)	24
Figure 2-5. Experimentally measured optical spectra ((a)-(c)) and frequency responses of an ultra-strong optical injection-locked laser ((d)-(f)) for various detuning conditions. The injection ratio is kept at 12 dB. (a) and (c): frequency detuning $\Delta f = -42$ GHz; (b) and (d): $\Delta f = -14$ GHz; (c) and (f): $\Delta f = 22$ GHz. For comparison, optical spectrum and frequency response of the free-running laser are depicted as dot lines in (a) and (c), respectively. Three vertical solid lines in the optical spectra represent positive detuning edge, free-running lasing wavelength, and negative detuning edge from left to right.	28
Figure 2-6. Injection locking stability as a function of injection ratio R and frequency detuning Δf	31
Figure 2-7. Calculated frequency responses of ultra-strong ($R = 10$ dB) injection-locked lasers under various frequency detuning values.	33
Figure 2-8. Calculated frequency responses for various injection ratios. Frequency detuning Δf is set at the positive edge of the locking range.....	34
Figure 2-9. Normalized amplitude of an injection-locked laser as a function of frequency detuning.	35
Figure 2-10. Resonance frequency as a function of frequency detuning.	35
Figure 2-11. Measured optical spectra showing the tunability of cavity mode at an injection ratio of $R = 16$ dB. (a) $\Delta f = 7.5$ GHz (b) $\Delta f = 38$ GHz.....	36
Figure 2-12. Experimental results showing broadband response. The injection ratio R is set at 18 dB.....	37
Figure 2-13. Experimental results showing a high resonance frequency with a narrowband enhancement of RF response of 13 dB.....	38
Figure 3-1. Optical spectra illustrating optical single sideband generation in directly-modulated semiconductor lasers with strong optical injection locking. (a) Optical spectrum of a free-running laser without RF modulation. (b) Optical spectrum of an injection-locked laser without RF modulation. (c) Optical spectrum of a free-running laser modulated by RF signal, f_m . (d) Optical spectrum of an injection-locked laser modulated by RF signal, f_m	41
Figure 3-2. Experimental setup for optical single sideband generation. (ECTL: external cavity tunable laser; EDFA: Erbium-doped fiber laser; Attn.: optical attenuator; Pol. cont.: polarization controller; OSA: optical spectrum analyzer; RF-SA; RF spectrum analyzer)	43
Figure 3-3. Measured optical spectra showing asymmetry between modulation sidebands in injection-locked DFB lasers. (a) $\Delta f = -43$ GHz (b) $\Delta f = -37$ GHz	

(locked) (c) $\Delta f = -25$ GHz (locked) (d) $\Delta f = 2$ GHz (locked). The injection ratio R is fixed at 11 dB and the RF-modulation frequency f_m is 15 GHz. Injection-locked lasers operating with positive detuning side exhibits pronounced asymmetry as shown in (d).	44
Figure 3-4. Measured optical spectra of RF-modulated slave laser ($f_m = 20$ GHz) under various conditions. (a) free-running; (b) injection locking with $\Delta f = -8.2$ GHz; and (c) injection locking with $\Delta f = -38$ GHz.	46
Figure 3-5. Measured frequency response of the slave laser under various conditions. (a) free-running; (b) injection locking with $\Delta f = -8.2$ GHz; and (c) injection locking with $\Delta f = -38$ GHz.	46
Figure 3-6. Measured optical power difference between lower and upper sideband versus frequency detuning with fixed modulation frequency at 20 GHz.	47
Figure 3-7. Measured optical power difference between lower and upper modulation sidebands versus modulation frequency with a fixed frequency detuning $\Delta f = -8.2$ GHz and injection ratio $R \sim 11$ dB.	47
Figure 3-8. Fiber chromatic dispersion effect on RF signal transmission.	48
Figure 3-9. Calculated RF power versus fiber transmission distance for symmetric modulation sidebands.	50
Figure 3-10. Calculated RF power versus modulation frequency for symmetric modulation sidebands.	50
Figure 3-11. RF power versus modulation frequency for various power differences between sidebands.	51
Figure 3-12. Measured optical spectrum of RF-modulated injection-locked laser ($f_m = 20$ GHz).	52
Figure 3-13. Measured fiber transmission response for a free-running laser and injection-locked laser.	53
Figure 4-1. Schematic of link gain improvement by series-connected lasers, after [94].	54
Figure 4-2. Monolithic versions of cascaded lasers (a) vertically integrated (b) laterally integrated	55
Figure 4-3. Gain-lever effect in semiconductor lasers.	56
Figure 4-4. Benefits of injection-locked gain-lever lasers in terms of modulation response.	57
Figure 4-5. (a) Illustration of the cross-sectional structure (b) Top-view of a fabricated device.	58
Figure 4-6. Experimental setup for measuring RF performances of an injection-	

locked gain-lever DBR laser.....	59
Figure 4-7. Wavelength tunability of a gain-lever DBR laser.	60
Figure 4-8. Measured L-I curves showing the effect of gain-lever modulation.....	61
Figure 4-9. Measured modulation responses of the gain-lever DBR laser for various operating conditions. RF signal is applied to the section facing the output facet.	63
Figure 4-10. Measured modulation responses of the gain-lever DBR laser for various operating conditions. The RF signal is applied to the gain section adjacent to the phase section.....	63
Figure 4-11. Measured RF spectra of directly-modulated gain-lever DBR laser: (a) I_1 $= 50$ mA, $I_2 = 50$ mA; (b) $I_1 = 4.5$ mA, $I_2 = 50$ mA. RF modulation frequency is 2 GHz.....	64
Figure 4-12. Schematic of optically injection-locked gain-lever DBR lasers.	65
Figure 4-13. Measured frequency responses of a free-running and injection-locked gain-lever laser for various bias conditions. The bias currents for the free- running laser with uniform bias: $I_1 = 50$ mA, $I_2 = 50$ mA; free-running gain- lever state: $I_1 = 4.5$ mA, $I_2 = 50$ mA; injection-locked gain-lever state: $I_1 = 4.5$ mA, $I_2 = 50$ mA.	66
Figure 4-14. Measured frequency response of an injection-locked gain-lever DBR laser for various frequency detuning values. ($I_1 = 4.5$ mA, $I_2 = 25$ mA)	67
Figure 4-15. Measured RIN for a gain-lever DBR laser under free-running and injection-locked condition.	68
Figure 4-16. Measured RF spectra of a gain-lever DBR laser modulated by a single- tone 2-GHz RF signal for a (a) free-running gain-lever and (b) injection-locked gain-lever laser.....	69
Figure 4-17. 2HD versus modulation frequency for various operation conditions. The second harmonic product is measured at twice the RF modulation frequency.	70
Figure 4-18. Measured RF spectra of a gain-lever DBR laser modulated by a two- tone RF signal ($f_1 = 2.0$ GHz, $f_2 = 2.1$ GHz) for (a) free-running gain-lever and (b) injection-locked gain-lever states.	71
Figure 4-19. Measured SFDR of the link with a directly-modulated gain-lever DBR laser.....	72
Figure 4-20. Optical spectra of a free-running gain-lever DBR laser and injection- locked gain-lever DBR laser under $R = 11$ dB and $\Delta f = -2.4$ GHz.....	73
Figure 4-21. Measured frequency responses of a free-running, strong injection-locked ($R = -1$ dB), ultra-strong ($R = 11$ dB) gain-lever DBR laser. Frequency detuning Δf of the injection-locked states is fixed at -2.4 GHz.	74

Figure 4-22. Measured RF spectra of a directly-modulated gain-lever DBR laser with RF signal at 2 GHz. (a) a free-running gain-lever DBR laser, (b) an ultra-strong injection-locked gain-lever DBR laser.	75
Figure 5-1. Schematics of injection locking system: (a) Conventional injection locking; (b) New monolithic injection locking scheme.....	78
Figure 5-2. Two-section DFB lasers for the demonstration of mutual locking in monolithic DFB lasers: (a) Schematic structure; (b) Longitudinal cross-sectional structure illustrating independent lasing; (c) Horizontal cross-sectional profile; (d) Scanning electron micrograph (SEM) of the laser before metallization.....	80
Figure 5-3. Top-view layout of various waveguides and multi-section laser designs...	82
Figure 5-4. Straight-bent-bent-straight waveguide design (type A) showing lateral displacement.	84
Figure 5-5. Single-mode yield for (a) low κ wafer (b) high κ wafer.	86
Figure 5-6. Experimental setup.	87
Figure 5-7. Measured optical spectrum. (a) Mutually-locked ($I_1 = 45.2$ mA, $I_2 = 50$ mA) and (b) Unlocked ($I_1 = 45.2$ mA, $I_2 = 61$ mA).....	88
Figure 5-8. Measured tuning characteristic for each mode when the bias current of section 2 ($= I_2$) is varied and section 1 ($= I_1$) is biased at a fixed value of 45.2 mA.	89
Figure 5-9. Optical spectra measure at the facet facing at (a) section 1 and (b) section 2. Bias current is $I_1 = 30$ mA and $I_2 = 21$ mA.....	90
Figure 5-10. Measured frequency responses for various DC bias values on section 2. Section 1 is DC biased at a fixed value of at 45.2 mA and RF-modulated.	91
Figure 5-11. Measured second harmonic distortion versus I_2 . Section 1 is biased at 45.2 mA and modulated by a 9-GHz RF signal.....	92
Figure 5-12. . Measured RF spectra when section 1 is modulated by a 6-GHz RF signal: (a) free-running ($I_1 = 45.2$ mA, $I_2 = 0$ mA); (b) mutually-locked ($I_1 = 45.2$ mA, $I_2 = 35$ mA).	92
Figure 5-13. The SFDR of the link with directly-modulated two-section DFB laser at $f_1 = 7.5$ GHz and $f_2 = 7.6$ GHz.	93
Figure 5-14. Waveforms measured by an oscilloscope at a 20-GHz RF modulation for free-running and injection-locked states.....	94
Figure 5-15. Measured SFDR at 18.1 GHz. The laser is modulated by a two-tone signal ($f_1 = 18.0$ GHz, $f_2 = 18.1$ GHz) under mutually-locked state.....	95
Figure 5-16. Fabricated device and fully packaged injection-locked DFB laser module. (a) Integrated master-slave laser on submount with 25- Ω termination	

for direct modulation (b) Fully packaged module with output fiber, optical isolator, master laser power monitor, TEC control, and GPO connector for RF input.	95
Figure 5-17. Experimental setup for measuring BER performance of the two-section DFB lasers. (variable attn.: optical variable attenuator; OSA: optical spectrum analyzer)	96
Figure 5-18. Measured optical spectra of the two-section DFB lasers under direct modulation with 10-Gb/s NRZ data: (a) $I_1 = 90$ mA, $I_2 = 0$ mA; (b) $I_1 = 90$ mA, $I_2 = 30$ mA. The optical power is measured in linear scale. The optical spectra without data modulation are depicted as dotted lines.	97
Figure 5-19. Measured eye diagram for (a) $I_1 = 90$ mA, $I_2 = 0$ mA, back-to-back; (b) $I_1 = 90$ mA, $I_2 = 30$ mA, back-to-back; (c) $I_1 = 90$ mA, $I_2 = 0$ mA after 80-km fiber transmission; (d) $I_1 = 90$ mA, $I_2 = 30$ mA after 80-km fiber transmission. ..	98
Figure 5-20. Measured BER performances: (a) back-to-back measurement; (b) 80-km fiber transmission.	99
Figure 6-1. Schematic illustrating large-signal modulations with (a) digital and (b) analog signals.	103
Figure 6-2. Challenges in directly-modulated lasers for analog signal transmission when the lasers are (a) DC-biased at low level and (b) DC-biased at high level.	104
Figure 6-3. Temporal responses of a free-running laser. The laser is modulated by a large-sinusoidal signal at 2 GHz. The DC bias of the laser is (a) 8.5 mA and (b) 34.3 mA.	105
Figure 6-4. Temporal responses of (a) a free-running laser, and (b) an externally injection-locked laser with an injection ratio of -11 dB. The slave laser is DC-biased at $I = 1.5 \cdot I_{th}$ and modulated by a large- sinusoidal signal at 1 GHz.	106
Figure 6-5. Three-section DFB laser for large-signal modulation with high extinction ratio.	107
Figure 6-6. Measured optical spectrum from the facet near the slave section (= section 1).	109
Figure 6-7. Measured light-versus-current curve of the monolithic optical injection-locked DFB laser with bent waveguide. The optical power is shown in both logarithmic (left) and linear (right) scales. The master section current, I_2 , is maintained at 50 mA and tuning section current, $I_3 = 0$ mA.	110
Figure 6-8. Intensity contour plot as a function of bias currents I_1 and I_2 . Current bias for wavelength tuning is fixed at 0 mA. ($I_3 = 0$ mA)	111
Figure 6-9. Measured small-signal frequency responses for various I_1 . I_2 is fixed at	

(a) 0 mA, and (b) 50 mA.	112
Figure 6-10. Measured time domain waveform of the mutually injection-locked laser. $I_1 = 8.5$ mA, $I_2 = 50$ mA and $I_3 = 0$ mA. The laser is modulated by an RF source with 15-dBm output power at 2 GHz.	113
Figure 6-11. Schematic of optical injection locking for millimeter-wave generation.	115
Figure 6-12. (a) Two-section DFB laser used for millimeter-wave generation. (b) Concept of optical millimeter-wave generation by sideband locking in a monolithic laser.	116
Figure 6-13. Measured optical spectrum. Inset is a measured RF spectrum.	117
Figure 6-14. Measured relative frequencies of the master and slave sections when the master current is tuned from 58 to 72 mA.	118
Figure 6-15. Optically generated millimeter-waves (a) without and (b) with a 12-GHz modulation on the slave section. ($I_1 = 45.2$ mA and $I_2 = 69$ mA). Insets are RF spectra measured in 50-GHz span.	119
Figure 6-16. Optically generated millimeter-wave signal at 30 GHz by tuning the bias current on the master section ($I_1 = 45.2$ mA, $I_2 = 64$ mA). The modulation frequency on the slave laser is 15 GHz.	119
Figure 6-17. RF spectra showing the tunability by changing RF modulation frequency. (a) 15.6-GHz RF modulation (b) 15.8-GHz RF modulation. Bias conditions are same as in Figure 6-16. ($I_1 = 45.2$ mA, $I_2 = 64$ mA)	120
Figure 6-18. Measured phase noise at a 30-GHz millimeter-wave signal.	121
Figure 7-1. Schematic of (a) standard OEO and (b) OEO using ultra-strong injection- locked lasers.	123
Figure 7-2. Schematic of monolithic analog optical source array comprising two- section DFB lasers and electroabsorption modulators.	124

LIST OF TABLES

Table 1-1. Historical main accomplishments of injection locking.	3
Table 2-1. Limitations of directly-modulated systems for analog signal transmission.	19
Table 2-2. Limitations of directly-modulated systems for digital signal transmission.	19
Table 2-3. Values used for calculations	30
Table 5-1. Coverage of κL products	84
Table 5-2. Summary of device characterization.	86

ACKNOWLEDGEMENTS

The completion of this thesis would not have been possible without many people who have supported me throughout my life and my graduate career.

I am extremely grateful to my advisor, Professor Ming C. Wu, for giving me a chance to work with him. His technical guidance and the way of thinking have inspired me to overcome the challenges that I faced during my graduate career and accomplish the best I can. I would like to thank Professor Connie Chang-Hasnain for providing me a lot of valuable advice and guidance and for helping me to keep my research on track. I also wish to thank Professor Costas P. Grigoropoulos for serving on my thesis committee and Professor Ali Niknejad for serving on my qualifying examination committee.

I especially thank Erwin K. Lau, Thomas Jung and Wendy Xiaoxue Zhao for their helpful discussion and contribution throughout my graduate study. I also would like to thank my colleagues in the Integrated Photonics Laboratory at Berkeley - Sagi Mathai, Ki-Hun Jung, David Leuenberger, Eric P. Y. Chiou, Chao-Hsi (Josh) Chi, Jin Yao, Aaron Ohta, and Ming-Chun (Jason) Tien, for having made my graduate study an experience to remember as well as giving me their many great and helpful ideas. Additional thanks goes to my project collaborators, Multiplex Inc. and Dr. K. -Y. Liou.

Most importantly I would like to thank my parents, who guided me to where I am by just showing me how they lived. Last, I declare my deepest debt of gratitude to my wife, Soo-Jin, who always trusts me and for her sacrifices. The laughter of my son, Junho, and daughter, Da-Hyun, gives me everlasting inspiration and happiness.

This work was partially supported by the Defense Advanced Research Projects Agency (DARPA). I also gratefully acknowledge partial financial support from the Korean government - Institute of Information Technology Assessment.

Chapter 1 Introduction

Optical fibers have become the media of choice for transmitting digital data over long distances, thanks to the extremely low propagation loss of light in fibers. The inherent bandwidth of fiber, on the order of tens of THz, offers enormous capacity, limited only by the transmitters, receivers, and fiber nonlinearity. Recently, there is increasing interest to use fibers to transmit not just digital but analog and radio-frequency (RF) signals. The light weight and immunity to electromagnetic interference (EMI) makes fiber an ideal media for antenna remoting. Optical processing of RF signals is also possible in the optical domain. Directly-modulated semiconductor lasers are the most compact source for fiber optic systems. However, their applications have been limited to low frequency systems (~ 10 Gb/s or 10 GHz) due to relaxation oscillation and chirp. The purpose of this thesis is to show that we can greatly enhance the performance of semiconductor lasers by strong optical injection locking, and extend their applications to larger bandwidth, higher performance systems, perhaps beyond 100 GHz.

To improve laser performance and further develop new applications, optical injection locking of semiconductor lasers has been widely investigated because injection-locked lasers can provide many advantages over free-running lasers. The advantages include laser linewidth reduction [1-3], suppression of mode hopping, reduction of mode-partition noise [4] and various modulation performance improvements [5-15]. In addition, lasers under certain injection locking conditions provide a variety of functionalities that might be useful, but not achievable by the free-running lasers [16-26].

1.1 Fundamentals of Optical Injection Locking

1.1.1 History

Locking phenomenon can occur between oscillators. It was first observed in two swinging pendulums by Huygens in the 1600s. Later, Adler established a theoretical study on locking phenomena in electric oscillators [27]. He found that the original oscillation frequency of a free-running oscillator can be locked to the frequency of an injecting oscillator with a constant phase value. This locking concept was adapted to a laser. The first “optical” injection locking was demonstrated by Stover and Steier using two HeNe lasers in 1966 [28]. Theoretical and experimental investigations on optical injection locking in the 1970s had been focused on the understanding of physical phenomena.

In the 1980s, thanks to the development of semiconductor lasers with spectral purity, optical injection locking had been widely investigated for communications applications. Using AlGaAs lasers, Kobayashi *et al.* demonstrated stable single-mode operation of Fabry-Perot (F-P) lasers [29] and phase modulation (PM) in an injection-locked laser through a frequency modulation (FM) of a master laser [20]. The primary focus was on coherent optical communications. Optical injection locking has also been applied to digital communication systems because the chirp of injection-locked lasers can be greatly reduced [5-7, 9, 30]. Since the 1990s, many advantages in the injection-locked lasers over free-running lasers has been achieved, including modulation bandwidth enhancement [10, 14, 31-39], resonance frequency increase [36, 39-42], nonlinear distortion reduction [12,

43, 44], relative intensity noise (RIN) reduction [10, 40, 45-48], and link gain improvement [49]. Table 1-1 summarizes the key milestones of injection locking research.

Year(s)	Main accomplishments	Researcher(s)
1600s	Observation of synchronization between two pendulums	C. Huygens
1946	First theoretical foundation on locking phenomena in electric oscillators	R. Alder [27]
1966	First demonstration of optical injection locking in lasers (two HeNe lasers)	Stover and Steier [28]
1980-1982	<ul style="list-style-type: none"> - Injection locking of semiconductor lasers (in AlGaAs lasers) - Single-mode operation of F-P lasers - Phase modulation using injection-locked lasers 	Kobayashi <i>et al.</i> [20, 29]
1984	<ul style="list-style-type: none"> - Dynamic linewidth reduction - Chirp reduction 	Lin <i>et al.</i> [5]
1995-1996	<ul style="list-style-type: none"> - Relative intensity noise (RIN) reduction - Modulation bandwidth enhancement 	Simpson <i>et al.</i> [10]
1998	First demonstration of nonlinear distortion reduction by optical injection locking	Meng <i>et al.</i> [12, 43]
2000	Injection locking of distributed Bragg reflector (DBR) lasers	Lee <i>et al.</i> [14]
2002	Injection locking of vertical cavity surface emitting lasers (VCSELs) at 1550 nm	Chang <i>et al.</i> [15]

Table 1-1. Historical main accomplishments of injection locking.

1.1.2 Basic Operation

The standard optical injection locking technique requires two optical sources - a master laser and a slave laser as shown in Figure 1-1. Light emitted from the master laser is injected into the slave laser. When injection locking conditions are satisfied, the frequency of the slave laser is locked to that of the master laser with a constant phase offset. Two important injection locking parameters are frequency detuning, Δf , which is the frequency difference between the master and the free-running slave lasers, and injection ratio, R , which is ratio between the injected power from the master laser and the lasing power of the free-running slave laser.

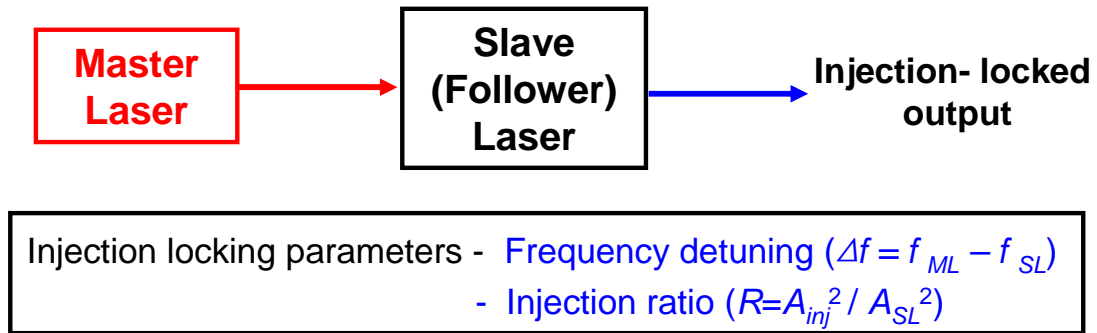


Figure 1-1. Schematic of optical injection locking.

The injection locking dynamics can be described by coupled rate equations, which represent the field amplitude, field phase, and carrier number of the slave laser under optical injection. The detailed theoretical and experimental investigations of optical injection locking will be discussed in Chapter 2. Here, we provide some overview of the

injection locking phenomena. Figure 1-2 illustrates the evolution of the intensity of the slave laser under optical injection when frequency detuning values are varied while the injection ratio, R , is kept constant. As shown in the figure, the spontaneous emission of the slave laser is significantly suppressed throughout the locking range, resulting in RIN reduction of the injection-locked laser. The intensity of the injection-locked laser also changes with the frequency detuning.

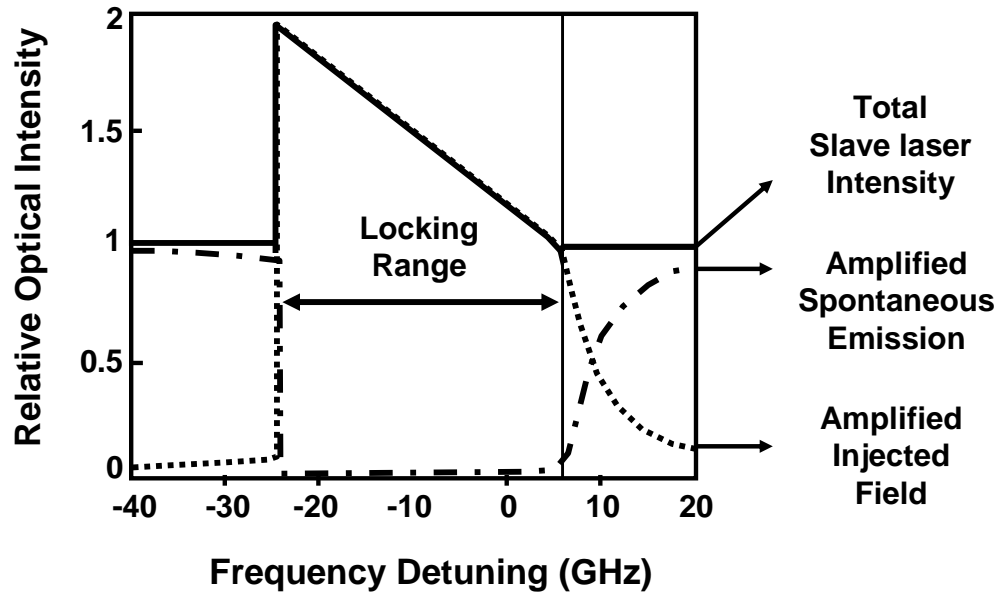


Figure 1-2. Calculated slave laser intensity, which consists of amplified spontaneous emission and amplified injected field, versus the frequency detuning, after [40].

Figure 1-3 and 1-4 show typical optical spectra of a free-running and injection-locked DFB and F-P lasers, respectively. For a DFB laser, two independent optical spectra are observed in an unlocked state, in which one peak is from a master laser and the other is from a slave laser. When the master laser wavelength is sufficiently close to the slave laser wavelength (i.e., tuned within injection locking range), a single injection-

locked peak is observed. In an injection-locked F-P laser, the optical injection from the master laser suppresses all other F-P modes except the injection-locked wavelength as shown in Figure 1-4(b).

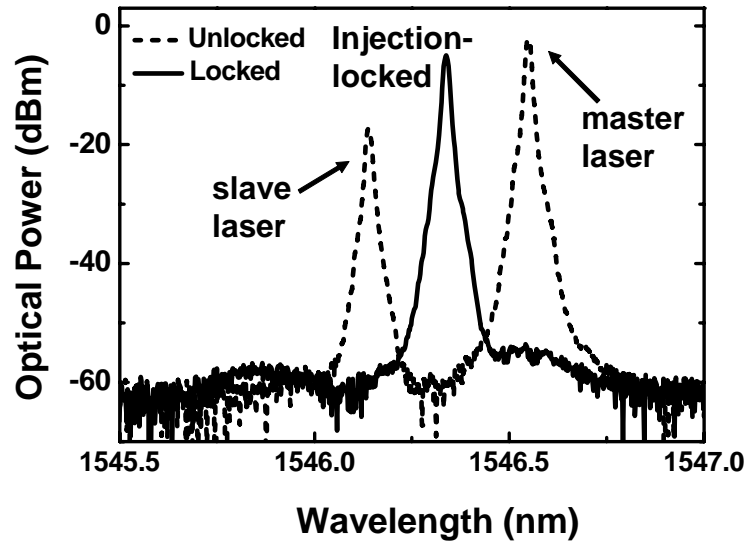


Figure 1-3. Experimentally measured optical spectra for an unlocked (dotted line) and injection-locked (solid line) DFB laser.

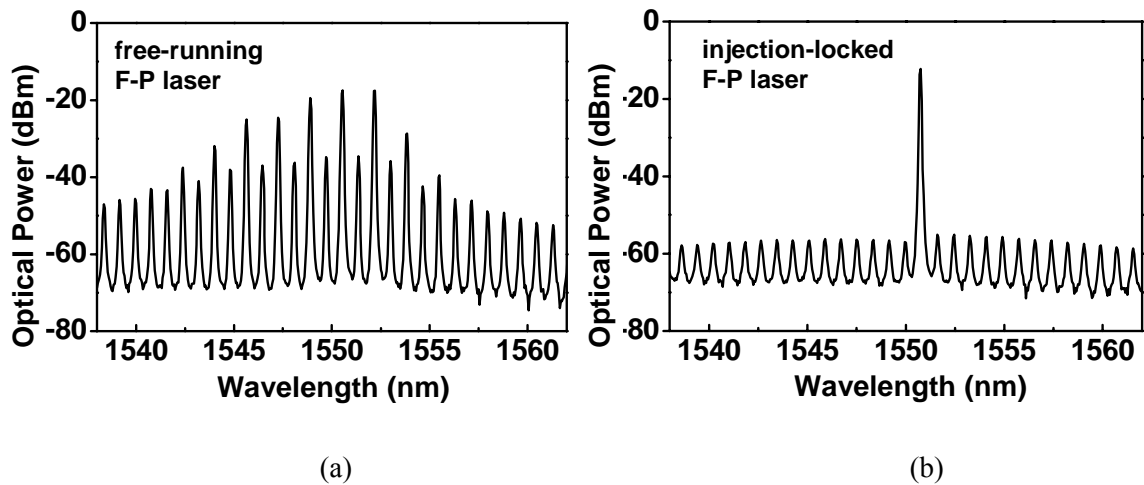


Figure 1-4. Experimentally measured optical spectra of a (a) free-running and (b) injection-locked F-P laser.

1.2 State of the Art of Optical Injection Locking

1.2.1 Modulation Bandwidth Enhancement

Bandwidth enhancement of directly-modulated semiconductor lasers has been demonstrated in various device structures, including short-cavity multiple-quantum well lasers [50], detuned loaded InGaAsP distributed Bragg reflector (DBR) lasers [51], and coupled-cavity injection grating lasers [52]. Modulation bandwidth enhancement by optical injection locking has been also reported by many authors, both theoretically and experimentally [10, 14, 31-39, 41, 49, 53, 54]. The enhanced resonance frequency can be much higher than the original relaxation oscillation frequency. Figure 1-5 shows the frequency response of an injection-locked DFB laser for various injection ratios. The resonance frequency increases with injection ratio, and is four times higher than that of the free-running laser at -6 dB injection ratio.

1.2.2 Link Linearity Improvement

In analog fiber optic links such as cable-TV video distribution and antenna remoting, the link performance is characterized by modulation bandwidth, link gain, noise figure, and spurious-free dynamic range (SFDR) [55, 56]. Directly-modulated semiconductor lasers experience nonlinear distortions due to the nonlinear coupling between carriers and photon [57, 58]. The distortions become more severe when the laser is modulated by signals with frequency components close to a relaxation oscillation frequency, where the nonlinear coupling is strongest. Meng *et al.* [43] and Chrostowski *et al.* [44, 59] demonstrated the reduction of nonlinear distortion and SFDR improvement as well as the

modulation bandwidth increase by an injection-locked DFB laser and vertical cavity surface emitting laser (VCSEL), respectively.

Figure 1-6 shows the two-tone intermodulation distortion of an injection-locked DFB laser. The laser is modulated by RF signals at $f_1 = 2.0$ GHz and $f_2 = 2.1$ GHz. The resonance frequency increases from 4.1 GHz to 13.6 GHz by injection locking. The SFDR is improved by 5 dB, which is mainly due to the resonance frequency increase in the injection-locked laser. Figure 1-7 shows the SFDR improvement as a function of injection ratio in a VCSEL. The experiment demonstrates that the increasing injection ratio leads to an increasing SFDR. The SFDR measurement was performed at 1-GHz range, while the numerical simulation at 2.4-GHz range. The data are plotted on two separate x -axes to demonstrate qualitative agreement between the experiment and the simulation.

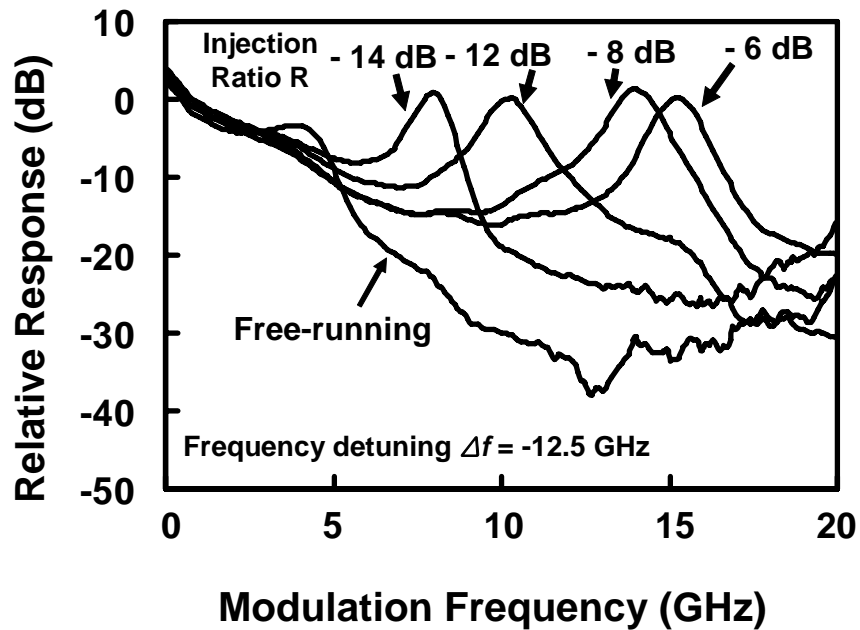


Figure 1-5. Measured frequency responses of an injection-locked DFB laser, after [35].

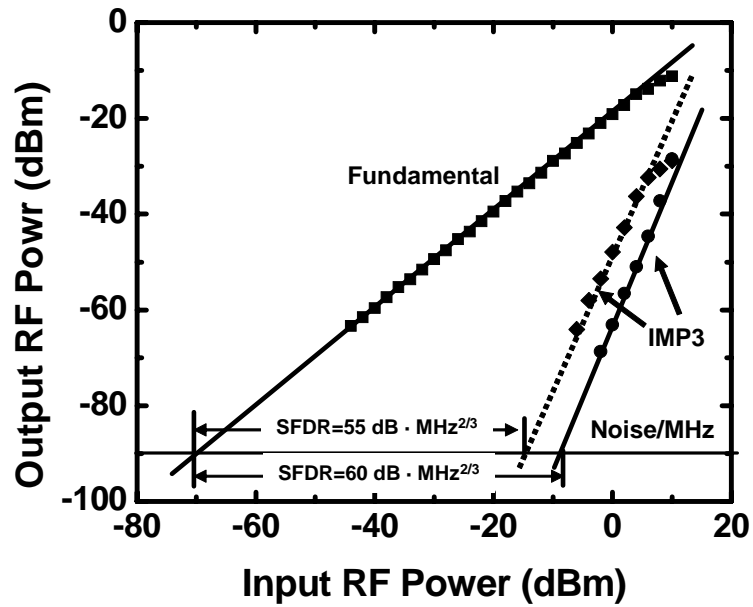


Figure 1-6. Measured RF fundamental power and third-order intermodulation products for a free-running laser and injection-locked DFB laser, after [43].

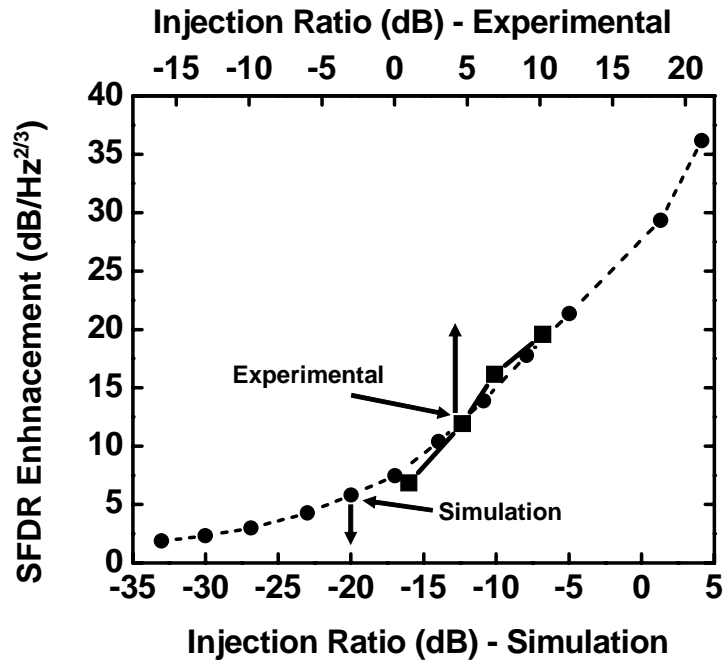


Figure 1-7. Measured SFDR improvement versus injection ratio for an injection-locked VCSEL, after [44].

1.2.3 Millimeter-Wave Generation

Transmission of analog or digital signals over high-frequency carriers (\sim a few tens of GHz) through an optical fiber has attracted great interest because optical fibers have very low propagation loss. In radio-over-fiber (RoF) systems, millimeter-wave signals are generated by optical sources in a central office (CO), and transmitted through fibers from CO to a base station (BS). Several schematics have been proposed to optically generate the millimeter-wave signals with a low phase noise. Goldberg *et al.* first demonstrated the millimeter-wave generation by sideband injection locking [60, 61]. In the demonstration, the coherence between two independent optical sources (= two slave lasers) are achieved by locking them to two modulation sidebands of the master laser. Using a millimeter-wave carrier generated by sideband injection locking, Braun *et al.* have reported a 155-Mb/s data transmission on a carrier of 64 GHz over 12.8-km standard single-mode fiber [17, 62]. By employing a similar but simpler technique, Noel *et al.* [63] demonstrated high-purity tunable millimeter-wave generation using one master laser and one RF-modulated slave laser. Recently, injection locking for millimeter-wave generation has been extended to the techniques using monolithic devices, including passively mode-locked DBR lasers [64] or two-section DFB lasers [65, 66].

1.2.4 Optical Injection Phase-Locked Loop (OIPLL)

Synchronization of lasers is a key issue in coherent optical communication system [67] and RF photonics applications. It can be attained either in the electric domain by phase-locked loops (PLL) or in the optical domain by optical injection locking [68].

Recently, optical injection phase-lock loop (OIPLL) has been demonstrated by A. J. Seed's group [69]. The OIPLL combines electric phase locking with optical injection locking (Figure 1-8), achieving superior performance than when individual technique is used alone. Figure 1-9 shows the measured power spectral densities (PSD) for a homodyne optical PLL (OPLL) and the OIPLL system. The theoretical PSD of the OIPLL system is also shown in the same figure. Clearly, the addition of optical injection locking improves its phase noise performance, overcoming the limitations of either OPLL or optical injection locking.

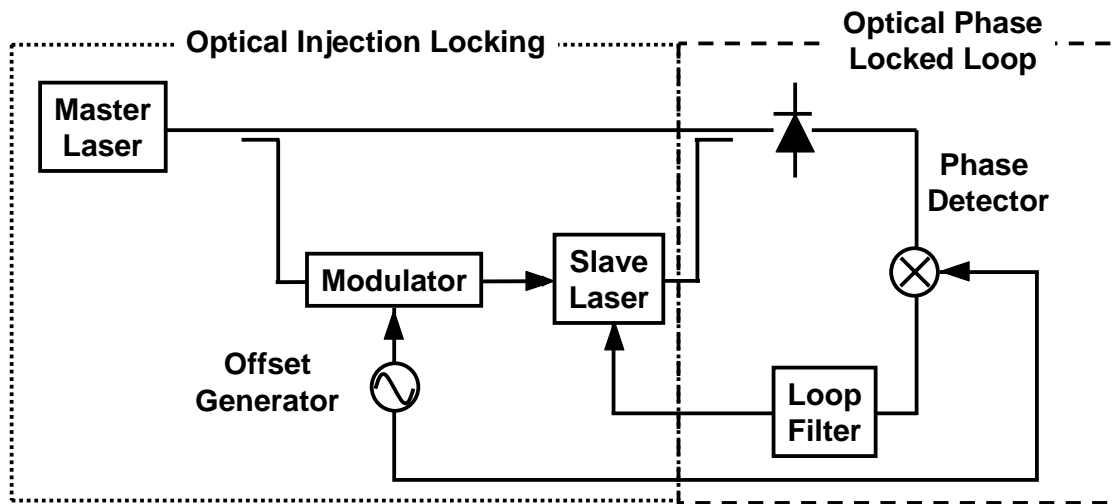


Figure 1-8. Schematic of optical injection phase-locked loop (OIPLL) for heterodyne systems. Synchronization is achieved by both optical injection locking and optical phase-locked loop, after [69].

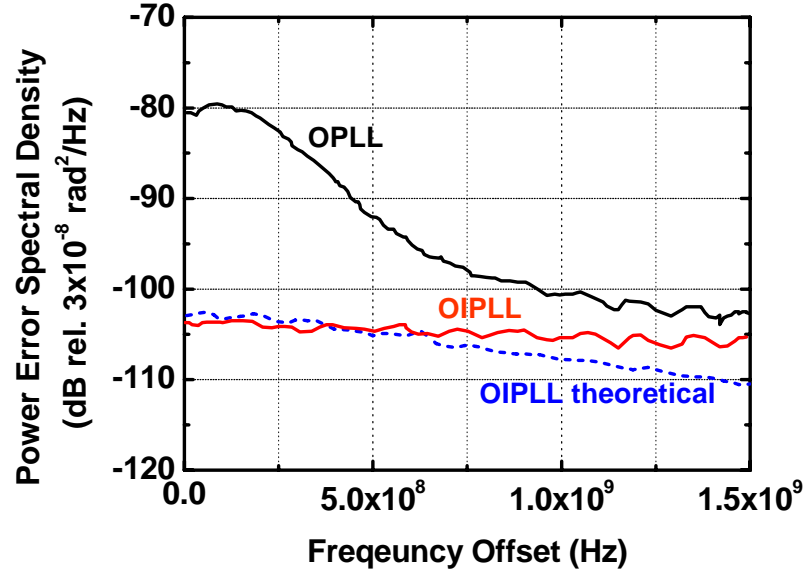


Figure 1-9. Power error spectral densities for homodyne OPLL and OIPLL systems, after [69].

1.2.5 Injection Locking of Mode-Locked Lasers

Channelization is a broadband RF signal processing technique that “chops” the RF signals into N consecutive frequency bands and convert them into an array of N intermediate frequency (IF) signals with smaller $(1/N)$ bandwidth. The channelization of broadband (~ 100 GHz) RF signals can be conveniently performed in the optical domain using coherent optical receivers if one can synchronize the RF-modulated optical carrier with an optical frequency comb (OFC) local oscillator. The OFC is typically generated by an external-cavity mode-locked laser or a passively mode-locked laser.

Injection locking of a mode-locked laser has been demonstrated to generate a coherent OFC at remote locations. This is potentially useful for coherent optical communication systems with subgigahertz channel spacing [70-73]. Figure 1-10 shows the schematic of the injection-locked OFC for coherent channelizer. By injecting light

from a CW master laser [70, 73] or a mode-locked laser [71, 72], phase coherence is established between the master and the injected mode. The grating disperses the OFC and the optical signals at the corresponding frequency onto a linear array of photodetectors for coherent demodulation.

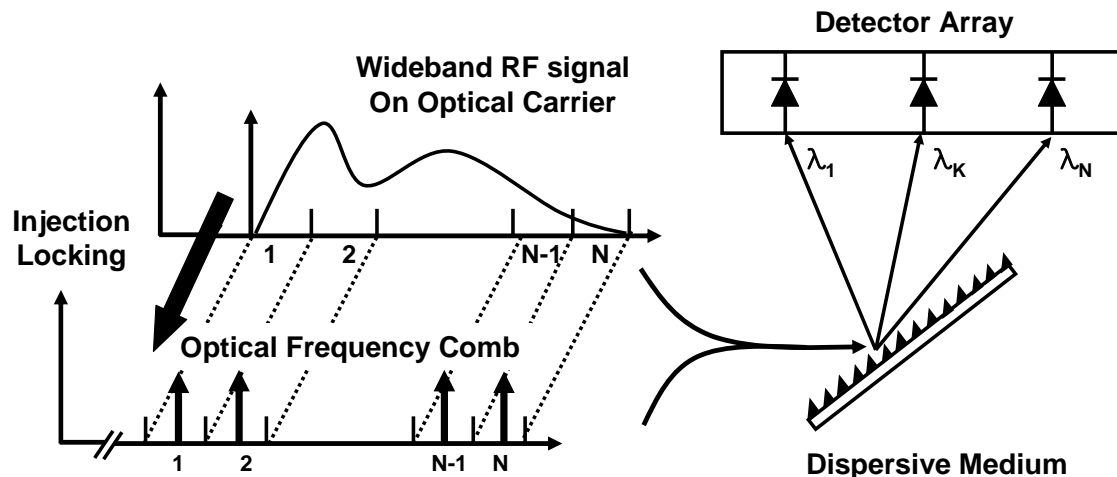


Figure 1-10. Conceptual architecture of coherent channelizer, after [70].

1.2.6 Optical Signal Processing and Other Applications

All-optical signal processing can alleviate the requirement of electric circuits in high-speed photonic networks. Clock recovery, which is essential to digital communication, can be achieved by injection locking a passively mode-locked laser [74]. All-optical signal regeneration has drawn considerable attention. It has been realized by using an injection-locked DFB laser [75], a sidemode injection-locked DFB laser [76], and a two-mode injection-locked F-P laser [77].

Figure 1-11 shows the schematic of waveform reshaping by optical injection locking. The reshaping process is based on the switching of locking stability as a function of

injection ratio. When the frequency detuning is fixed, the locked or unlocked state depends on the injection power. When the optical power higher than locking threshold is injected to a slave laser, the slave laser is locked to the master laser frequency, f_m . On the other hand, when the injection power is small, the slave laser operates at the original frequency, f_s . Due to the threshold behavior of the locking and unlocking processes, distorted signals can be reshaped, resulting in a frequency-modulated signal with a reduced noise. The signal from the slave laser is then filtered by bandpass filter, so that the reshaped signal can be obtained. Injection locking for all-optical processing also provides additional all-optical signal processing functions, such as optical inverter [78], all-optical format converter [79], and polarization controller [80].

Injection locking of uncooled VCSELs can potentially be used for low-cost transmitters for WDM (Wavelength Division Multiplexing) systems [81]. Optical single sideband modulation, which substantially reduces fiber chromatic dispersion effect, can be generated by strong optical injection locking [82].

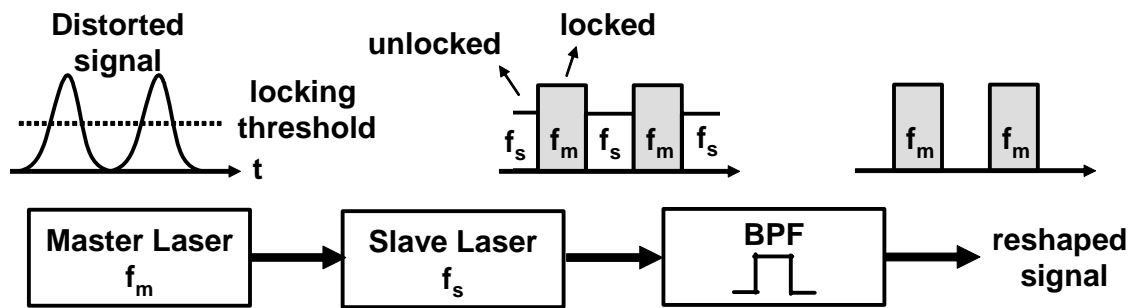


Figure 1-11. Schematic of optical waveform reshaping by injection locking, after [75].

1.3 Organization of the Dissertation

Chapter 2 starts with the limitations of directly-modulated lasers and introduces the motivation of ultra-strong optical injection locking ($R \sim 10$ dB). Experimental observation on optical spectra and frequency responses of ultra-strong injection-locked lasers reveals three distinctive modulation characteristics under different frequency detuning, Δf : (1) increase of amplitude modulation (AM) response, (2) broad 3-dB bandwidth, and (3) high resonance frequency with a narrowband RF gain. In Chapter 3, we propose a novel approach to produce optical single sideband (SSB) modulation by strong optical injection locking. Modulation sidebands with > 10 -dB asymmetry between the upper and lower sidebands have been achieved. The RF performance of the optical SSB has been demonstrated by transmitting the optical SSB over optical fibers.

In Chapter 4, we present the fabrication of gain-lever distributed Bragg reflector (DBR) lasers. We also demonstrate the injection locking of gain-lever DBR lasers for the first time. By combining gain-lever modulation with optical injection locking, an improvement of AM modulation efficiency, increase of modulation bandwidth, reduction of nonlinear distortions, and increase of SFDR have been achieved simultaneously.

In Chapter 5, we propose a monolithic injection locking scheme using two-section DFB lasers. The two-section DFB lasers exhibit mutual locking phenomena similar to those observed in externally injection-locked lasers, including increased modulation bandwidth, enhanced resonance frequency, and reduced laser chirp.

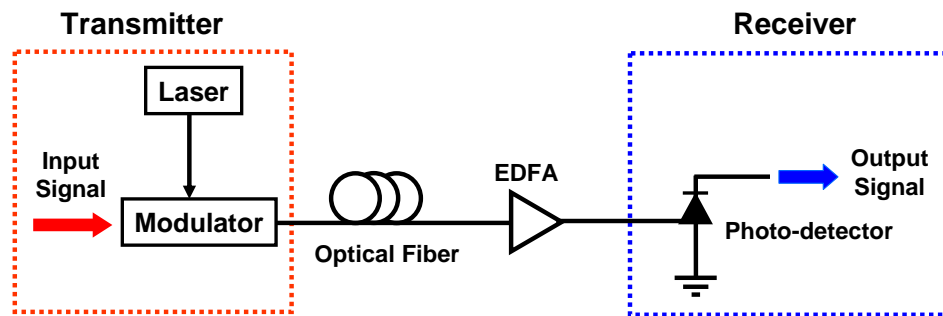
In Chapter 6, we describe two applications of the monolithic injection-locked lasers. The first is the extinction ratio improvement under large-signal modulation. The second is

optical millimeter-wave generation using two-section DFB lasers. Spectrally pure millimeter-waves with high power are generated by monolithic sideband injection locking. Chapter 7 summarizes the work presented in this dissertation and comments on future directions and the applications of optical injection locking.

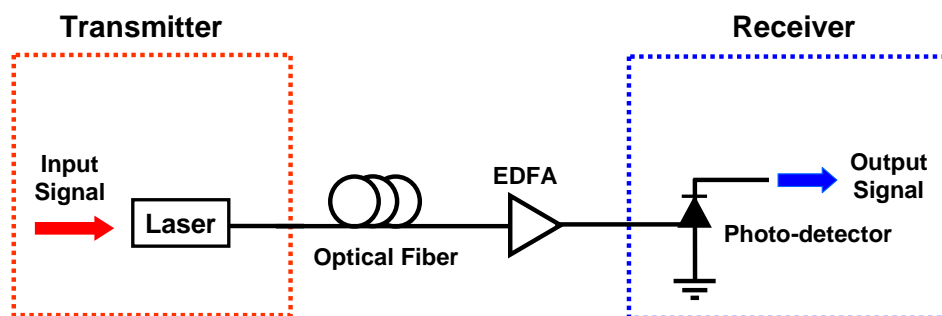
Chapter 2 Strong Optical Injection Locking

2.1 Limitations of Directly-Modulated Lasers

Figure 2-1 shows the schematics of fiber optic links with (a) external and (b) direct modulations. Typically, direct modulation is used in low-cost systems, while external modulation is employed in high performance applications. In addition to optical communication networks, fiber optic links are also used in analog/RF systems such as cable-TV video distribution, antenna remoting in cellular networks, and radio-over fiber (RoF) systems [55, 83, 84]. The requirements for analog and digital signal transmissions are quite different. Table 2-1 summarizes the limitations of directly-modulated fiber-optic links for analog signal transmission. The modulation bandwidth is limited by the relaxation oscillation frequency of the laser. The nonlinear coupling between electron and photon generates undesired signal distortions such as harmonic and intermodulation distortions. Electron-photon conversion loss (< 1) results in a link loss. On the other hand, digital links require low frequency chirp and high extinction ratio, different from analog links. Fortunately, most of these limitations can be improved by optical injection locking.



(a) External Modulation



(b) Direct Modulation

Figure 2-1. Schematics of fiber optic links using (a) external modulation (b) direct modulation.

System Requirements	Limitations of Direct Modulation
High modulation bandwidth	Relaxation oscillation
Low signal distortion	Nonlinear electron-photon coupling
Low relative intensity noise (RIN)	Spontaneous emission of lasers
Low RF link loss	Electron-photon conversion loss

Table 2-1. Limitations of directly-modulated systems for analog signal transmission.

System Requirements	Limitations of Direct Modulation
High modulation bandwidth	Relaxation oscillation
Low chirp	frequency change under modulation
High extinction ratio	Laser turn-on transient

Table 2-2. Limitations of directly-modulated systems for digital signal transmission.

2.2 Motivation for Ultra-Strong Injection

The history optical injection locking research can be divided into three periods. In the 1980s, most of the experiments were in the weak injection regime ($R < -10$ dB) [3, 4, 20, 21, 29, 68]. Injection ratio R , here, is defined as the power ratio between the injected power and the lasing power of the free-running slave laser. Phase modulation [20], laser

linewidth reduction [2, 3], and sidemode suppression of F-P lasers [29] have been demonstrated. The primary driving force at that time was coherent optical communications.

In the 1990s, thanks to the development of high-power, continuous-wave (CW) semiconductor lasers, strong optical injection locking ($-10 < R < 0$ dB) properties have been intensely investigated. The lasers exhibit resonance frequency enhancement [36, 41], modulation bandwidth increase [10, 14, 31, 32, 34-36], chirp reduction [9], and nonlinear distortion suppression [12, 43], in addition to the benefits of the weak injection locking. These benefits improved the performance of both analog and digital fiber optic links. For example, laser chirp in directly-modulated lasers can be significantly reduced by injection locking because the slave laser's wavelength is locked to the master's. The 3-dB modulation bandwidth can be improved by increasing the resonance frequency of injection-locked lasers. The increase of resonance frequency can be explained as follows: for strong injection-locked lasers, the carrier density of the slave laser changes as a function of injection locking parameters - frequency detuning and injection ratio. This modified carrier density causes a wavelength shift of the original cavity mode of the free-running slave laser [36, 40]. As a result of an interaction between the injection-locked wavelength and the shifted cavity mode, the injection-locked laser exhibits a resonance enhancement.

The properties of the resonance frequency increase depend on injection locking parameters. Recently, Simpson *et al.* [41] and Murakami *et al.* [36] demonstrated this resonance frequency increase in strong injection-locked semiconductor lasers experimentally and theoretically. According to the theory and experimental results [36,

40-42], the performances of injection-locked lasers improve with stronger injection ratio. Using injection locking of VCSELs, Chrostowski *et al.* [44] achieved a high resonance frequency of > 50 GHz as shown in Figure 2-2. Figure 2-3 shows the measured stable locking range versus injection ratio. Stronger injection increases the stable locking range. At the injection ratio of -6 dB, stable locking range is ~ 20 GHz. Injection locking system with stronger injection is robust and exhibits improved performance compared with weaker injection locking system.

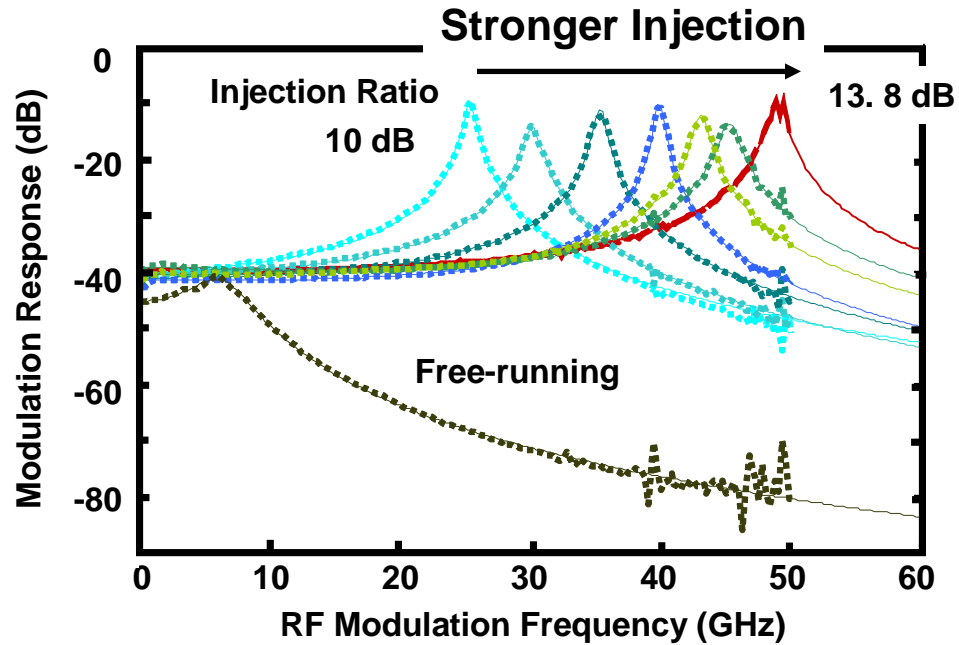


Figure 2-2. Frequency responses of free-running and injection-locked VCSELs for various injection ratios, after [44].

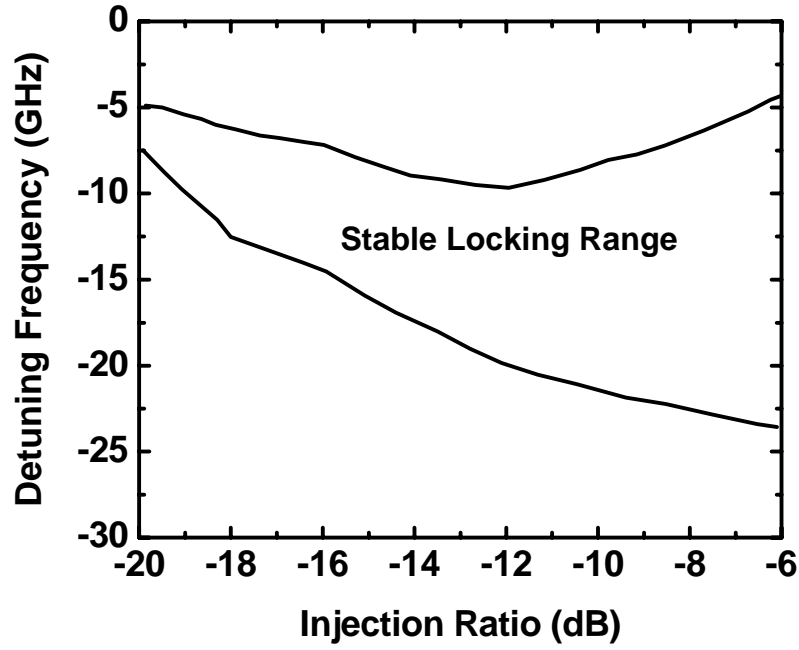


Figure 2-3. Injection locking range of DFB lasers as a function of injection ratio, after [35].

In this Chapter, we will extend the study of strong injection locking to *ultra-strong* injection locking regime, where the injection ratio, R , is ~ 10 dB. We have performed a systematic study on ultra-strong injection-locked DFB lasers through experimental observations of optical spectra and corresponding frequency responses with various injection locking parameters. We will show that the measured frequency responses exhibit three distinctive regimes, depending on the frequency detuning.

2.3 Experimental Observations

2.2.1 Experimental Setup

Figure 2-4 is a schematic of the experimental setup to characterize the optical spectra and electric modulation properties of ultra-strong optical injection-locked DFB lasers. A master laser module consists of an external-cavity tunable laser (ECTL) that provides wide frequency tunability and an Erbium-doped fiber amplifier (EDFA) that enables ultra-strong injection. An EDFA followed by a variable optical attenuator controls the injection ratio. Polarization matching between the master laser and a slave laser is achieved by a polarization controller. To couple the incident light from the master laser module to the slave lasers, an optical head with a pig-tailed fiber and an optical circulator with > 40 -dB isolation between ports are used. The optical isolator prevents undesired light coupling from the slave laser to the master laser module. It also protects the slave laser against the back-reflected light. The slave laser is a DFB laser with two electrically-isolated gain sections. Only the section facing the coupling lens is pumped and the other section is left unbiased.

The optical and RF spectra of the free-running slave laser is carefully observed to ensure a stable single-mode operation without exhibiting self-pulsation or multi-mode lasing throughout the measurements presented in this Chapter. The optical output of the injection-locked laser is monitored on an optical spectrum analyzer (OSA) with a resolution of 0.01 nm ($= 1.25 \text{ GHz}$). To measure the frequency responses, modulation signals from a network analyzer are applied to the slave laser through a bias-tee. The output is sent to a high-speed (34 GHz) photodetector followed by the network analyzer

or an RF-spectrum analyzer (RF-SA).

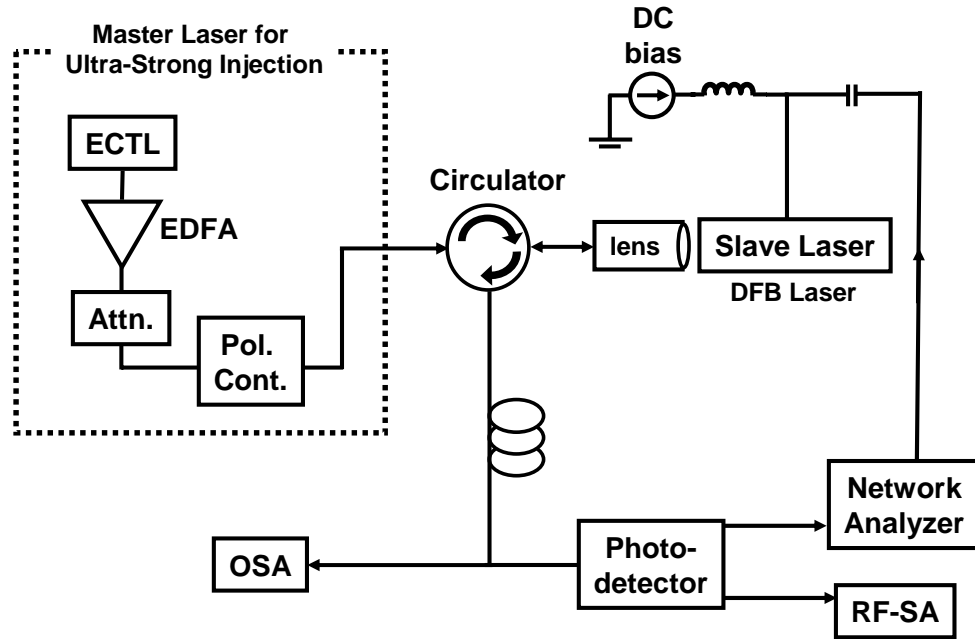


Figure 2-4. Experimental setup for ultra-strong optical injection locking. The optical spectrum and the RF modulation responses are monitored simultaneously. (ECTL: external cavity tunable laser; EDFA: Erbium-doped fiber laser; Attn.: optical attenuator; Pol. cont.: polarization controller; OSA: optical spectrum analyzer; RF-SA: RF-spectrum analyzer)

2.2.2 Measured Optical Spectra and Modulation Responses

Figure 2-5(a)-(c) show the measured optical spectra under various frequency detuning conditions. Figure 2-5(d)-(f) depict their corresponding frequency responses. The threshold current of the free-running slave laser is 9 mA. It is DC-biased at 19 mA ($= 2.1 \cdot I_{th}$) throughout the measurement. The lasing wavelength at this bias current is thermally stabilized at 1545.91 nm by a heat sink with temperature controller. The output

power of the free-running slave laser is measured to be -3 dBm at the pig-tailed output fiber of the coupling lens.

As shown in the dotted lines in Figure 2-5(a) and (d), the free-running optical spectrum exhibits stable single-mode performance with SMSR of >50 dB and the relaxation oscillation frequency is measured at 4.2 GHz. To achieve the ultra-strong injection-locked state, the optical power of the master laser is boosted by an EDFA, so that the injection ratio R of ~ 12 dB is attained. Systematic variation of frequency detuning Δf has been achieved by changing piezo voltage of the ECTL while maintaining injection ratio at a constant value. The frequency detuning, Δf , is defined as the frequency difference between the master laser and free-running slave laser ($\Delta f = f_{\text{master}} - f_{\text{free,slave}}$). The injection locking range is measured by observing the optical spectra in OSA and the beating frequency in RF-SA. The measured injection locking range with respect to the wavelength of the free-running laser is drawn by the thin vertical lines at $\lambda = 1545.71$ and 1546.30 nm in Figure 2-5(a)-(c). The thin vertical line at wavelength $\lambda = 1545.91$ nm represents the zero-detuning point ($\Delta f = 0$). The area between the two vertical lines is the stable locking range. The corresponding frequency detuning values are -48.75 and 25 GHz, respectively. The asymmetry of the locking range is due to the linewidth enhancement factor (Henry's factor) [1, 40, 85, 86].

Experimentally, the transition from locked to unlocked state at the negative detuning edge can be easily observed through a sudden jump from injection-locked wavelength to the free-running slave laser mode. However, because there is no such wavelength hop at the positive detuning edge, the locking range for the positive detuning edge is defined as the frequency detuning value corresponding to the point where SMSR between the

injection-locked peak and residual cavity mode is 35 dB. Within this range, no unstable locking or unlocked phenomena such as four-wave mixing, pulsation, or chaos have been observed, so that the slave laser is still locked to the master laser despite the existence of the cavity mode.

In the large negative locking regime ($\Delta f = -42$ GHz), where the master laser is injected into the longer wavelength of the free-running slave laser, the optical spectrum in Figure 2-5(a) shows a single mode with SMSR > 50 dB. The corresponding frequency response exhibits an enhanced amplitude response at low frequency (DC to ~3 GHz). The increase of the amplitude response results from a cavity resonance effect. Since the cavity mode is very close to the injected frequency, the resulting resonance frequency is low.

When the master laser is tuned towards the center of the locking regime ($\Delta f = -14$ GHz), a single-mode spectrum is maintained with SMSR of 45 dB. The cavity mode is believed to be hidden under the envelope of the injection-locked spectrum due to the small amplitude, thus the limitation of the resolution of the OSA. In the corresponding frequency response in Figure 2-5(e), the 3-dB bandwidth is significantly increased to 21 GHz, which is more than a four-fold increase of the relaxation oscillation frequency of the free-running laser. This broad 3-dB bandwidth originates from the moderate resonance enhancement of the cavity mode. This resonance compensates the RC roll-off of the free-running laser. Therefore, the flat frequency response and broad 3-dB modulation bandwidth are observed.

Finally, the master laser is tuned to the edge of the positive frequency detuning regime. The cavity mode becomes observable, showing a reduced SMSR and increased wavelength spacing between injection-locked frequency and the cavity mode. As shown

in Figure 2-5(c), the wavelength of the cavity mode is shifted to the longer wavelength compared with the original wavelength of the free-running slave laser. The shift of the cavity mode results from the carrier density-dependent refractive index change in the injection-locked laser [36, 40]. The injection of photon from the master laser depletes carrier in the slave laser. In the optical spectrum in Figure 2-5(c), the wavelength difference between the injection-locked wavelength and cavity mode is measured as 0.264 nm (= 33 GHz). Correspondingly, the resonant peak is located at 33 GHz in the frequency response in Figure 2-5(f). The resonant peak originates from the resonance enhancement of the cavity mode. Since the cavity mode is on the longer wavelength side, only the upper wavelength sideband is resonantly amplified. This can be used for single sideband modulation and will be discussed in detail in Chapter 3. The amount of the wavelength shift and the power evolution of the cavity mode is a strong function of injection locking parameters, which allow us to control the height and frequency of the resonant peak.

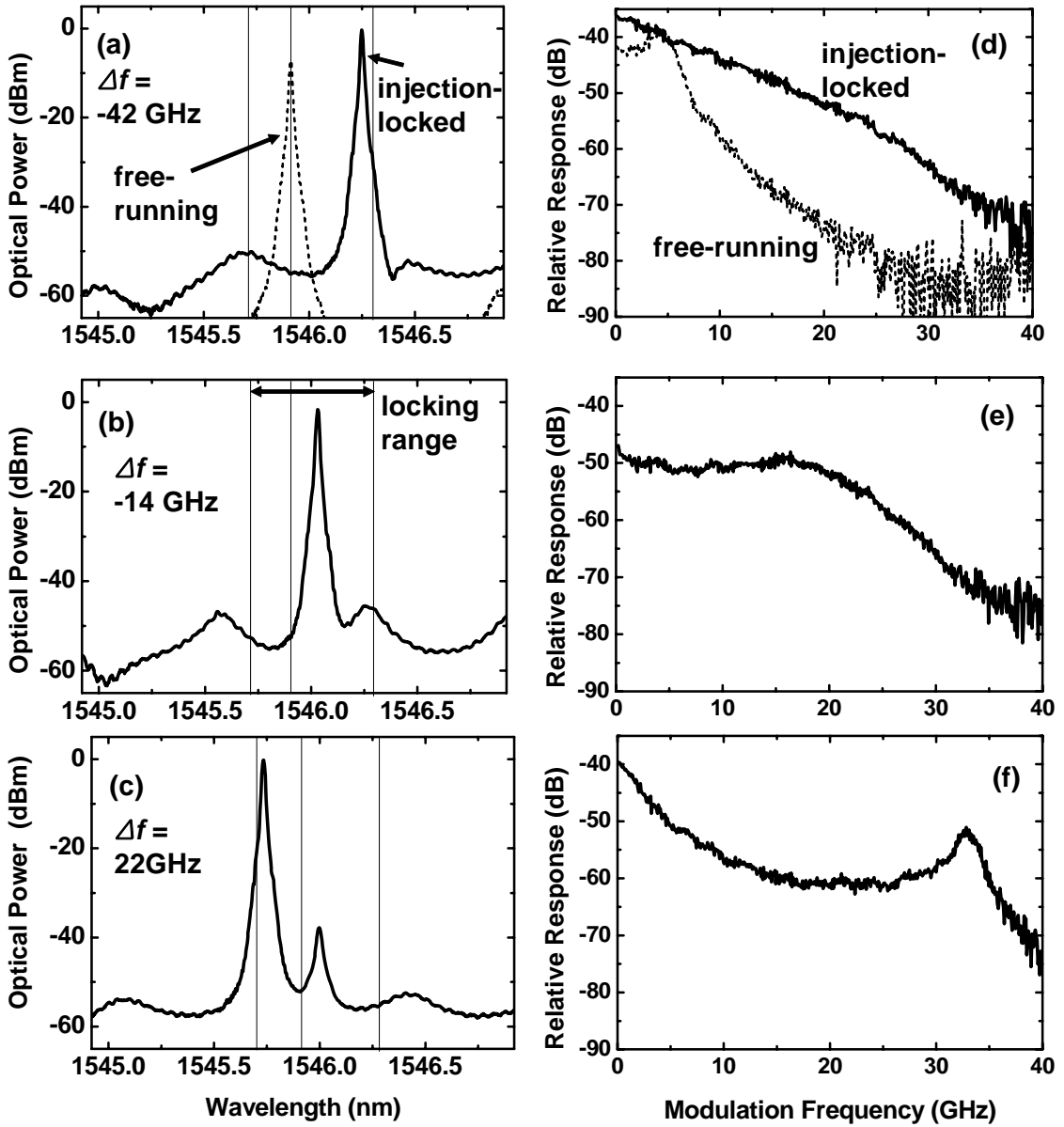


Figure 2-5. Experimentally measured optical spectra ((a)-(c)) and frequency responses of an ultra-strong optical injection-locked laser ((d)-(f)) for various detuning conditions. The injection ratio is kept at 12 dB. (a) and (c): frequency detuning $\Delta f = -42$ GHz; (b) and (d): $\Delta f = -14$ GHz; (c) and (f): $\Delta f = 22$ GHz. For comparison, optical spectrum and frequency response of the free-running laser are depicted as dot lines in (a) and (c), respectively. Three vertical solid lines in the optical spectra represent positive detuning edge, free-running lasing wavelength, and negative detuning edge from left to right.

2.4 Theoretical Model

Recently, several researchers have investigated and demonstrated the resonance frequency increase in directly-modulated semiconductor lasers with strong optical injection locking, both experimentally and theoretically [10, 32, 36, 37, 42, 49]. To model the three distinctive frequency responses observed experimentally, the dynamics of injection-locked lasers are simulated by rate equations which couple the temporal variations of the amplitude, the phase and the number of carriers of the slave laser:

$$\frac{dA(t)}{dt} = \frac{1}{2} g [N(t) - N_{th}] A(t) + \kappa A_{inj} \cos \phi(t) \quad (2.2)$$

$$\frac{d\phi(t)}{dt} = \frac{\alpha}{2} g [N(t) - N_{th}] - \kappa \frac{A_{inj}}{A(t)} \sin \phi(t) - 2\pi \Delta f \quad (2.3)$$

$$\frac{dN(t)}{dt} = J - \gamma_N N(t) - \{\gamma_p + g [N(t) - N_{th}]\} A^2(t) \quad (2.4)$$

where $A(t)$ is the field amplitude, defined as $A^2(t) = S(t)$, where $S(t)$ is the photon number. $\phi(t)$ is the phase difference between the temporal laser field of the slave laser and master laser. $N(t)$ is the carrier number and J is the injection current. For all calculations done in this section, J is set at $3 \cdot J_{th}$. N_{th} is the threshold carrier number, g is the linear gain coefficient, γ_p is the photon decay rate, $\kappa (= 1/\tau_{in})$ is coupling coefficient, τ_{in} is the cavity round-trip time of the slave laser, α is the linewidth enhancement factor of the slave laser, and γ_N is the carrier decay rate. N_{th} also defines the carrier number at the onset of lasing, and contains both transparency carrier number and photon loss rate: $N_{th} \equiv N_{tr} + \gamma_p / g$.

The values used for the calculation are listed in Table 2-3. Regarding the injection condition, A_{inj} is the field amplitude injected into the slave laser and Δf is the lasing

frequency difference (i.e., frequency detuning) between the master and the free-running slave lasers. Dynamics of the slave laser are governed by the injection locking parameters, including frequency detuning Δf and injection power ratio $R (= A_{inj}^2 / A_{free}^2)$, where A_{free} is the field amplitude of the free-running slave laser.

Symbol	Quantity	Value
g	linear gain coefficient	$5.667 \times 10^3 \text{ s}^{-1}$
N_{th}	threshold carrier number	2.088×10^8
κ	coupling coefficient	$1.002 \times 10^{11} \text{ s}^{-1}$
α	linewidth enhancement factor	3
γ_N	carrier decay rate	$1/(1 \times 10^{-9} \text{ s})$
γ_P	photon decay rate	$1/(3 \times 10^{-12} \text{ s})$

Table 2-3. Values used for calculations

By applying small-signal linear approximation and stability analysis to the above rate equations [9, 17, 22], the injection locking range, $\Delta\omega_L$, and locking stabilities can be derived and plotted

$$-\sqrt{1+\alpha^2} \kappa \left(\frac{A_{inj}}{A_0} \right) < \Delta\omega_L < \kappa \left(\frac{A_{inj}}{A_0} \right) \quad (2.5)$$

where A_0 is the stationary amplitude of the slave laser under optical injection. The regions

of injection locking stability are shown as a function of injection locking parameters in Figure 2-6. Equation (2.5) and Figure 2-6 illustrate that stronger optical injection broadens the stable injection locking range.

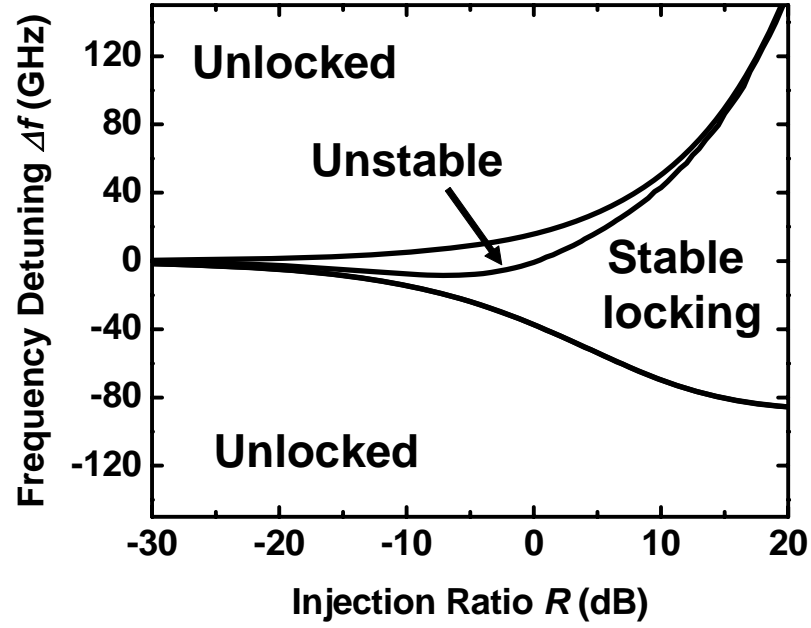


Figure 2-6. Injection locking stability as a function of injection ratio R and frequency detuning Δf . Stronger optical injection broadens locking range.

Using the small-signal approximation of the coupled rate equations, the small-signal modulation response of the injection-locked lasers can be derived as [36, 86]

$$H(s) = \frac{\frac{1}{2} g A_0 \left(s + a_{22} - \frac{a_{12}a_{23}}{a_{13}} \right)}{s^3 + A s^2 + B s + C} \quad (2.6)$$

$$A = a_{11} + a_{22} + a_{33} \quad (2.7)$$

$$B = a_{11}a_{33} + a_{22}a_{33} + a_{11}a_{22} - a_{21}a_{12} - a_{31}a_{13} \quad (2.8)$$

$$C = a_{11}a_{22}a_{33} - a_{21}a_{12}a_{33} + a_{31}a_{12}a_{23} - a_{31}a_{22}a_{13} \quad (2.9)$$

where

$$\begin{aligned} a_{11} &= -\frac{1}{2}g(N_s - N_{th}), & a_{12} &= \kappa \cdot A_{inj} \cdot \sin(\phi_s), & a_{13} &= -\frac{1}{2}g \cdot A_0 \\ a_{21} &= \kappa \cdot \sin(\phi_s) \cdot \frac{A_{inj}}{A_0^2}, & a_{22} &= \kappa \cdot \cos(\phi_s) \cdot \frac{A_{inj}}{A_0}, & a_{23} &= -\frac{1}{2}\alpha \cdot g \\ a_{31} &= 2 \cdot A_s \left(\frac{1}{\tau_p} + g(N_s - N_{th}) \right), & a_{32} &= 0, & a_{33} &= \frac{1}{\tau_n} + g \cdot A_0^2 \end{aligned}$$

Figure 2-7 shows the calculated frequency responses of the injection-locked lasers. The frequency responses calculated from equation (2.6) are normalized by the free-running DC optical power for amplitude response comparison. To confirm the various modulation responses depending on frequency detuning values, the frequency detuning values are varied, while fixing the injection ratio at 10 dB.

As shown in Figure 2-7, the calculated frequency response at large negative detuning ($\Delta f = -60$ GHz) shows an increase of low frequency amplitude response. A broad 3-dB bandwidth is attained when the frequency detuning Δf is set at -5 GHz, which is near the center of the locking range. A high resonant peak at 48.3 GHz is demonstrated at the detuning value Δf of 42 GHz. These distinctive modulation characteristics of ultra-strong optical injection-locked lasers are well matched with the measurement results shown in Section 2.2.3. In addition, the frequency of the resonant peak is controllable and can be increased with stronger injection. By performing a small-signal linear analysis on the coupled rate equations, we can derive an approximate formula for the resonance frequency, ω_R , of the injection-locked laser [36, 40],

$$\omega_R^2 \approx \omega_{R0}^2 + \kappa^2 \left(\frac{A_{inj}}{A_0} \right)^2 \sin^2 \phi_0 \quad (2.5)$$

where ω_{R0} is the relaxation oscillation frequency of the free-running slave laser and ϕ_0 is the steady-state phase difference between the injection-locked slave laser and the master laser. Here, we see that increasing the injection ratio enhances the resonance frequency.

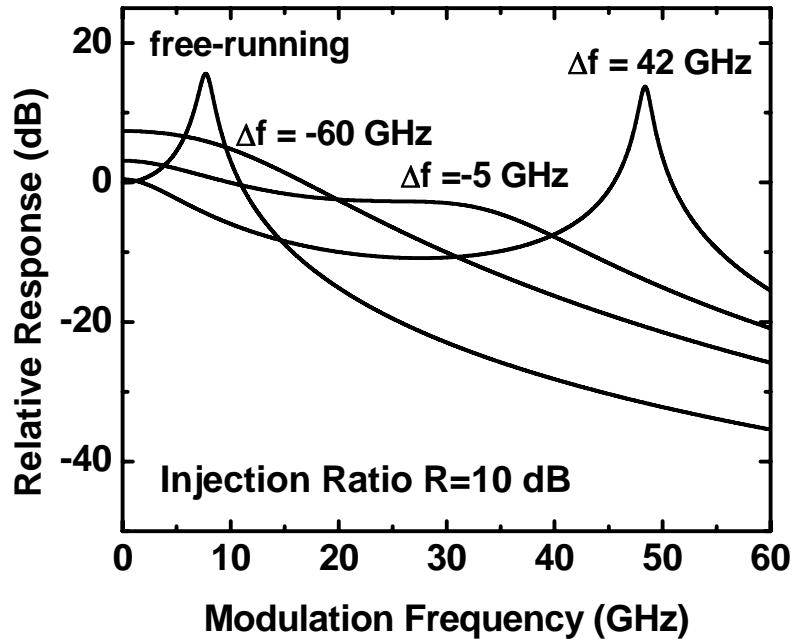


Figure 2-7. Calculated frequency responses of ultra-strong ($R = 10$ dB) injection-locked lasers under various frequency detuning values.

Figure 2-8 shows the calculated frequency response curves, where the resonance frequency increases with injection ratio. In Figure 2-9 and 2-10, amplitude and resonance frequency evolution of injection-locked lasers are shown as a function of frequency detuning throughout an entire locking range. For the calculations, injection ratio is set at 10 dB. The amplitude of the injection-locked laser increases at large negative frequency

detuning. Consequently, three distinctive locking regimes match well with the experimental observations.

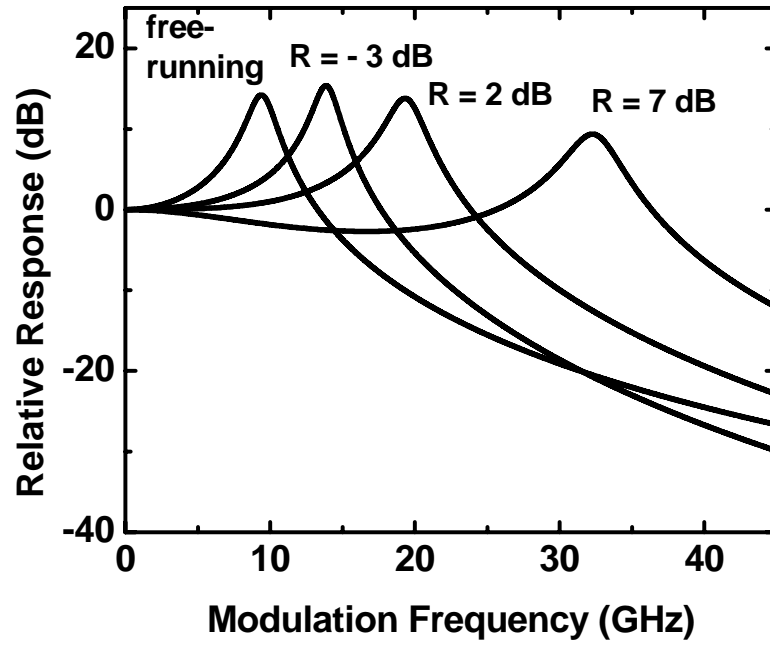


Figure 2-8. Calculated frequency responses for various injection ratios. Frequency detuning Δf is set at the positive edge of the locking range.

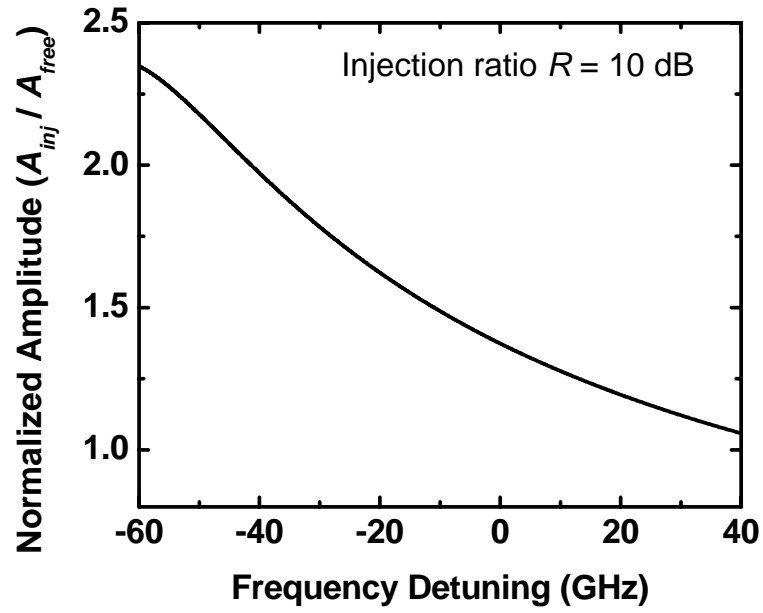


Figure 2-9. Normalized amplitude of an injection-locked laser as a function of frequency detuning. Injection-locked amplitude, A_{inj} is normalized by the free-running amplitude A_{free} .

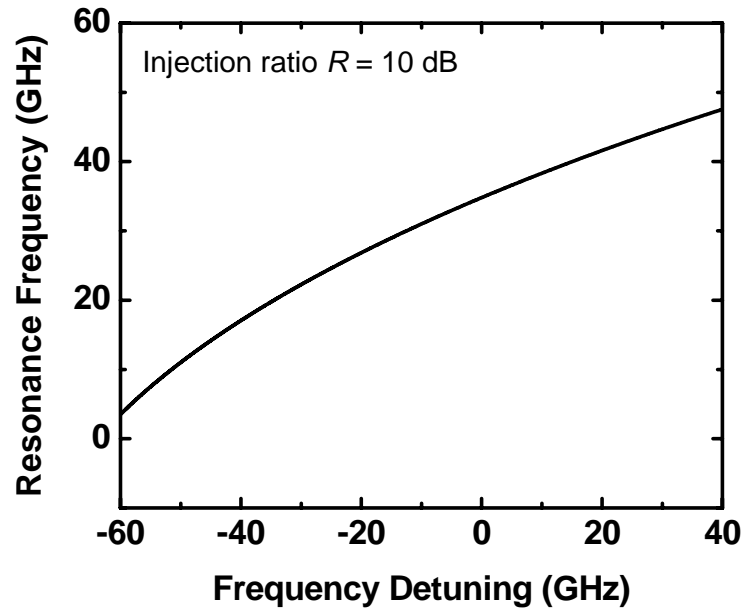


Figure 2-10. Resonance frequency as a function of frequency detuning.

2.5 Broad 3-dB Bandwidth and High Resonance Frequency with Narrowband RF Gain

As demonstrated in Sections 2.3 (experimentally) and 2.4 (theoretically), the resonance frequency and the 3-dB bandwidth of ultra-strong injection-locked lasers are greatly improved by stronger injection. Figure 2-11(a) and (b) are optical spectra of the ultra-strong injection-locked laser showing the tunability of the spacing between the injection-locked wavelength and cavity mode. In the measurement, injection ratio is fixed at 16 dB and frequency detuning is changed from 7.5 GHz (Figure 2-11(a)) to 38 GHz (Figure 2-11(b)). When the master laser is injected more into the positive frequency detuning edge (i.e., shorter wavelength side), spacing between the injection-locked and cavity modes are increased from 36 GHz (Figure 2-11(a)) to 71 GHz (Figure 2-11(b)). By adjusting the frequency detuning, tunable resonance frequency can be achieved.

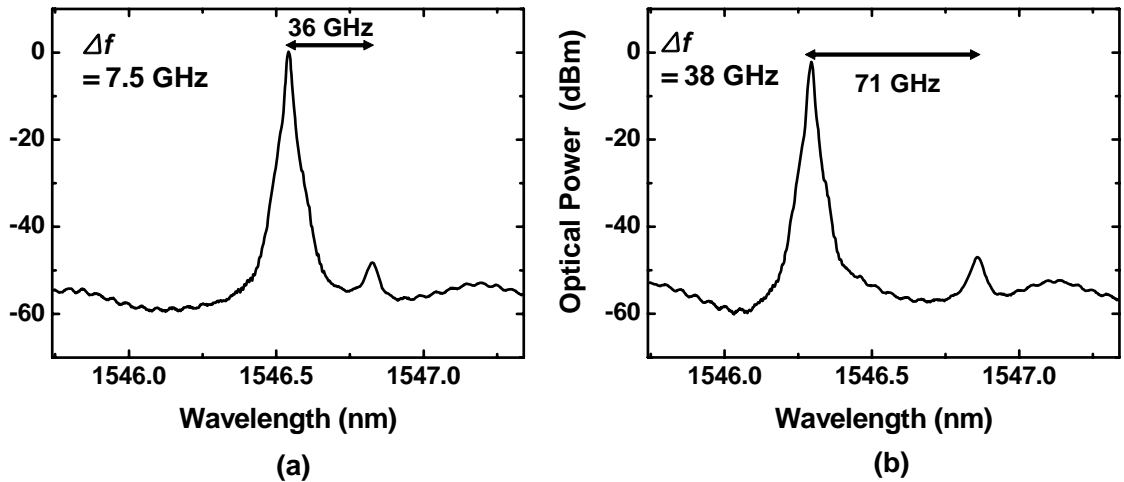


Figure 2-11. Measured optical spectra showing the tunability of cavity mode at an injection ratio of $R = 16$ dB. (a) $\Delta f = 7.5$ GHz (b) $\Delta f = 38$ GHz.

Two representative modulation responses are shown by optimizing the injection ratio and frequency detuning. One of the improvements allows us to obtain broad 3-dB bandwidth. Figure 2-12 shows the frequency response of an injection-locked laser with injection ratio of 18 dB and frequency detuning of -22 GHz. The 3-dB bandwidth is 33 GHz, which is four times higher than the free-running bandwidth. To achieve enhanced resonance frequency, the injection ratio and frequency detuning are tuned to 16 dB and +8 GHz, respectively. A high resonance frequency of 31 GHz with enhanced modulation efficiency of 13 dB is observed as shown in Figure 2-13. These results illustrate that strong optical injection locking can be optimized for different applications.

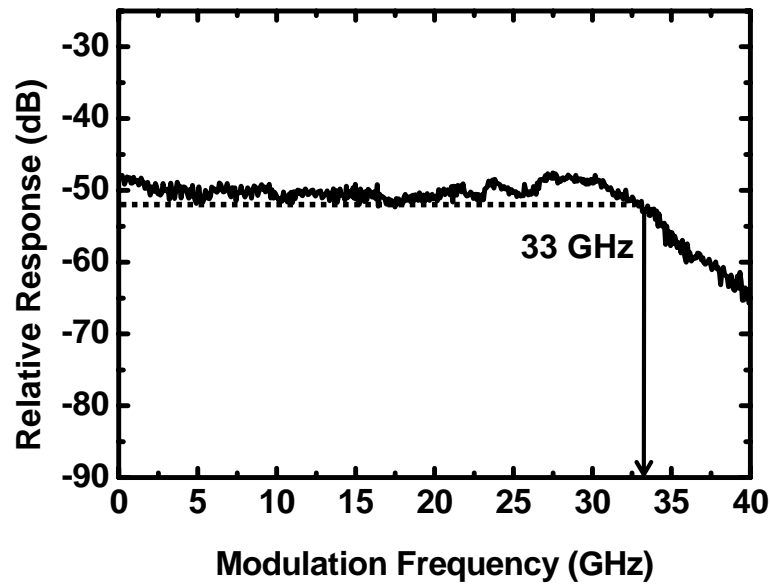


Figure 2-12. Experimental results showing broadband response. The injection ratio R is set at 18 dB.

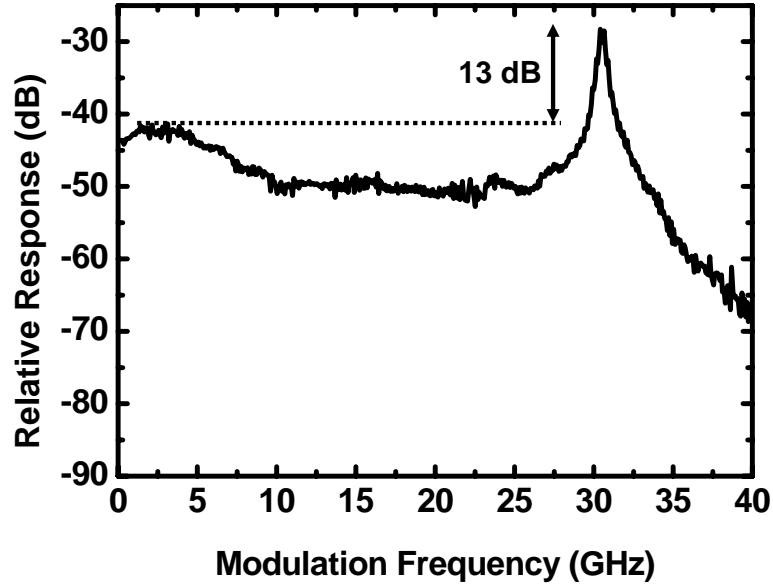


Figure 2-13. Experimental results showing a high resonance frequency with a narrowband enhancement of RF response of 13 dB.

2.6 Summary

We experimentally investigated the optical properties and electrical modulation characteristics of ultra-strong ($R \sim 10$ dB) injection-locked DFB lasers. Measured frequency responses exhibit three distinctive modulation characteristics, depending on the frequency detuning values.

In the large negative detuning regime, the optical spectrum shows a single mode spectrum with high SMSR. The frequency response shows enhanced modulation efficiency in low frequency. Broad 3-dB bandwidth has been demonstrated when the frequency detuning is set around the center of the locking regime. A flat modulation response has been attained by compensating laser parasitics-limited response with the resonance of the cavity mode. At the edge of the positive detuning regime, the frequency

response exhibits a pronounced resonance peak at high frequency (> 30 GHz). The optical spectrum showed both the injection-locked frequency and cavity mode. The resonance frequency is equal to the difference between the locked and the cavity mode frequencies.

These experimental results agree well with the calculation using coupled rate equations. By optimizing ultra-strong injection locking conditions, we have experimentally demonstrated broad 3-dB bandwidth of 33 GHz and a resonance frequency of 31 GHz with a narrowband RF enhancement of 13 dB. The distinctive optical properties and modulation performances can be exploited in various applications such as analog fiber optic links, broadband digital communications, RF photonics and opto-electronic oscillators.

Chapter 3 Optical Single Sideband Generation Using Strong Optical Injection-Locked Semiconductor Lasers

3.1 Asymmetric Modulation Sidebands in Strong Optical Injection-Locked Lasers

A novel single sideband (SSB) modulation technique is demonstrated using direct modulation of strong injection-locked semiconductor lasers. Under certain frequency detuning conditions, we have found that, in addition to enhancement of resonance frequency and reduction of chirp, the lower frequency (i.e., longer wavelength) sideband is enhanced, resulting in a 12-dB asymmetry for 20-GHz RF modulation sidebands. This is due to the resonant amplification of the modulation sideband on the longer wavelength side by the cavity mode [36, 41]. The amount of the asymmetry depends on the frequency detuning, Δf . We have measured the RF performance of the free-running and injection-locked link over 80-km fibers. The dispersion-limited RF bandwidth has been increased by this SSB scheme.

3.2 Principles and Experimental Results

Figure 3-1 illustrates the concept of the optical SSB generation by direct modulation of strong optical injection-locked semiconductor lasers. Strong injection-locked lasers tuned in certain locking regime - typically tuned towards positive frequency detuning - exhibit both an injection-locked frequency f_{inj} and a residual cavity mode f_c , as shown in Figure 3-1(b) [36, 40].

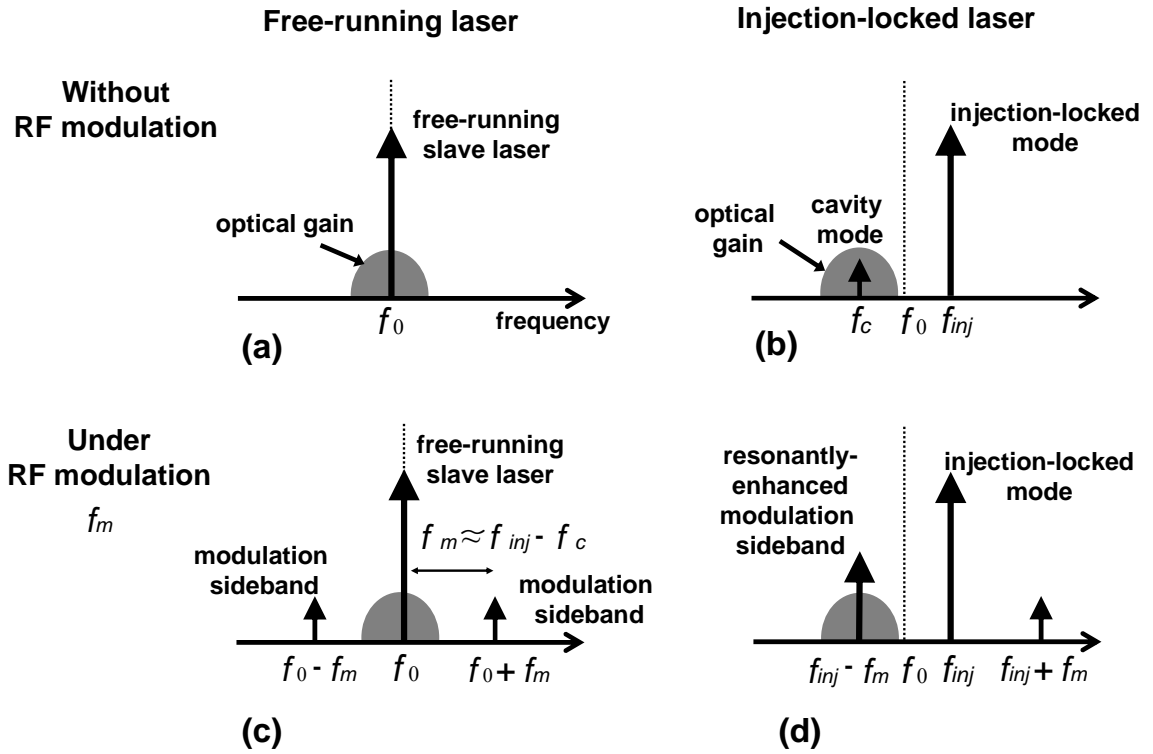


Figure 3-1. Optical spectra illustrating optical single sideband generation in directly-modulated semiconductor lasers with strong optical injection locking. (a) Optical spectrum of a free-running laser without RF modulation. (b) Optical spectrum of an injection-locked laser without RF modulation. (c) Optical spectrum of a free-running laser modulated by RF signal, f_m . (d) Optical spectrum of an injection-locked laser modulated by RF signal, f_m .

Directly-modulated free-running lasers generate symmetric modulation sidebands on both upper and lower sides of an optical carrier f_0 regardless of modulation frequency (Figure 3-1(c)). However, when the injection-locked laser is modulated by RF signals at f_m close to the frequency difference between the injection-locked and cavity mode frequencies ($f_m \approx f_{inj} - f_c$), the modulation sidebands become asymmetric because the lower modulation sideband (= longer wavelength) is resonantly amplified by the cavity mode. The asymmetry can be optimized by fine-tuning injection locking parameters.

Figure 3-2 shows the experimental setup to demonstrate the optical SSB generation using the strong injection-locked DFB lasers. To demonstrate transmission performance, an 80-km-long optical fiber with negative dispersion (Corning MetroCor, $D \sim -8$ ps/km/nm) is added to the link. To compensate for the loss of the fiber link, the transmitted signal is amplified by an EDFA. The transmission performance will be presented in Section 3.4. Figure 3-3 shows the measured optical spectra of the strong injection-locked DFB laser with various frequency detuning values. The laser is modulated at $f_m = 15$ GHz. The injection ratio is kept constant at 11 dB. In the unlocked state (Figure 3-3(a)), both wavelengths from the slave and the master laser exist. The modulation sidebands of the slave laser are symmetric. When the master laser wavelength is tuned to the edge of the negative frequency detuning regime (Figure 3-3(b)), only one optical carrier at the master laser's wavelength exists. Modulation sidebands are still symmetric. Finally, the injection-locked laser tuned towards positive frequency detuning shows asymmetric modulation sidebands (Figure 3-3(c) and (d)). The longer wavelength sideband is resonantly amplified. The asymmetry can be maximized by optimizing frequency detuning as shown in Figure 3-3(d).

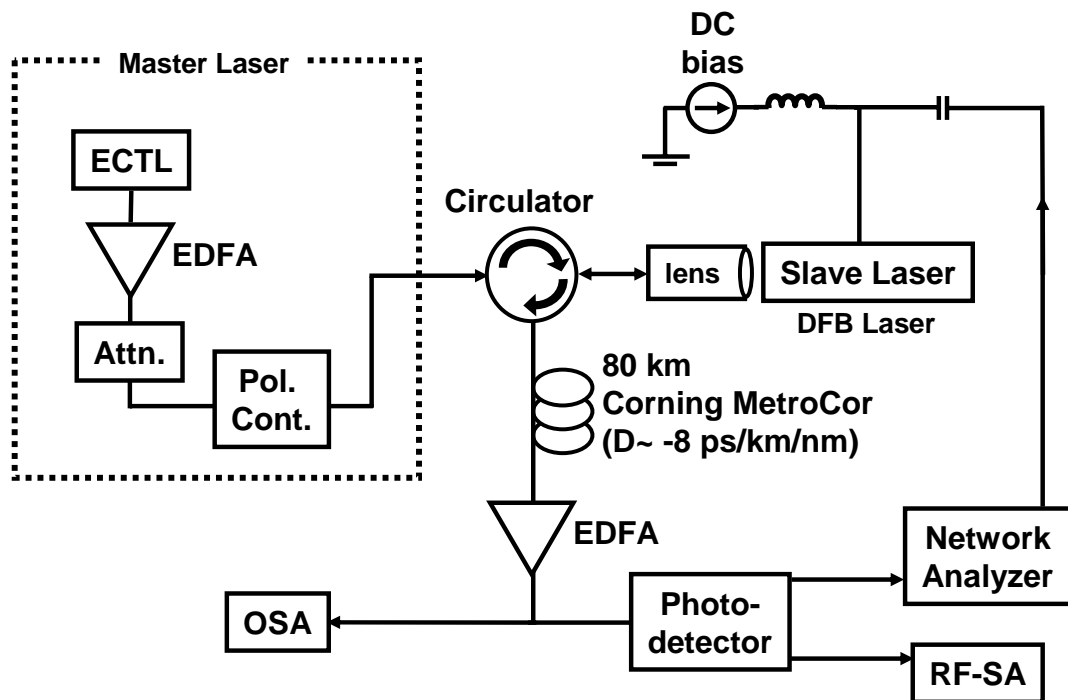


Figure 3-2. Experimental setup for optical single sideband generation. (ECTL: external cavity tunable laser; EDFA: Erbium-doped fiber laser; Attn.: optical attenuator; Pol. cont.: polarization controller; OSA: optical spectrum analyzer; RF-SA; RF spectrum analyzer)

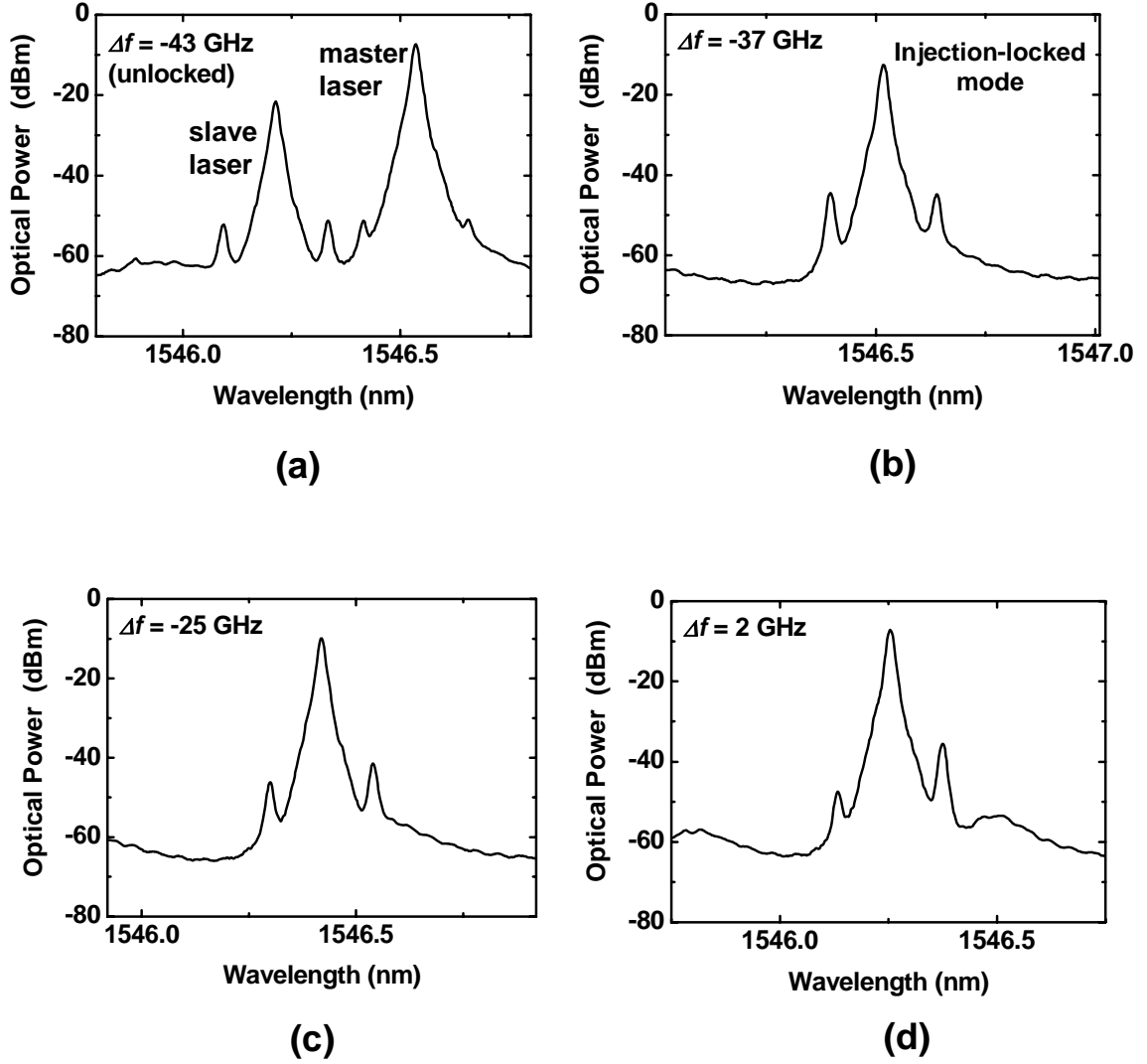


Figure 3-3. Measured optical spectra showing asymmetry between modulation sidebands in injection-locked DFB lasers. (a) $\Delta f = -43$ GHz (b) $\Delta f = -37$ GHz (locked) (c) $\Delta f = -25$ GHz (locked) (d) $\Delta f = 2$ GHz (locked). The injection ratio R is fixed at 11 dB and the RF-modulation frequency f_m is 15 GHz. Injection-locked lasers operating with positive detuning side exhibits pronounced asymmetry as shown in (d).

Figure 3-4 shows the measured optical spectra of the RF-modulated slave laser ($f_m = 20$ GHz) under (a) free-running, and (b) injection locking with -8.2 GHz and (c) -38 GHz detuning. As shown in Figure 3-4 (b), the asymmetry is maximized when Δf is set at -8.2 GHz. Figure 3-5 shows the corresponding frequency responses. The relaxation oscillation frequency of the free-running laser is approximately 3 GHz. When the laser is injection-locked, the enhancement or damping of the new resonance frequency is observed. For $\Delta f = -8.2$ GHz, the injection-locked laser shows the enhanced resonance frequency (> 20 GHz) beyond the measurable range of our equipment at that time. The injection-locked laser shows highly-damped frequency response for $\Delta f = -38$ GHz. The phenomena are explained by the cavity resonance in Chapter 2.

The amount of asymmetry is controllable by varying frequency detuning, Δf , as shown in Figure 3-6. The asymmetry is maximized when Δf is set around -10 GHz, at which the spacing between injection-locked and cavity mode frequencies is tuned to the modulation frequency f_m ($= 20$ GHz). When the detuning value is set to the negative detuning edge ($\Delta f = -40$ GHz), the optical power difference ($= P_{lower} - P_{upper}$) becomes negligible, showing symmetric modulation sidebands. This characteristic results from the evolution of the cavity mode across the locking range as discussed in Chapter 2. Figure 3-7 shows the measured asymmetry between a lower and upper sideband as a function of modulation frequency. The locking conditions are fixed at $\Delta f = -8.2$ GHz and $R = 11$ dB. The asymmetry is maximized when the injection-locked laser is modulated by an RF signal at 22 GHz because the injection-locked and cavity mode frequencies are spaced by that amount.

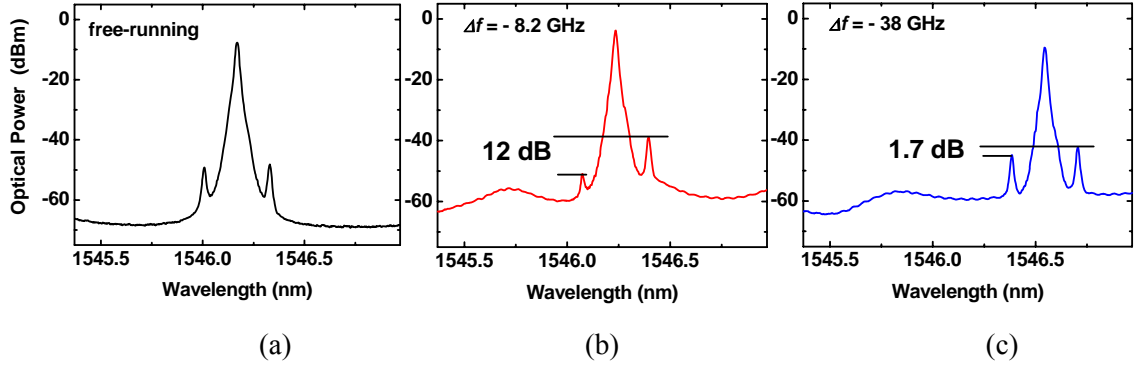


Figure 3-4. Measured optical spectra of RF-modulated slave laser ($f_m = 20$ GHz) under various conditions. (a) free-running; (b) injection locking with $\Delta f = -8.2$ GHz; and (c) injection locking with $\Delta f = -38$ GHz.

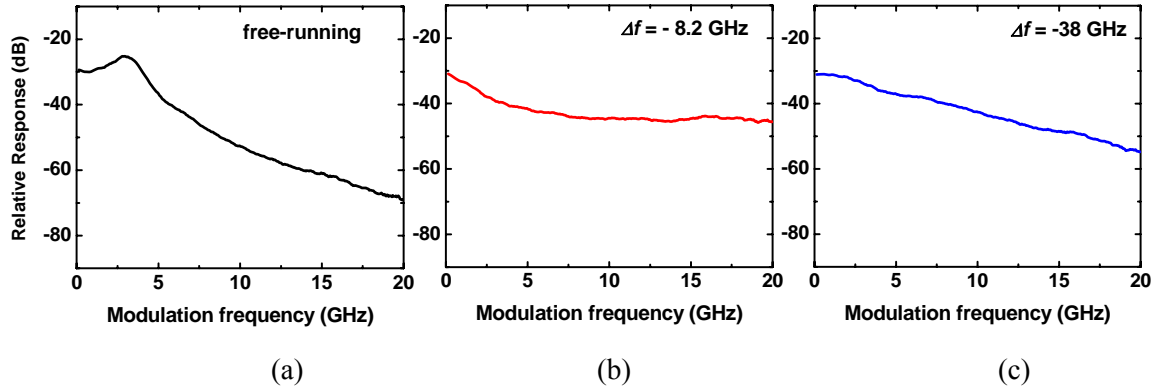


Figure 3-5. Measured frequency response of the slave laser under various conditions. (a) free-running; (b) injection locking with $\Delta f = -8.2$ GHz; and (c) injection locking with $\Delta f = -38$ GHz.

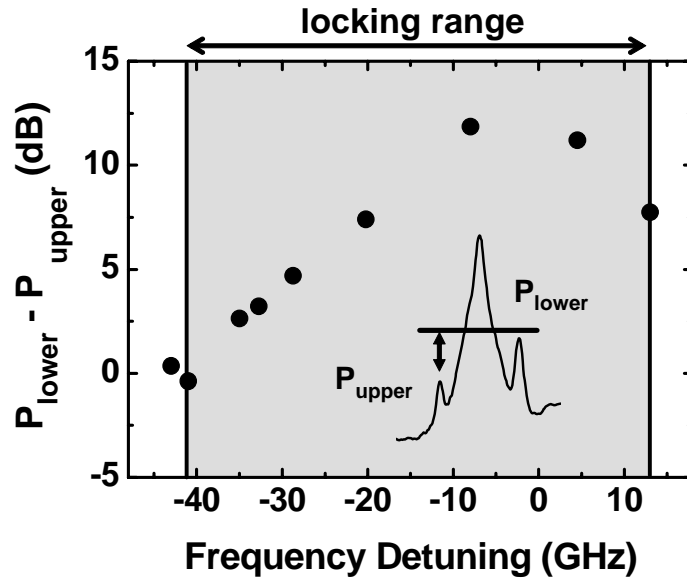


Figure 3-6. Measured optical power difference between lower and upper sideband versus frequency detuning with fixed modulation frequency at 20 GHz.

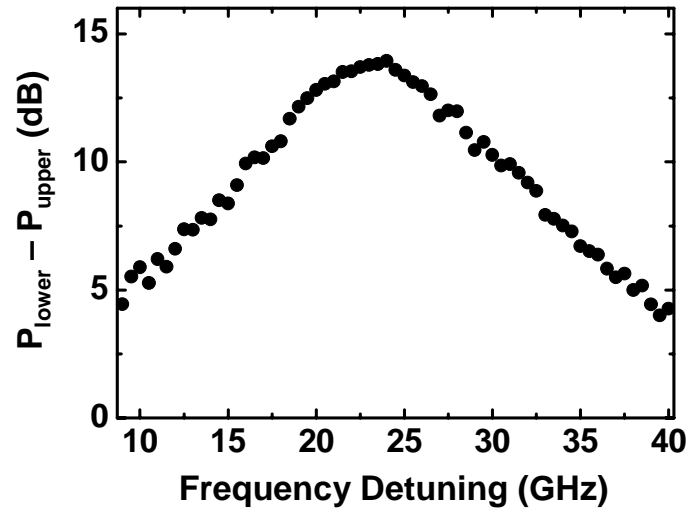


Figure 3-7. Measured optical power difference between lower and upper modulation sidebands versus modulation frequency with a fixed frequency detuning $\Delta f = -8.2$ GHz and injection ratio $R \sim 11$ dB.

3.3 Fiber Chromatic Dispersion Effect on Modulation Sidebands

The RF link performance is degraded by fiber chromatic dispersion when the signal travels through optical fibers. Standard modulation generates two symmetric signal sidebands at both sides of the optical carrier. The dispersion in fibers causes a walk-off in the phases of the sidebands, resulting in distance- and frequency-dependent attenuation of the RF signals [87, 88]. This imposes a limit on the product of RF carrier frequency and fiber transmission distance, as shown in Figure 3-8. We can express the detected RF power from an optical field transmitted through optical fibers. Only two modulation sidebands are considered for simplicity, which is a good approximation for small modulation index ($m_+ < 0.5$ and $m_- < 0.5$) [89].

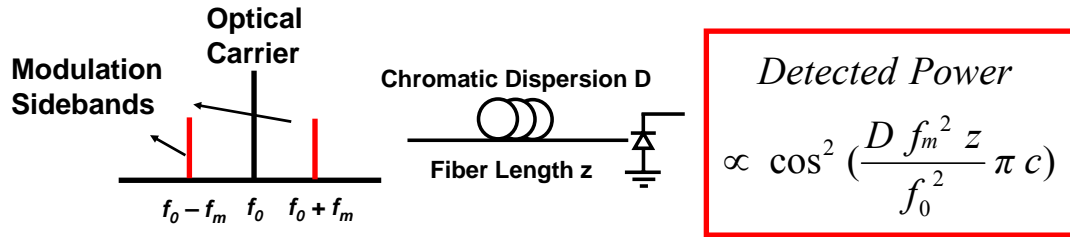


Figure 3-8. Fiber chromatic dispersion effect on RF signal transmission.

Neglecting fiber transmission loss, the optical field incident on a photodetector can be expressed by

$$E \cong E_0 \left[\cos(\omega_0 t - \beta_0 z) + \frac{m_+}{2} \left[\cos((\omega_0 + \omega_m)t - \beta + z) \right] + \frac{m_-}{2} \left[\cos((\omega_0 - \omega_m)t - \beta - z) \right] \right] \quad (3.1)$$

where ω_0 is the angular frequency of the optical carrier ($= 2\pi f_0$), ω_m is the angular frequency of RF modulation signal ($= 2\pi f_m$), m_+ and m_- are the modulation indices for the upper and the lower sidebands, respectively. β_0 , β_+ and β_- are the propagation constants at the corresponding frequencies. They can be described as functions of angular frequency:

$$\beta(\omega) = \beta_0 + \beta_1(\omega - \omega_0) + \frac{1}{2}\beta_2(\omega - \omega_0)^2 + \dots \quad (3.2)$$

where β_0 is the constant phase. β_1 and β_2 are the first and second derivative of the propagation constant, respectively. Other higher order terms are neglected. Fiber dispersion parameter D is related to the second derivative of the propagation constant. By using $\omega = 2\pi c / \lambda$, fiber dispersion parameter D can be expressed as

$$D = -\frac{2\pi c}{\lambda^2} \cdot \beta_2 \quad (3.3)$$

where λ is the carrier wavelength. Because the photodetector is a square law device, the output current of the photodetector can be expressed as

$$i = E \cdot E^* \propto \sqrt{\cos^2 \theta \left(\frac{m_+}{2} + \frac{m_-}{2}\right) + \sin^2 \theta \left(\frac{m_+}{2} - \frac{m_-}{2}\right)} \quad (3.4)$$

where $\theta = \beta_2 \omega_m^2 z / 2$. For symmetric sidebands ($m_+ = m_-$), (3.4) becomes the general expression describing the fiber chromatic dispersion effect on symmetric modulation sidebands.

$$i = E \cdot E^* \propto \cos \theta = \cos\left(\frac{1}{2}\beta_2 \omega_m^2 z\right) = \cos\left(\frac{D \lambda^2 f_m^2 \pi z}{c}\right) \quad (3.5)$$

Figure 3-9 and Figure 3-10 show the calculated RF power versus fiber transmission length and modulation frequency, respectively. The interference between the sidebands results in a frequency and fiber length dependent loss as described in (3.5). By introducing an asymmetry of 10 dB between the modulation sidebands, the power penalty

can be greatly alleviated as shown in Figure 3-11.

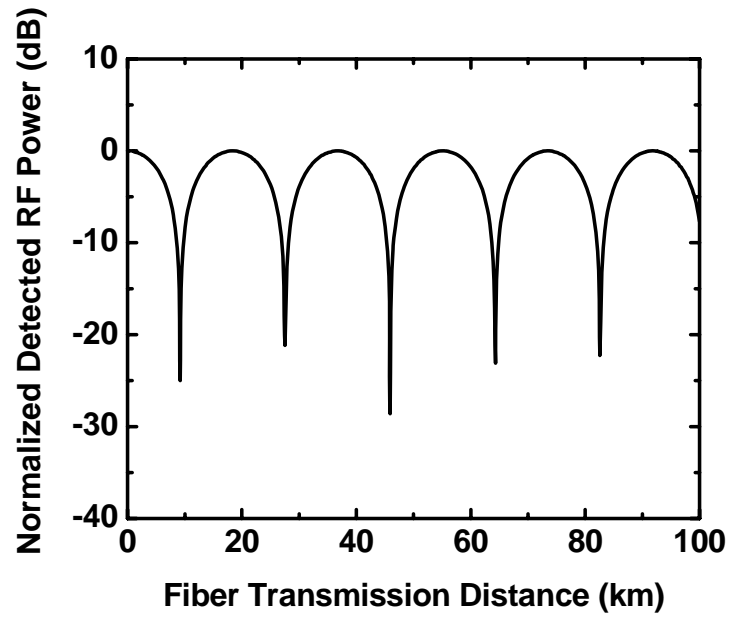


Figure 3-9. Calculated RF power versus fiber transmission distance for symmetric modulation sidebands.

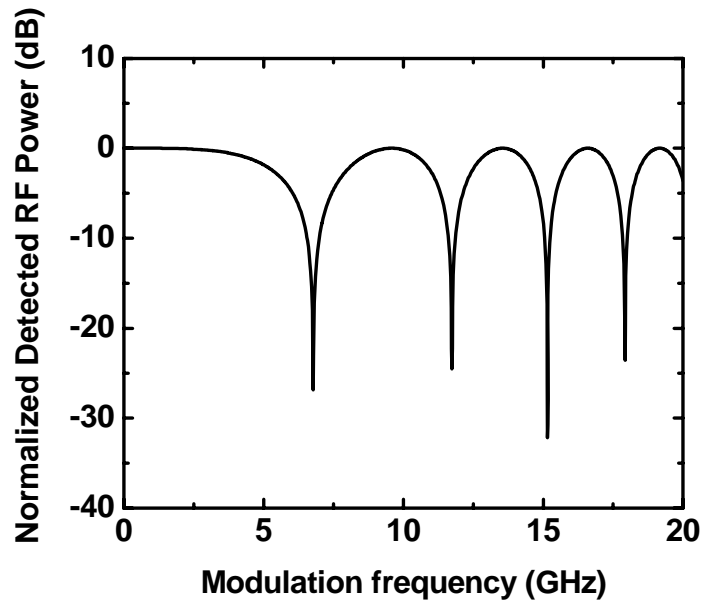


Figure 3-10. Calculated RF power versus modulation frequency for symmetric modulation sidebands.

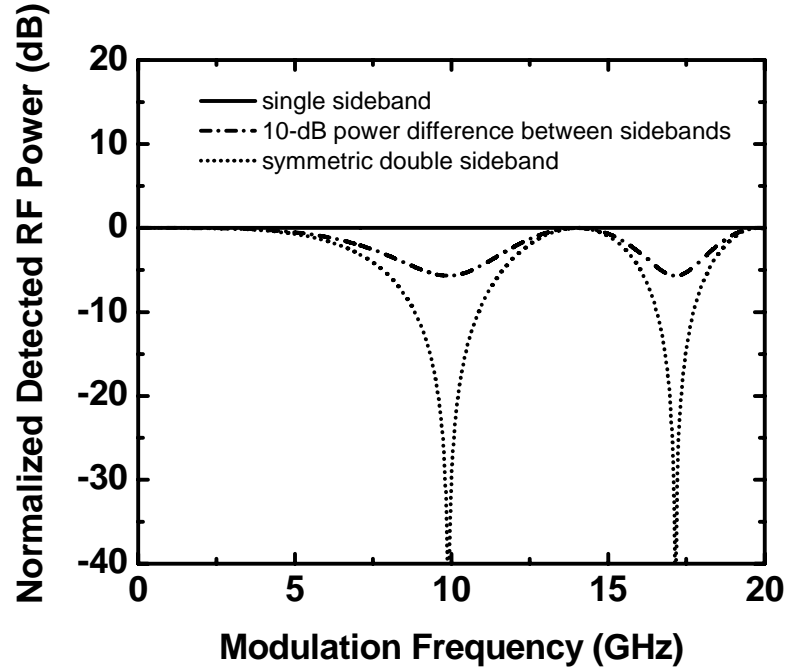


Figure 3-11. RF power versus modulation frequency for various power differences between sidebands.

3.4 Fiber Transmission Measurements

The SSB fiber transmission response is experimentally measured and normalized to the back-to-back frequency response of the laser using the setup shown in Figure 3-1. Figure 3-12 shows the measured optical spectrum under RF modulation ($f_m = 20$ GHz) for the injection-locked laser with a frequency detuning $\Delta f = -8.2$ GHz and an injection ratio $R \sim 11$ dB. Modulation sidebands show a 12-dB asymmetry, as compared to the symmetric modulation sidebands for the free-running laser as shown in the inset.

Figure 3-13 shows the measured transmission response through 80-km of negative dispersion fibers. In the free-running state, the fiber transmission response shows

pronounced dips of up to 27 dB at 13 and 19 GHz. The dips are due to the interference between the symmetric sidebands. The increase of the response in the low frequency range is due to the laser chirping combined with the fiber chromatic dispersion [87, 90]. The RF power variation has been reduced to 7 dB from DC to 20 GHz for the injection-locked laser. It is interesting to note that the low frequency hump is also suppressed due to chirp reduction.

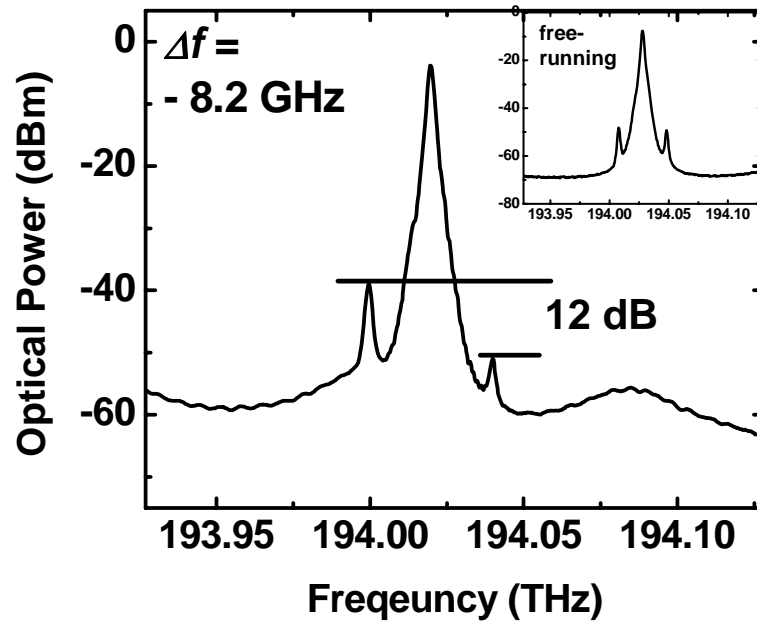


Figure 3-12. Measured optical spectrum of RF-modulated injection-locked laser ($f_m = 20$ GHz).

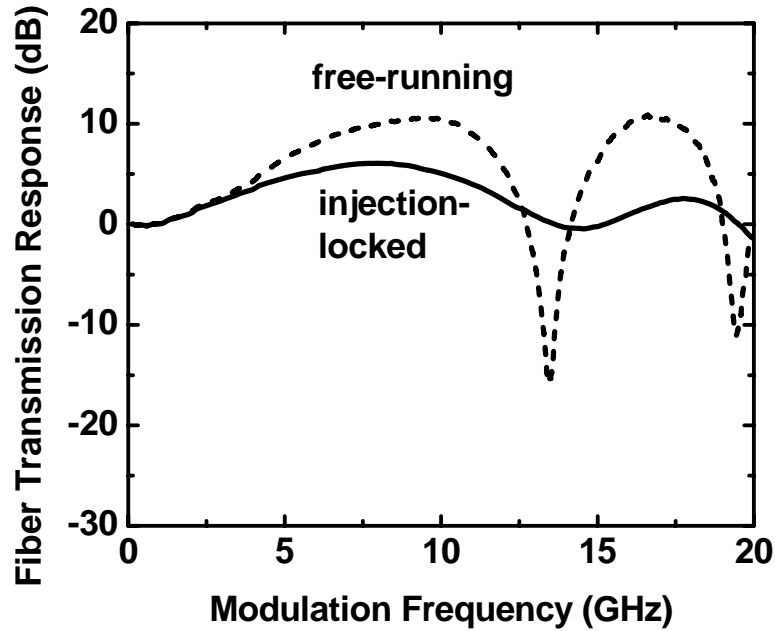


Figure 3-13. Measured fiber transmission response for a free-running laser and injection-locked laser.

3.5 Summary

Optical single sideband generation using strong optical injection-locked lasers has been demonstrated. The asymmetric modulation sidebands are achieved by utilizing the resonantly-amplified modulation sideband in strong injection-locked lasers. The asymmetry is controllable and depends on the frequency detuning of injection-locked lasers. By increasing the asymmetry and generating near-single sideband, the dispersion-limited power penalty of directly-modulated link has been greatly reduced across a 20-GHz band after 80-km transmission, a 20-dB improvement over the free-running laser.

Chapter 4 Optically Injection-Locked Gain-Lever Distributed Bragg Reflector (DBR) Lasers with Enhanced RF Performances

4.1 Fiber-Optic Link Gain Improvement

Low RF link loss and small nonlinear distortions are needed to achieve good analog performance. Unlike externally modulated links, the link loss of directly-modulated links is independent of the optical power. Rather, it is proportional to the square of the electrical-to-optical (E/O) conversion efficiency. This results in high link loss for most directly-modulated links. Several approaches have been proposed to increase the modulation efficiency of semiconductor lasers, including gain-lever modulation [91-93] and cascade lasers [94-96]. Narrowband techniques such as resonant modulation are outside the scope of this Chapter. Cascade lasers achieve higher efficiency by recycling the RF modulating current through multiple lasers that are connected in series. It was first proposed using discrete lasers [94], as shown in Figure 4-1.

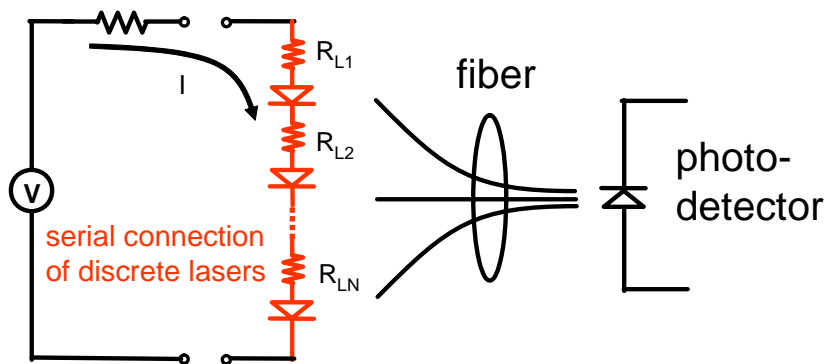


Figure 4-1. Schematic of link gain improvement by series-connected lasers, after [94].

Using the serial connection of six discrete lasers, positive link gain of 3.78 dB was demonstrated. However, the measured link bandwidth was about 60 MHz, while the 3-dB bandwidth of the individual lasers is greater than 3 GHz. This is due to the parasitics of the series connected lasers. To overcome the limitation and achieve a bandwidth closer to the individual components, monolithically integrated versions were proposed using surface-emitting lasers [95] (Figure 4-2(a)) and edge-emitting lasers [96] (Figure 4-2(b)). Improved link performances has been demonstrated exhibiting $> 100\%$ differential efficiency and an SFDR of $120 \text{ dB} \cdot \text{Hz}^{2/3}$ operating at 500 MHz [96].

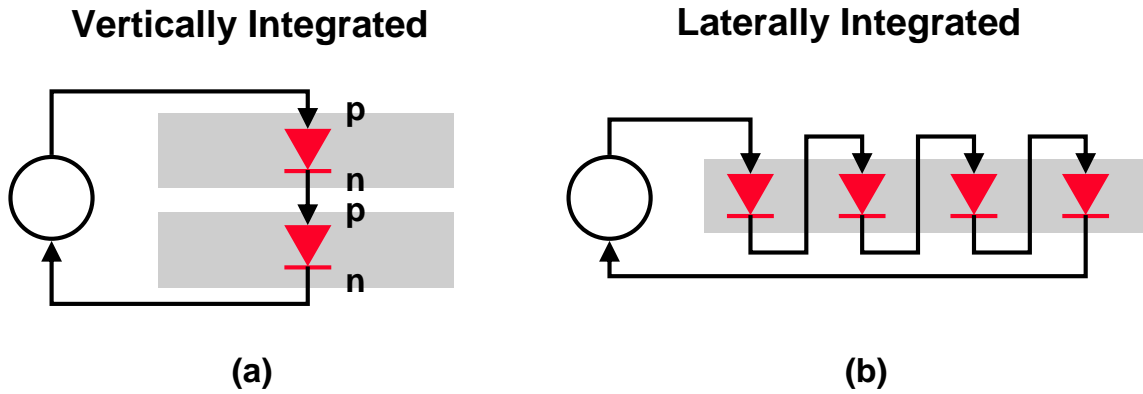


Figure 4-2. Monolithic versions of cascaded lasers (a) vertically integrated (b) laterally integrated

4.2 Gain-Lever Modulation Combined with Optical Injection Locking

Among the techniques discussed, the gain-lever lasers are simple structurally and directly compatible with standard fabrication process of conventional lasers. The gain-lever lasers take advantage of the nonlinear gain-versus-current characteristics in quantum-well gain media. Figure 4-3 illustrates the principle of gain-lever modulation.

The modulation efficiency is increased by modulating one of the two-gain section, which is biased at a higher slope of the gain profile while maintaining a constant total gain [91]. GaAlAs/GaAs single quantum well (QW) [91, 92] and InGaAsP/InP multiple QW [93] gain-lever lasers have been demonstrated. Unfortunately, the improved amplitude modulation (AM) efficiency is obtained at the expense of linearity. Furthermore, the previous gain-lever devices were Fabry-Perot (F-P) lasers operating in multiple longitudinal modes, and are not suitable for practical system applications.

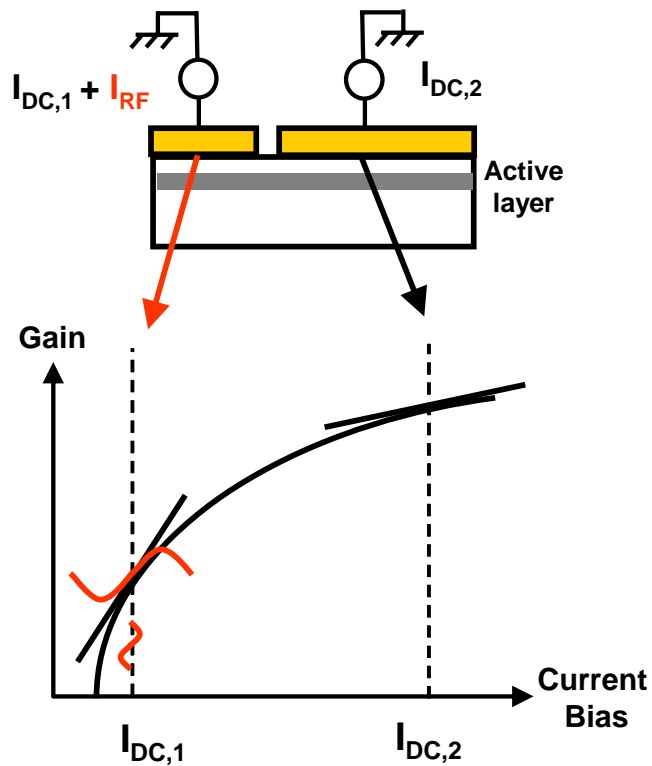


Figure 4-3. Gain-lever effect in semiconductor lasers.

In this chapter, the optical injection locking is combined with gain-lever modulation to simultaneously enhance AM efficiency, increase bandwidth, and suppress nonlinear distortions. Figure 4-4 illustrates the advantages of this approach. We use distributed Bragg reflector (DBR) lasers with two gain as well as a phase and a grating sections to achieve single mode operation with a sidemode suppression ratio of > 35 dB. With optical injection locking, a 10-dB increase in AM efficiency and a 15-dB suppression of third-order intermodulation distortions (IMD3) have been demonstrated, in addition to increased modulation bandwidth.

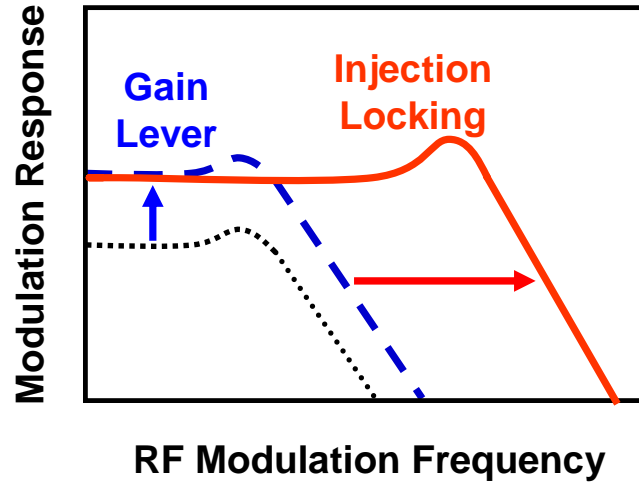


Figure 4-4. Benefits of injection-locked gain-lever lasers in terms of modulation response.

4.3 Device Fabrication: Gain-Lever DBR Lasers

The gain-lever DBR laser consists of four sections; a grating, a phase, and two-electrically isolated gain sections. The grating and phase sections are designed to achieve coarse and fine wavelength tuning with single-mode operation. Various split ratios, defined as the length of the small section divided by the total length, between the gain sections are used to investigate the optimum gain-lever geometry. The laser is realized in

a capped mesa buried heterostructure (CMBH). Figure 4-5(a) illustrates the cross-section structure, and Figure 4-5(b) shows the top-view of the fabricated gain-lever DBR laser. After epitaxial growth of the CMBH, a ridge of 3 ~ 4- μm height is formed to reduce parasitic capacitance. A 500-nm layer of silicon nitride passivates the surface. P-metal contacts for the grating, phase, and gain sections are formed using Ti/Pt/Au. The bottom n-contact comprises Au/Sn/Au. The contact resistance obtained was typically less than 10 Ω after annealing. A final isolation etch of 0.5- μm depth is performed to increase the electrical isolations among the different sections. The resistance between sections is greater than 4 k Ω .

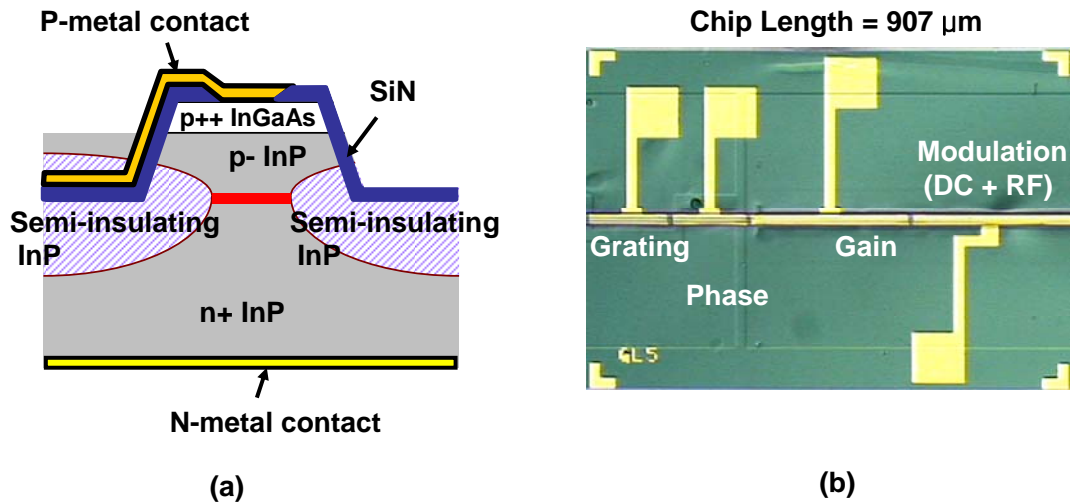


Figure 4-5. (a) Illustration of the cross-sectional structure (b) Top-view of a fabricated device.

4.4 Experimental Results

4.4.1 DC Performance of Gain-Lever DBR Lasers

Figure 4-6 shows the experimental setup for measuring the performance of the gain-lever DBR laser with optical injection locking. For all the measurements presented in this chapter, the gain-lever DBR laser with a split ratio of 0.5 is used. Figure 4-7 shows the measured optical spectra of the free-running gain-lever DBR laser. Wide wavelength tunability of 2.5 nm has been achieved by varying grating current with high SMSR of > 35 dB. Fine wavelength tuning is also achieved by modulating the phase section.

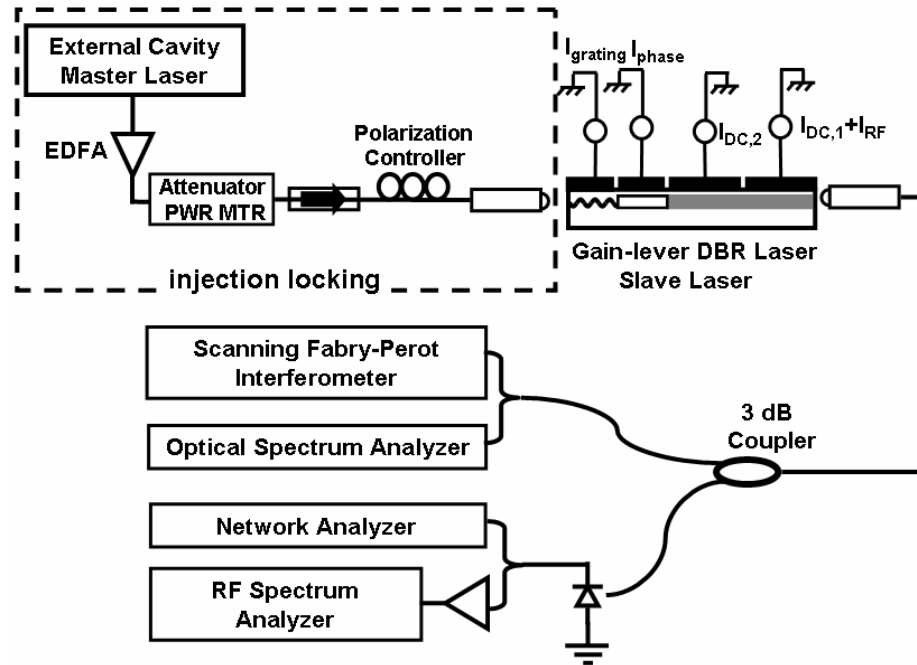


Figure 4-6. Experimental setup for measuring RF performances of an injection-locked gain-lever DBR laser.

The DC light-versus-current (L-I) curves are shown in Figure 4-8. The current I_2 (see Figure 4-6 for the definition of current symbols) is fixed at 50 or 25 mA while current I_1 is varied from 0 to 60 mA. As depicted in the shaded area in Figure 4-8, a three-fold increase of the quantum efficiency (equivalent to an RF efficiency increase of 9.5 dB) is achieved when the RF modulation section ($= I_1$) is biased at a low level (< 5 mA).

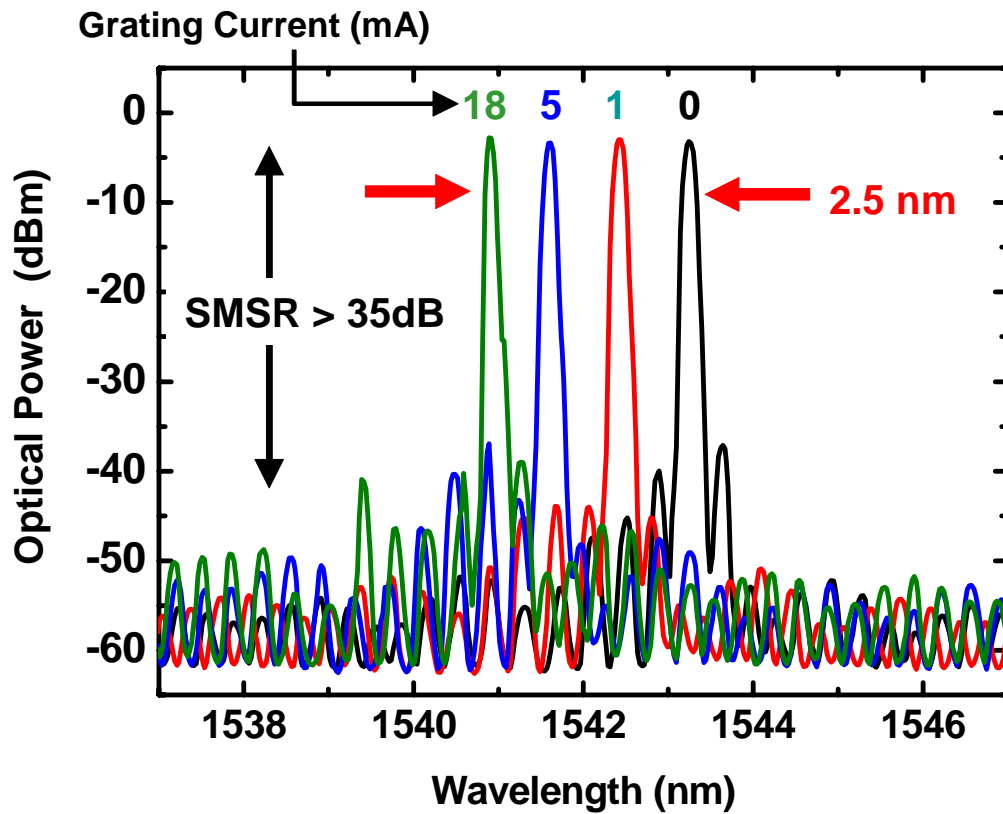


Figure 4-7. Wavelength tunability of a gain-lever DBR laser.

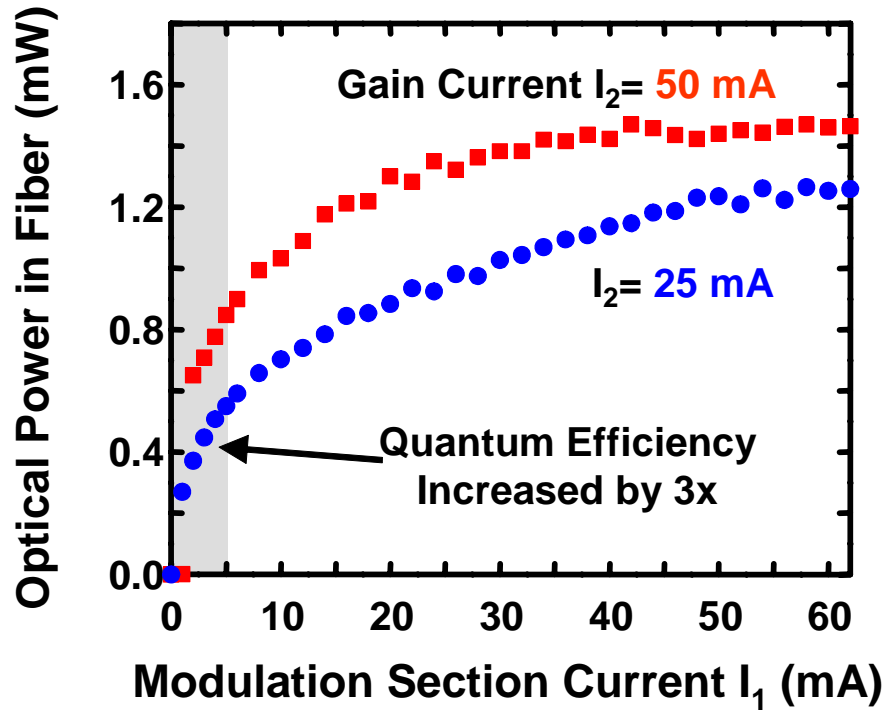


Figure 4-8. Measured L-I curves showing the effect of gain-lever modulation.

4.4.2 Modulation Performance of Gain-lever DBR Lasers

The modulation response of the gain-lever DBR laser with a split ratio of 0.5 is shown in Figure 4-9 for various bias currents. As the bias current on the modulation section ($= I_1$) decreases, the differential gain increases producing a higher modulation response. Compared with the uniformly biased condition ($I_1 = 25$ mA and $I_2 = 25$ mA), 9-dB improvement in modulation efficiency has been achieved by the gain-lever modulation ($I_1 = 4$ mA, $I_2 = 25$ mA). However, as a consequence of the low current bias necessary for gain-lever modulation, the modulation bandwidth decreases compared with the laser with uniform bias. The resonance frequency of the laser is decreased from 5 GHz to 3 GHz. To verify the dependence of the gain-lever effect on the location of the

modulation section, we also measured the frequency response with the RF signal applied to the other gain section (I_2). The measurement result is very similar to that of modulation I_1 (Figure 4-10).

Figure 4-11 is the measured RF spectra when I_1 is modulated by a 2-GHz RF signal. For the uniform bias ($I_1 = 50$ mA and $I_2 = 50$ mA) case, the second harmonic distortion (2HD) is measured at -24.1 dBc and the third harmonic distortion (3HD) is not observable. The received RF power at the fundamental tone (= 2 GHz) is increased by 11 dB when the laser operates in gain-lever mode ($I_1 = 4.5$ mA and $I_2 = 50$ mA). However, the 2HD is measured at -9.8 dBc and 3HD is -24 dBc, exhibiting an increase of 14 dB and > 24 dB, respectively.

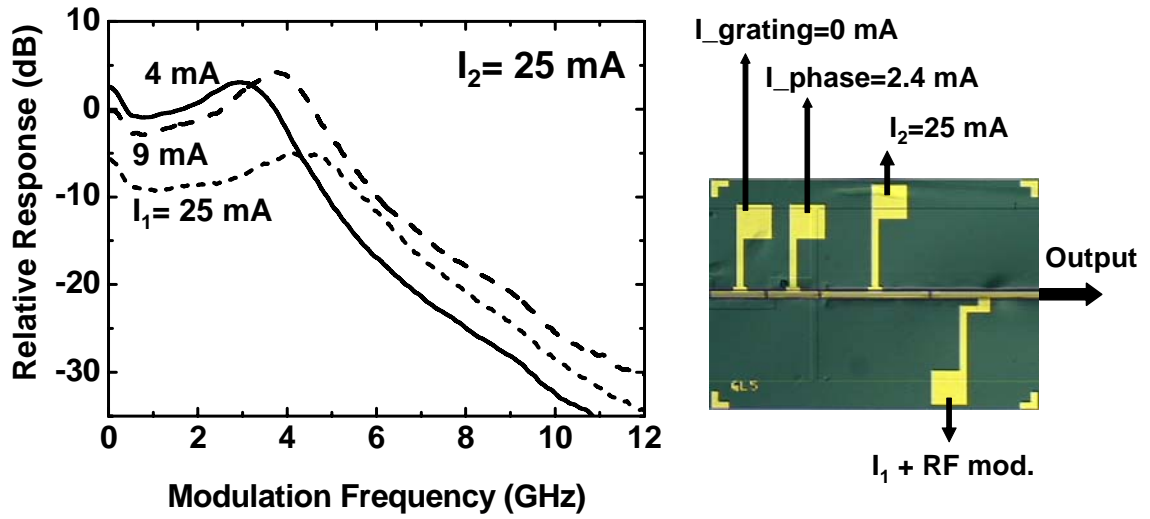


Figure 4-9. Measured modulation responses of the gain-lever DBR laser for various operating conditions. RF signal is applied to the section facing the output facet.

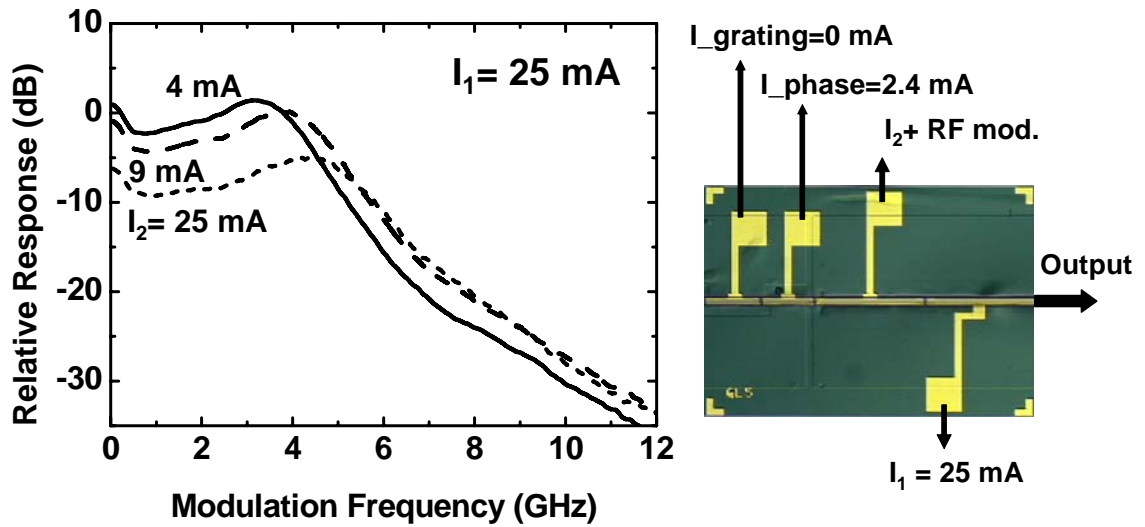


Figure 4-10. Measured modulation responses of the gain-lever DBR laser for various operating conditions. The RF signal is applied to the gain section adjacent to the phase section.

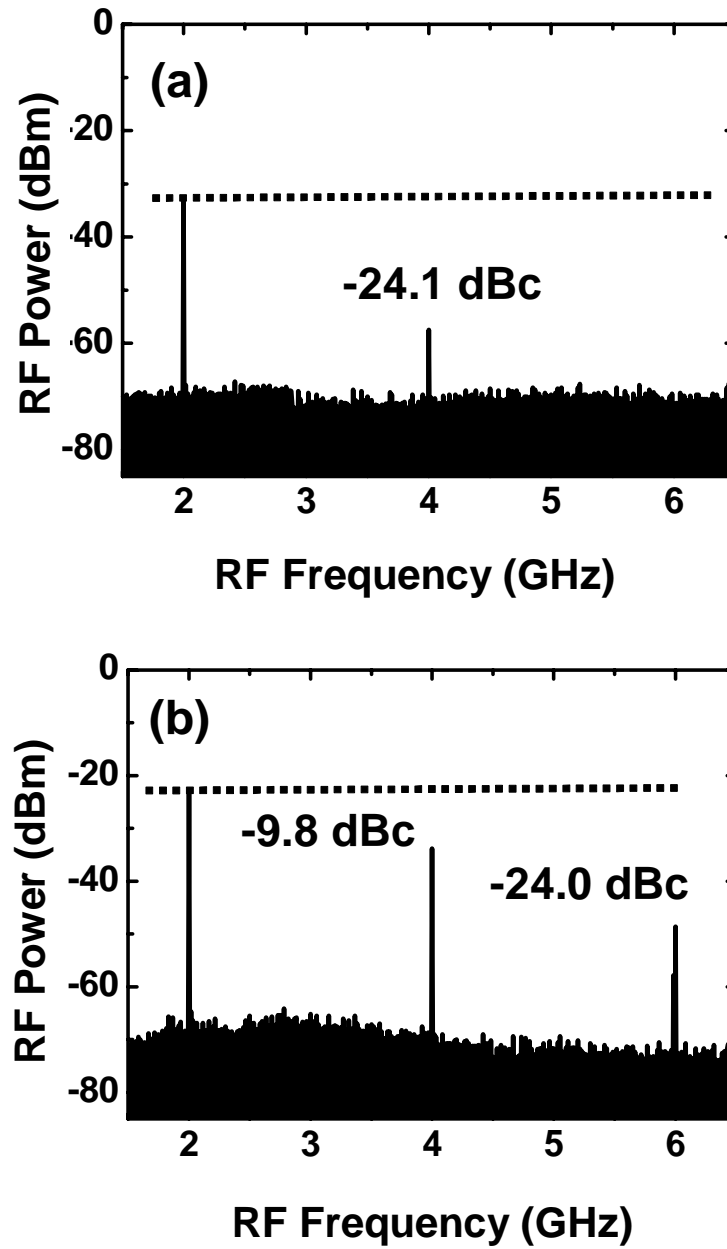


Figure 4-11. Measured RF spectra of directly-modulated gain-lever DBR laser: (a) $I_1 = 50$ mA, $I_2 = 50$ mA; (b) $I_1 = 4.5$ mA, $I_2 = 50$ mA. RF modulation frequency is 2 GHz.

4.4.3 Optical Injection Locking of Gain-Lever DBR Lasers

The linearity and modulation bandwidth of the gain-lever DBR laser can be improved by strong optical injection locking while maintaining the enhanced AM efficiency. Figure 4-12 shows the schematic of the directly-modulated gain-lever DBR lasers with optical injection locking.

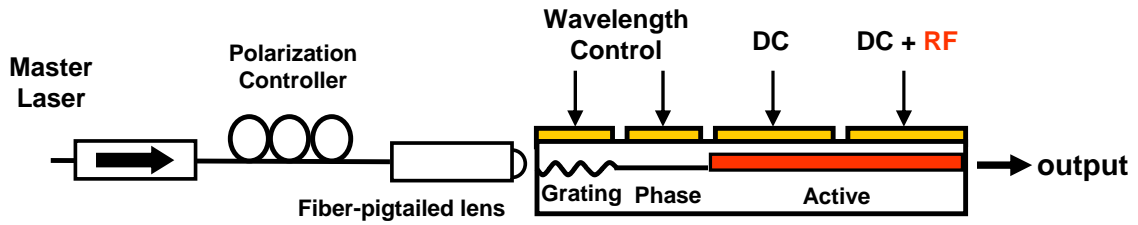


Figure 4-12. Schematic of optically injection-locked gain-lever DBR lasers.

The modulation bandwidth of the gain-lever DBR laser is measured using the setup in Figure 4-6. An external cavity laser is used as a master laser; the output of the master laser is amplified by an EDFA and attenuated with an inline power meter/attenuator before injecting into the gain-lever DBR laser. The output of the gain-lever DBR laser is monitored by an optical spectrum analyzer and a scanning F-P interferometer. The RF modulation performance, such as modulation response, RF link gain and SFDR, are measured by a network analyzer and an RF spectrum analyzer.

The frequency response of the gain-lever DBR laser is shown in Figure 4-13 for three operating conditions. First, in the free-running gain-lever state, the differential gain increases, resulting in a higher modulation response as the bias current on the modulation section decreases. Compared with uniform bias ($I_1 = 50$ mA, $I_2 = 50$ mA), the AM

efficiency is improved by ~ 12 dB at 2 GHz by gain-lever modulation ($I_1 = 4.5$ mA, $I_2 = 50$ mA). However, there is a trade off between modulation bandwidth and the AM efficiency. The resonance frequency of the laser decreases from 5 GHz to 3.6 GHz because of lower total current in gain-lever biasing. When the gain-lever DBR laser is injection-locked with a frequency detuning, Δf , of -20 GHz and an injection ratio R of -8 dB, the modulation bandwidth is increased to 7.8 GHz while maintaining the enhancement of the AM efficiency. The enhancement of AM efficiency is 10 dB around 2 GHz, and is greater than 7 dB from DC to 6 GHz.

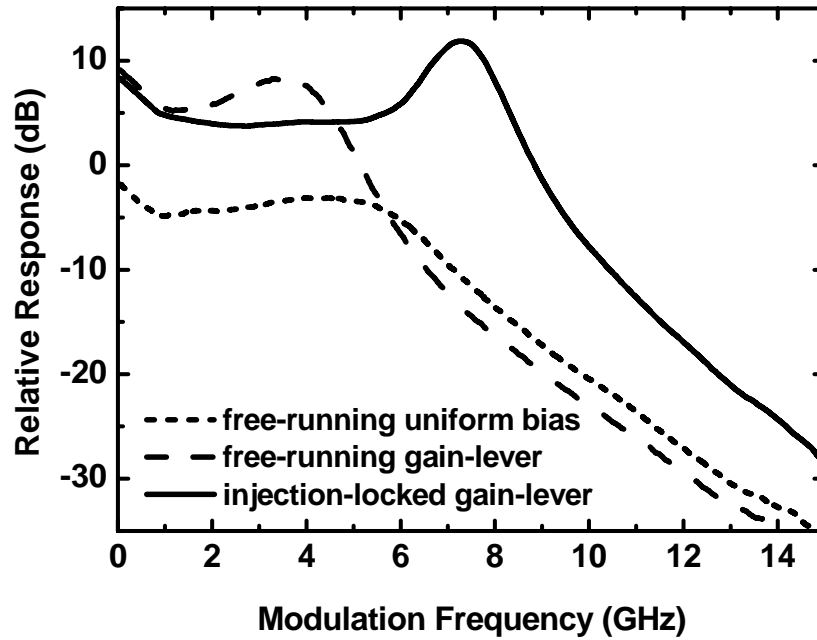


Figure 4-13. Measured frequency responses of a free-running and injection-locked gain-lever laser for various bias conditions. The bias currents for the free-running laser with uniform bias: $I_1 = 50$ mA, $I_2 = 50$ mA; free-running gain-lever state: $I_1 = 4.5$ mA, $I_2 = 50$ mA; injection-locked gain-lever state: $I_1 = 4.5$ mA, $I_2 = 50$ mA.

The frequency detuning controls both the height and the frequency of the resonance peak, as shown in Figure 4-14. Larger positive frequency detuning leads to high resonance frequency and sharp resonant peaks. This result is consistent with the works discussed in Chapter 2.

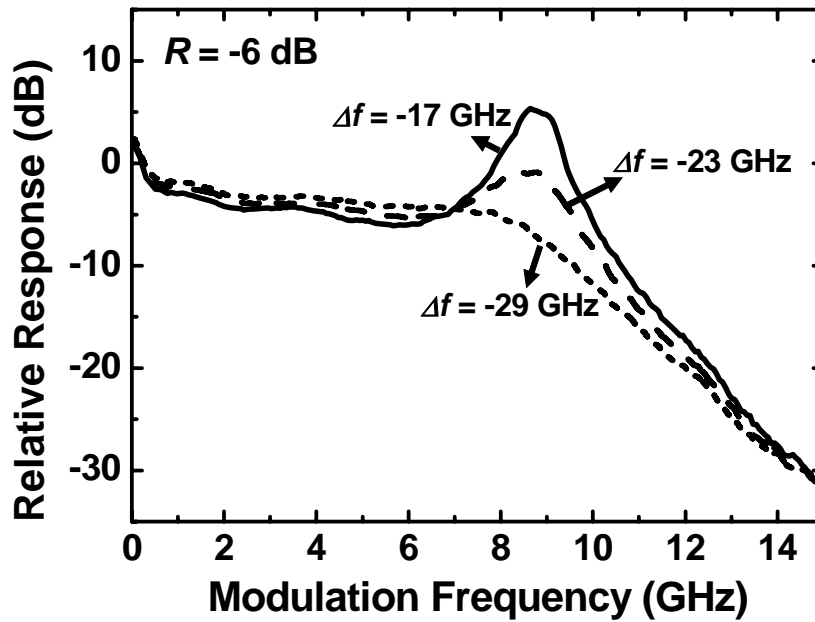


Figure 4-14. Measured frequency response of an injection-locked gain-lever DBR laser for various frequency detuning values. ($I_1 = 4.5$ mA, $I_2 = 25$ mA)

Injection-locked lasers also reduce relative intensity noise (RIN) as shown in Figure 4-15. RIN of the gain-lever DBR laser is measured by amplifying the output from a photodetector through a two-stage RF amplifier (gain = 60 dB). The noise from the photodetector is found to be limited by RIN of the laser, not by shot or thermal noise. This is confirmed by observing the relationship between the noise power detected in RF-SA and the optical power incident on the photodetector. When the optical power incident

on the photodetector was increased by 1 dB, the noise power detected in RF-SA increased by 2 dB. Therefore, the link that we investigate can be considered as RIN-limited. Figure 4-15 shows the measured RIN for the gain-lever DBR laser under the free-running gain-lever and injection-locked gain-lever states. The RIN of the free-running laser exhibits a peak at its relaxation oscillation frequency (≈ 3 GHz). When the gain-lever DBR laser is injection-locked, the RIN is reduced by 11 dB for both frequency detuning values of -8 GHz and -21 GHz. The RIN of the injection-locked laser operating in the larger negative detuning regime ($\Delta f = -21$ GHz) exhibits more reduction in the high frequency range (> 7 GHz) while the injection-locked laser at the detuning value of -8 GHz shows a RIN peak at 8.2 GHz. The RIN peak at 8.2 GHz originates from the resonance frequency of the injection-locked laser. Injection-locked laser at in the large negative detuning regime exhibits better performance in RIN reduction because its resonant peak is highly suppressed.

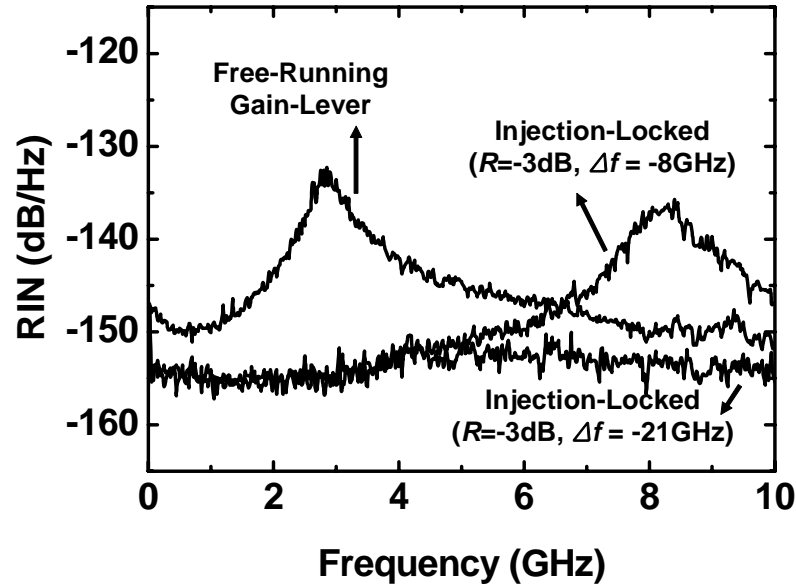


Figure 4-15. Measured RIN for a gain-lever DBR laser under free-running and injection-locked condition.

To measure the 2HD and 3HD, gain section 1 is modulated by a single-tone RF signal ($f = 2$ GHz). The second harmonic and third harmonic frequencies are at 4 GHz and 6 GHz, respectively. DC bias condition for the laser is set at $I_1 = 4.5$ mA and $I_2 = 50$ mA for both free-running and injection-locked cases. Injection locking parameters are $R = -8$ dB and $\Delta f = -20$ GHz. Figure 4-16 shows the measured RF spectra of the laser under gain-lever modulation with and without optical injection locking. For the free-running laser, the 2HD and 3HD are measured to be -9.8 and -24.0 dBc, respectively. With optical injection locking, the 2HD and 3HD are suppressed to -31.6 and -41.8 dBc, respectively.

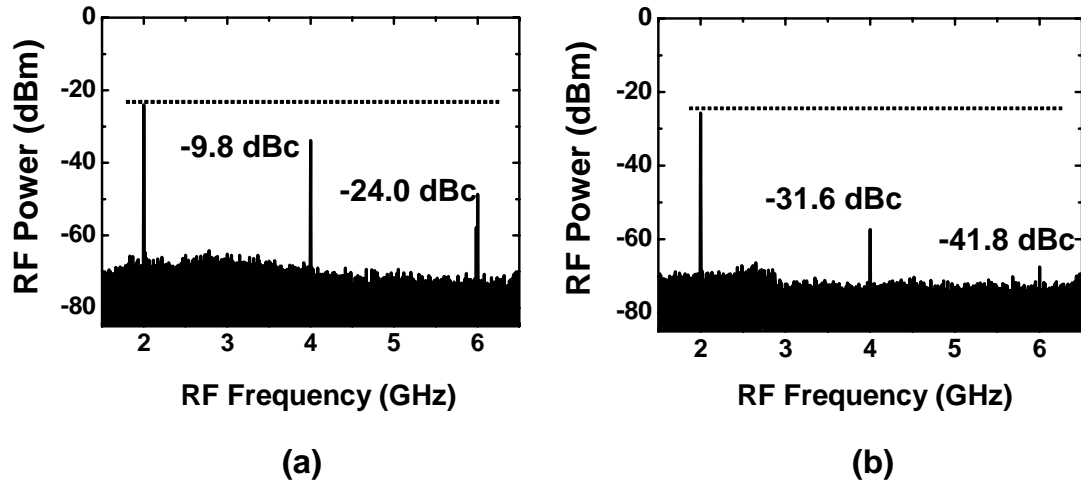


Figure 4-16. Measured RF spectra of a gain-lever DBR laser modulated by a single-tone 2-GHz RF signal for a (a) free-running gain-lever and (b) injection-locked gain-lever laser.

The measured 2HD as a function of the modulation frequency is shown in Figure 4-17. The free-running gain-lever laser ($I_1 = 4.5$ mA, $I_2 = 50$ mA) shows a maximum distortion of -9.8 dBc at 2 GHz because the modulation frequency is close to the relaxation oscillation frequency of the laser. The uniformly biased laser ($I_1 = 50$ mA, $I_2 = 50$ mA) shows the maximum distortion at 4.5 GHz near the relaxation oscillation

frequency corresponding to the bias condition. The 2HD of the uniformly biased laser is lower than the gain-lever laser because of higher relaxation oscillation frequency. In the injection-locked gain-lever device, the nonlinearity of the laser is suppressed by more than 20 dB at 2 GHz, compared with the free-running gain-lever laser.

To measure third order inter modulation distortion (IMD3), the gain-lever DBR laser is modulated by a two-tone RF signal ($f_1 = 2.0$ GHz, $f_2 = 2.1$ GHz). As shown in Figure 4-18, the IMD3 for the free-running laser is -37.2 dBc. In comparison, the IMD3 of the injection-locked state is reduced considerably to -52.2 dBc.

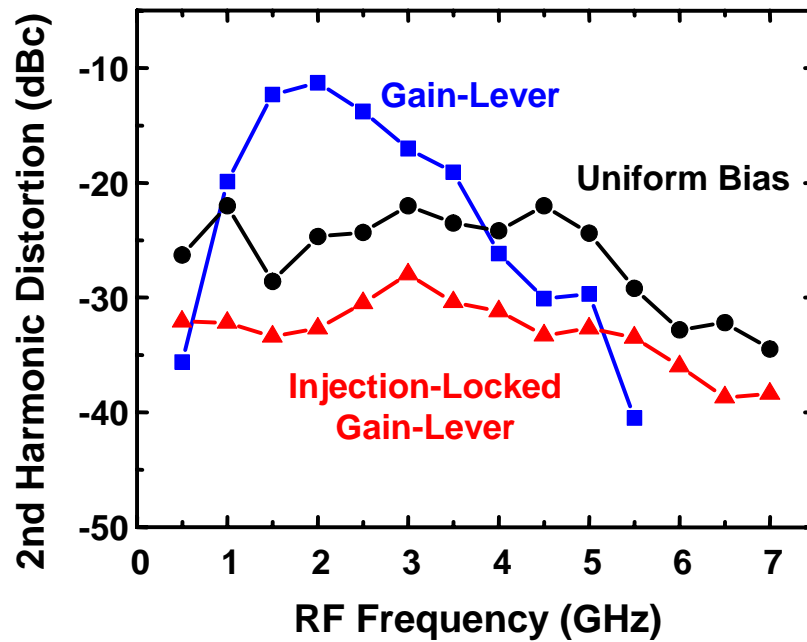


Figure 4-17. 2HD versus modulation frequency for various operation conditions. The second harmonic product is measured at twice the RF modulation frequency.

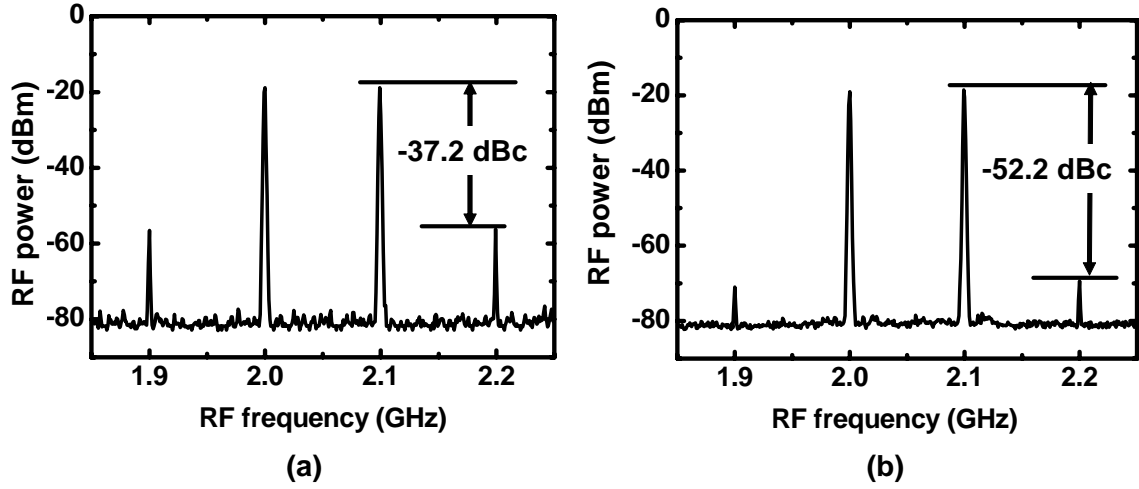


Figure 4-18. Measured RF spectra of a gain-lever DBR laser modulated by a two-tone RF signal ($f_1 = 2.0$ GHz, $f_2 = 2.1$ GHz) for (a) free-running gain-lever and (b) injection-locked gain-lever states.

One of the important figures-of-merit for fiber-optic links is SFDR. Figure 4-19 shows the received RF powers of the fundamental and the third-order inter-modulation product (IMP3) versus the input RF power for the free-running gain-lever, free-running uniform bias, and injection-locked gain-lever conditions. The received fundamental powers are almost equal for the gain-lever modulation with and without optical injection locking, both showing a 12-dB increase over the uniformly biased case. The SFDR of the injection-locked gain-lever DBR laser is increased by 12 dB compared with the free-running gain-lever states, 5 dB by IMP3 reduction and 7 dB by RIN reduction.

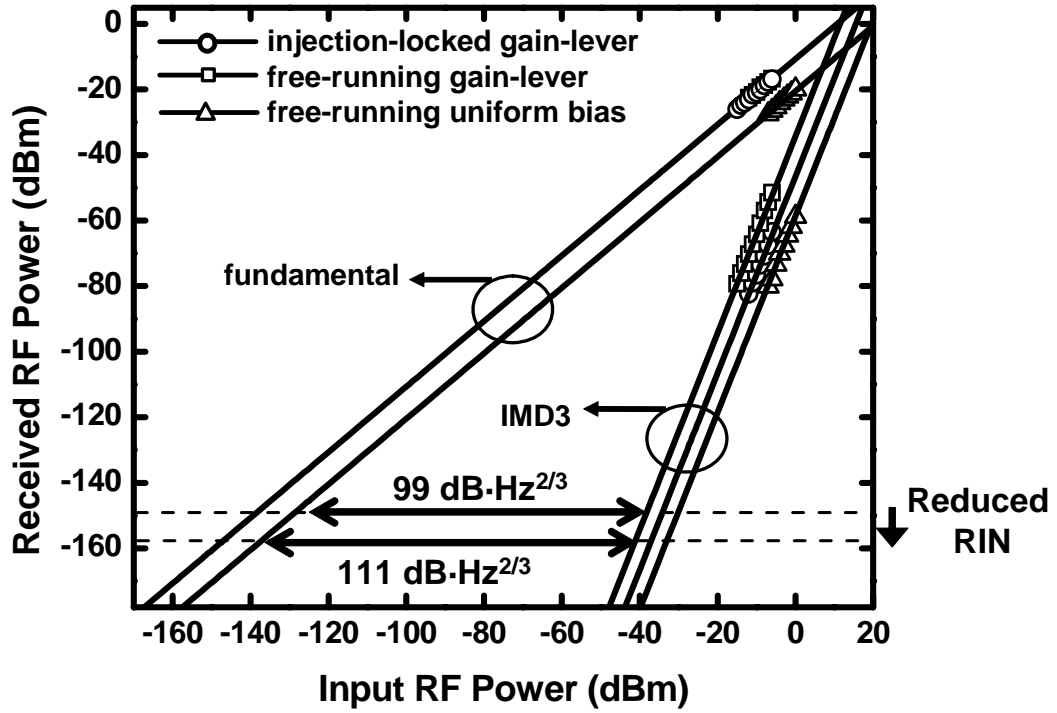


Figure 4-19. Measured SFDR of the link with a directly-modulated gain-lever DBR laser.

4.4.4 Ultra-Strong Injection-Locked Gain-Lever DBR Lasers

The performances of the injection-locked gain-lever DBR laser under ultra-strong injection ($R = 11$ dB) have been investigated experimentally. The ultra-strong injection is achieved by boosting up the injection power from a master laser by an EDFA. Figure 4-20 shows the measured optical spectrum of the injection-locked gain-lever DBR laser under $R = 11$ dB and $\Delta f = -2.4$ GHz. Optical power from the injection-locked laser is increased by 17 dB compared with the free-running laser due to the ultra-strong injection.

Figure 4-21 shows the measured frequency responses of the free-running, strong injection-locked ($R = -1$ dB) and ultra-strong injection-locked ($R = 11$ dB) gain-lever

DBR laser. The frequency responses are plotted after de-embedding the raw data from a network analyzer to remove the RC parasitic effect of the free-running laser [97]. The resonance frequency of the ultra-strong injection-locked gain-lever DBR laser is increased to 15.2 GHz from the original resonance frequency of the free-running laser, 3.5 GHz. Furthermore, AM response increases by 13 dB due to the increased optical power. The results observed in this measurement are agreed well with the results on the ultra-strong injection locking of DFB lasers discussed in Chapter 2.

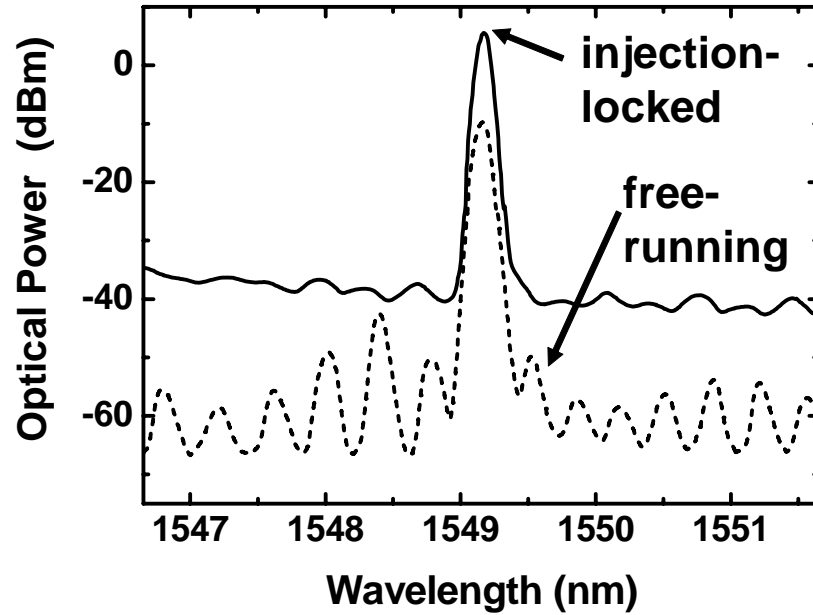


Figure 4-20. Optical spectra of a free-running gain-lever DBR laser and injection-locked gain-lever DBR laser under $R = 11$ dB and $\Delta f = -2.4$ GHz.

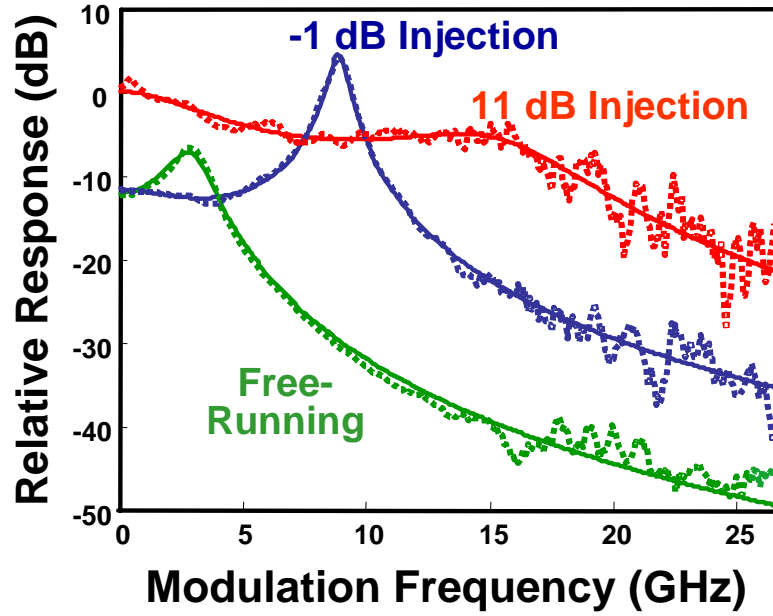


Figure 4-21. Measured frequency responses of a free-running, strong injection-locked ($R = -1$ dB), ultra-strong ($R = 11$ dB) gain-lever DBR laser. Frequency detuning Δf of the injection-locked states is fixed at -2.4 GHz.

RF performances of the ultra-strong injection-locked DBR lasers are investigated by direct modulation of the laser with a 2-GHz RF signal. Figure 4-22 shows the measured RF spectra for the free-running gain-lever DBR laser and the ultra-strong injection-locked gain-lever DBR laser under 2-GHz RF modulation. The Fundamental tone at 2 GHz for the injection-locked laser exhibits a 12.6-dB improvement of AM efficiency on top of gain-lever due to the increased optical power. The 2HD is reduced from -13.4 dBc to -32.7 dBc. Therefore, a 32-dB reduction in 2HD can be attained at equal received RF power.

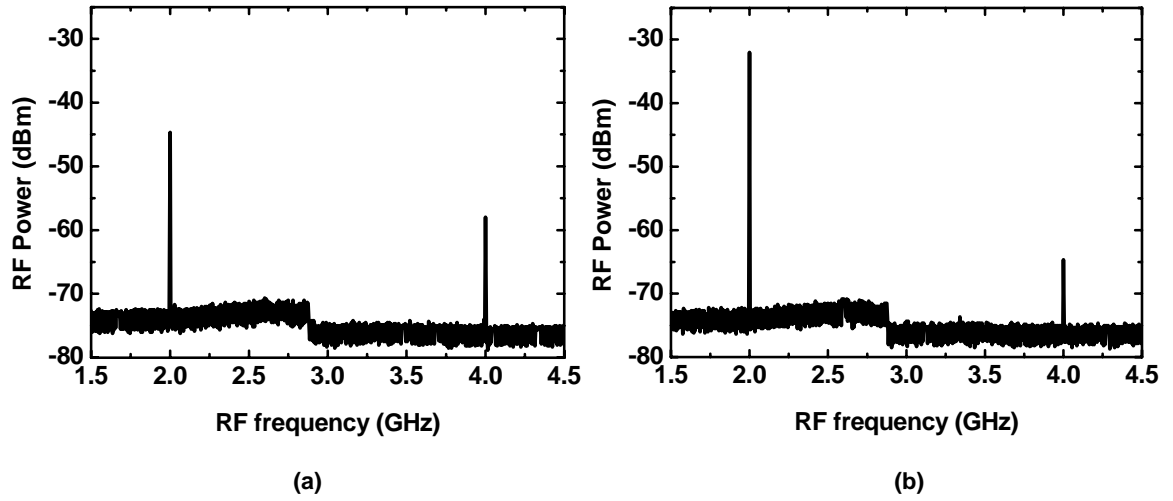


Figure 4-22. Measured RF spectra of a directly-modulated gain-lever DBR laser with RF signal at 2 GHz. (a) a free-running gain-lever DBR laser, (b) an ultra-strong injection-locked gain-lever DBR laser.

4.5 Summary

The first optically injection-locked gain-lever distributed Bragg reflector (DBR) laser has been successfully demonstrated. The gain-lever DBR laser fabricated exhibits high sidemode suppression ratio (SMSR) of > 35 dB and wide tunability. Amplitude modulation (AM) efficiency is improved by 11 dB by gain-lever modulation through a proper current bias on two gain sections. This improvement is attained at the expense of the laser linearity. By combining the gain-lever modulation with optical injection locking, modulation bandwidth of the laser is increased by three times over the free-running laser while maintaining the improved AM efficiency. The third-order intermodulation distortion (IMD3) has been suppressed by 15 dB and relative intensity noise (RIN) of the laser is reduced by 11 dB, resulting in a 12-dB improvement in spurious-free dynamic range (SFDR). Ultra-strong injection ($R = 11$ dB) increases AM efficiency by 12.6 dB on

top of the gain-lever effect with improved linearity. This new modulation scheme would improve the link loss, noise figure, and fidelity of directly modulated fiber-optic links.

Chapter 5 Monolithic Injection Locking in Multi-Section Distributed Feedback (DFB) Lasers

5.1 Introduction

The experimental setups used to achieve optical injection locking often require two light sources - an external cavity laser (ECL) or a wavelength-matched distributed feedback (DFB) laser as the master laser and another semiconductor laser as the slave laser. In a typical injection locking system, the master laser is isolated from the slave laser using optical isolators. The isolation is on the order of 30 - 40 dB with an insertion loss of 1 - 3 dB. Polarization controllers are also used in the injection path to maximize the interaction of the injected signal with the slave laser. For strong injection locking, the output power from the master laser needs to be much higher than the slave laser. Often an optical amplifier is used to boost the master laser power to achieve a high injection ratio.

Configuring and mounting these various system components on an optical bench as shown in Figure 5-1(a) limits the portability of injection locking technology. Although suitable for research applications, large-scale multi-component laser systems are not suitable for field use. In particular, the size constraints and the need for multiple optically linked system elements render these configurations impractical for many telecommunications applications. Consequently, a need exists for techniques and devices that enable the broader application of injection locking technology. Further, techniques are sought that provide improved frequency control and bandwidth without significantly increasing fabrication costs.

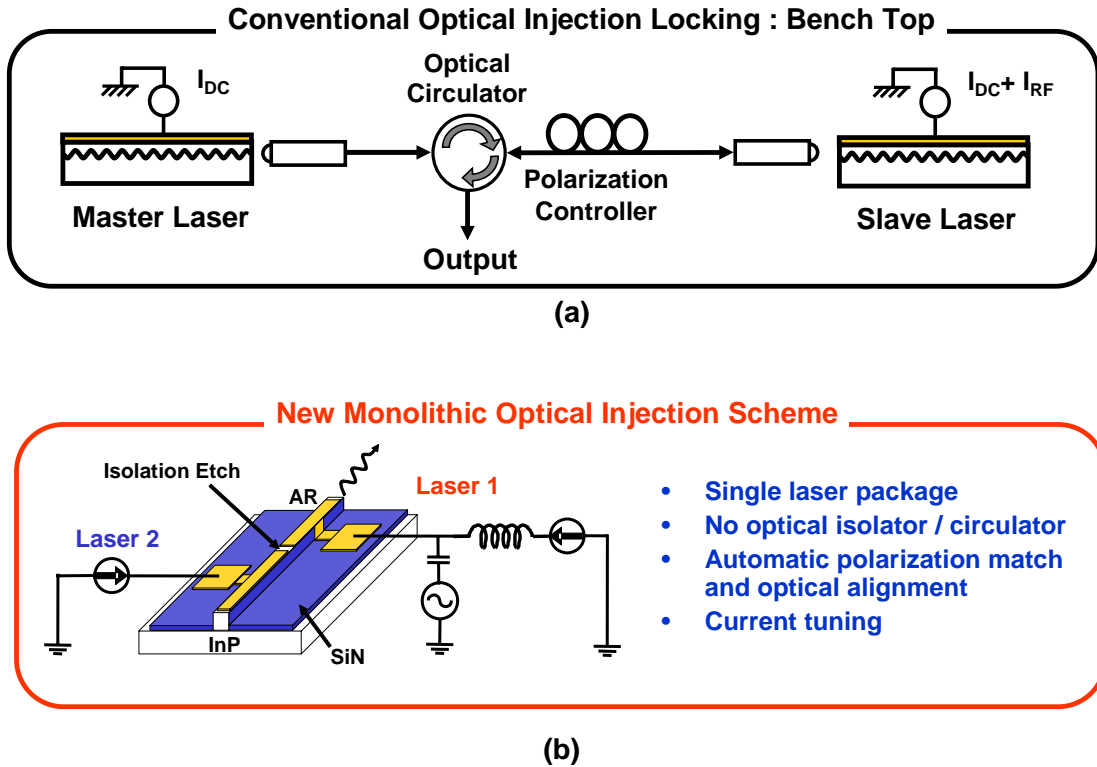


Figure 5-1. Schematics of injection locking system: (a) Conventional injection locking; (b) New monolithic injection locking scheme.

To overcome these issues, a monolithic injection-locked DFB laser with two separate gain sections are proposed and demonstrated. Figure 5-1(b) is a schematic of monolithic injection-locked DFB lasers. In two-section DFB lasers with strong gratings, each section can lase by itself. Locking/unlocking phenomenon between the modes from individual sections is observed by tuning the bias current on each section. When biased within the proper current range, the two sections operate at the same wavelength and exhibit a significant increase in the modulation bandwidth similar to optical injection locking with an external master laser. In addition, the nonlinear distortions such as second harmonic and intermodulation distortions are also suppressed. Chirp reduction in a directly-

modulated two-section DFB laser is also demonstrated. Using the monolithic devices, we achieved a > 2.5 -dB improvement of BER performance at 10-Gb/s transmission over 80-km.

5.2 Principles and Device Fabrication

As shown in Figure 5-2(a), the first laser section L_1 and the second laser section L_2 , share a common waveguide layer for transmitting light. Accordingly, both laser sections are automatically aligned along the waveguide and share a common laser cavity. The problems of optical alignment and polarization matching that would occur in a conventional injection locking configuration are thus avoided. Additionally, each laser section typically incorporates a shared grating that is incorporated in the unitary structure.

Figure 5-2(b) illustrates the principles of independent lasing which results in mutual locking by proper current tuning at each section. For each section to lase independently, a suitable grating is chosen such that each laser section can reach its own lasing threshold. In order to evaluate cavity sizes in various devices, a unitary structure of length L having a grating with a coupling constant κ can be analyzed in terms of the κL product. For devices with a small κL product, current tuning in each section fails to achieve independent operation at two distinct wavelengths. Thus, gratings with higher coupling coefficients are particularly suited for the mutual locking purpose.

Using laser wafer material supplied by our collaborators, Multiplex Inc., we have fabricated multi-section DFB lasers. Most of the fabrication processes are compatible with the gain-lever DBR lasers presented in Section 4.3. The DFB laser is designed with a very strong grating such that the κL product is approximately 3 to 4 for a single-section

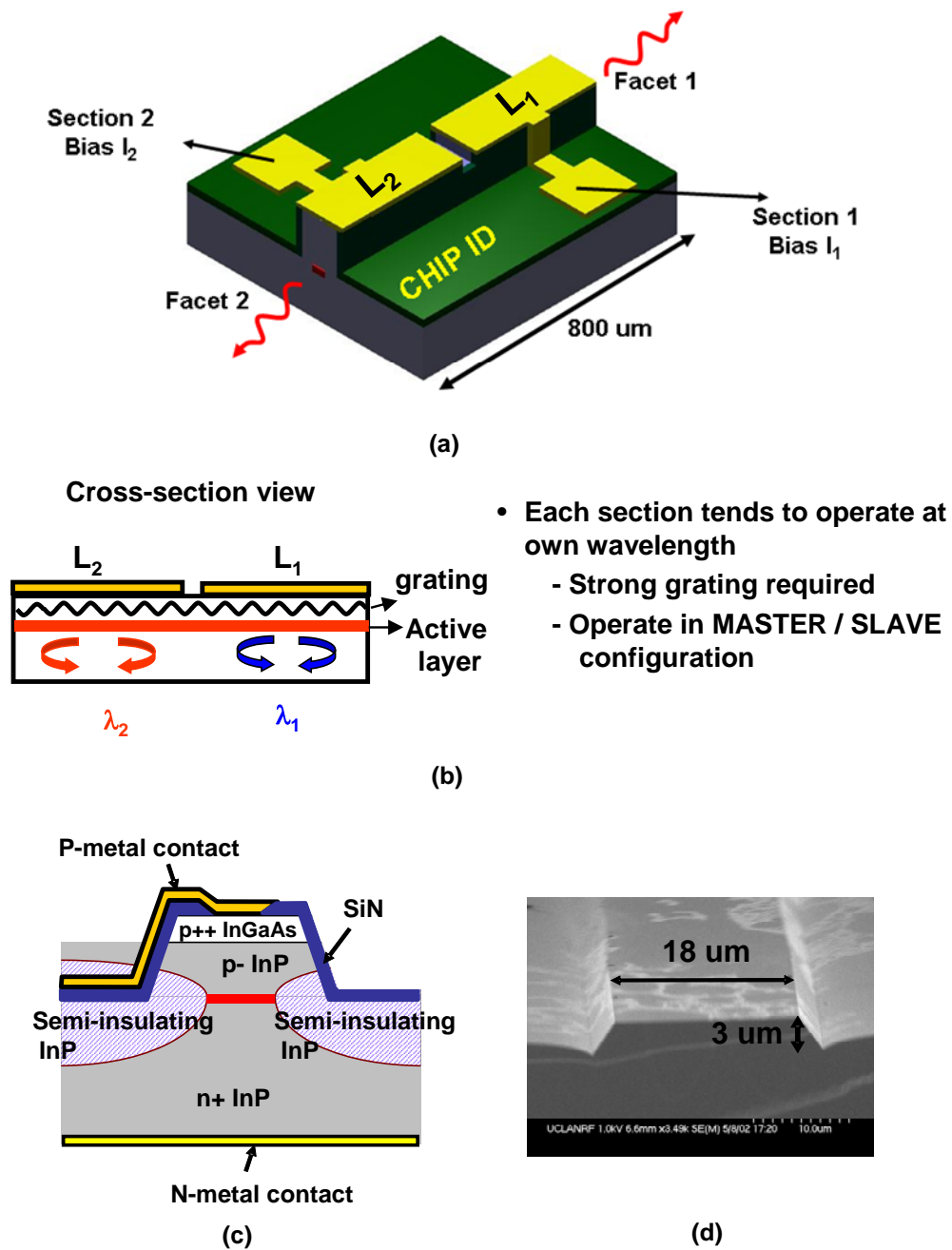


Figure 5-2. Two-section DFB lasers for the demonstration of mutual locking in monolithic DFB lasers: (a) Schematic structure; (b) Longitudinal cross-sectional structure illustrating independent lasing; (c) Horizontal cross-sectional profile; (d) Scanning electron micrograph (SEM) of the laser before metallization.

length of 400 μm . The wafer is etched to form an approximately 3 - 4 μm ridge and silicon nitride is used as a passivation layer as shown in Figure 5-2(c) and (d). The top metal contact is split into two or three sections with varying split ratio between sections. A 0.2- μm etch is then done between the laser sections and an electrical isolation larger than 4 k Ω is achieved. An anti-reflection (AR) coating of \sim 0.2- μm Zirconium dioxide (ZrO_2) layer with a reflectivity of less than 0.1% is deposited on one facet to suppress the Fabry-Perot (F-P) modes of the cavity.

5.3 Optimization of Multi-Section DFB Lasers for Mutual Locking Purpose

5.3.1 Introduction

For the mass production of the monolithic injection-locked DFB lasers, device yield is most critical. Therefore, we have fabricated various versions of multi-section lasers with systematic variations of coupling coefficient κ , waveguide shape and cavity length. By fabricating and testing devices with various design parameters, an optimized laser structure for high-yield and uniformity has been achieved. Figure 5-3 shows various waveguide and multi-section schematics we have designed and fabricated. The waveguides are depicted as red solid lines. Blue pads are drawn to represent metal pads for DC-bias and/or high-speed signal modulation. Electrical isolations between laser sections are done by etching the area between laser sections. This etching is done between two lasers for type A, B and D. Additional isolation is done in one of the laser sections in type C. The split contact version (type C) offers on-chip control of frequency detuning between laser sections. In terms of cavity length, all the device types are designed to have three different total cavity lengths of 600, 800 and 1000 μm .

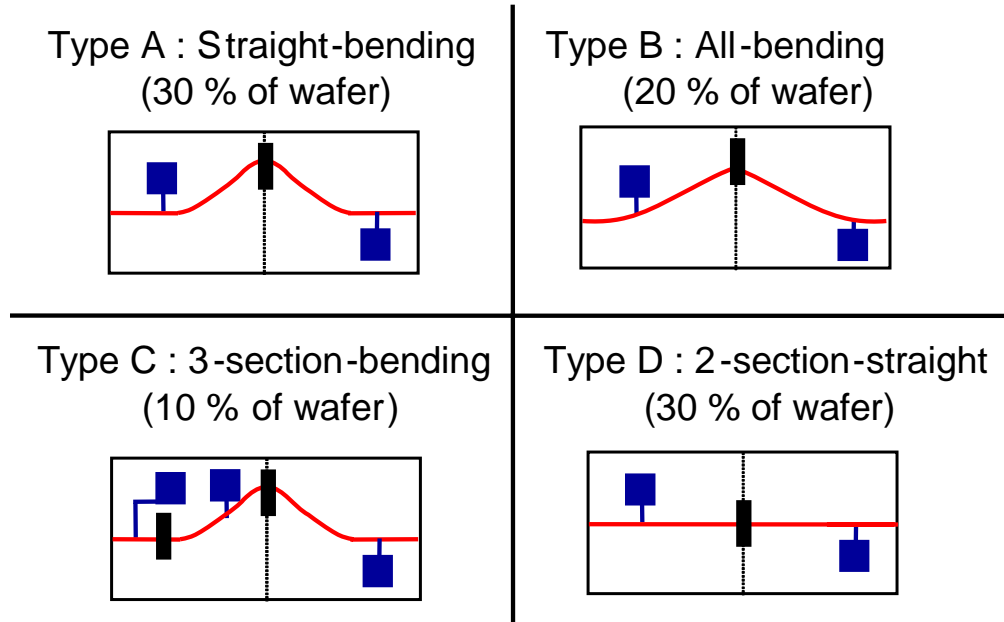


Figure 5-3. Top-view layout of various waveguides and multi-section laser designs.

5.3.2 Quarter-Wavelength Shifted DFB Lasers with Bent Waveguide

To further improve the performance of the monolithic injection-locked DFB laser, the use of quarter-wave-shifted DFB for both laser sections can be utilized. Normal DFB lasers have two degenerate modes located on either side of the stopband of the grating. They are usually referred to as -1 and +1 modes. Exactly which mode of the laser will lase in is difficult to predict. It is affected by the terminating phase of the grating at the laser facets, and the reflectivity of the facets. The situation in monolithic optical injection-locked laser is even more complicated.

The two-mode degeneracy of the DFB laser can be removed by using quarter-wave shifted gratings for both the master and the slave lasers. This is expected to improve the performance of monolithic optical injection locking. Quarter-wave shifted DFB lasers

operate in single longitudinal mode located in the middle of the stopband. This may be able to increase the stability of optical injection locking. By employing a curved waveguide, the grating pitch in the middle of the laser becomes larger. This results in a shift of the grating phases between the two straight sections of the waveguide [98]. By properly designing the waveguide bend, a quarter wave phase shift can be achieved without using sophisticated electron-beam lithography. Bent-waveguide DFB lasers are compatible with the standard laser fabrication processes. An example of the bent structures is shown in Figure 5-4. The bent section is implemented by a raised-sine function as

$$\begin{aligned}
 y(x) &= 0 \quad , \quad 0 \leq x \leq L_1 \\
 y(x) &= \frac{W}{L_B}(x - L_1) + \frac{W}{\pi} \sin\left(\pi \frac{L_1 - x}{L_B}\right) \quad , \quad L_1 \leq x \leq L_1 + 2 \cdot L_B \\
 y(x) &= 2 \cdot W \quad , \quad L_1 + 2 \cdot L_B \leq x \leq L
 \end{aligned} \tag{5.1}$$

In the equations, $2 \cdot W$ is the lateral transition in y-coordinates between $x = 0$ and $x = L$. L is the cavity length of a master laser or slave laser, $2 \cdot L_B$ is the length of bent region and L_1 ($= L - L_1 - 2L_B$) is the length of the straight section. As well as varying the waveguide shapes and cavity lengths, coupling coefficient κ of wafers has been also varied by two-different wafer growths from Multiplex, Inc. The purpose of varying κ is to achieve more uniform device performances in terms of mutual locking. The effect of monolithic injection locking originates from independent lasing in two laser sections. Two independent modes from each section are mutually locked by adjusting bias currents on each section. Therefore, κL product of the lasers is a critical parameter that characterizes the possibility and the degree of mutual locking.

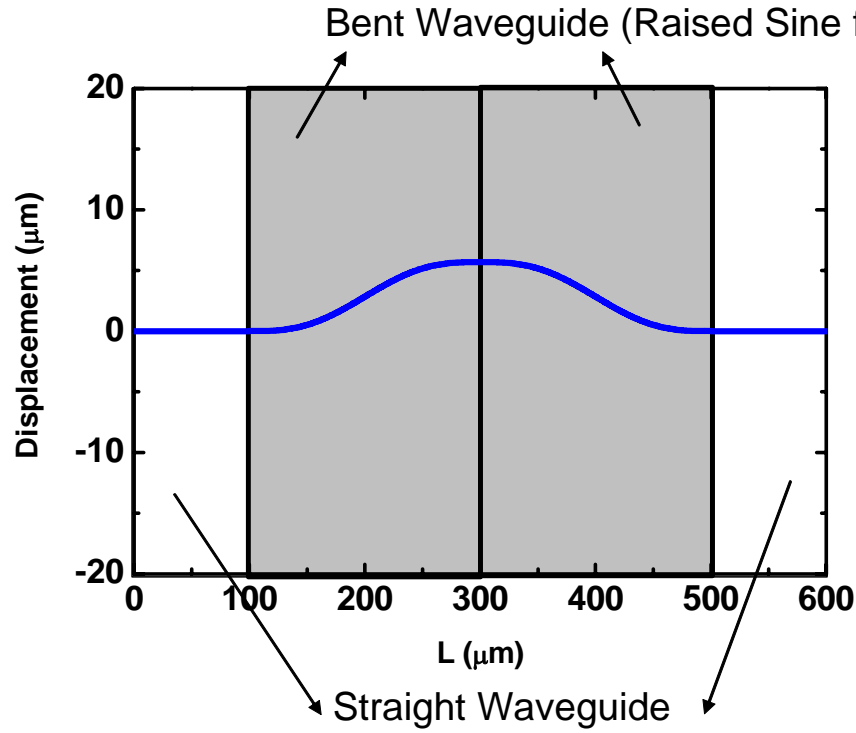


Figure 5-4. Straight-bent-bent-straight waveguide design (type A) showing lateral displacement.

The κL products of the lasers for mutual injection locking experiments are summarized in Table 5-1. The κL product ranges from 1.2 to 3.5.

Total cavity length (μm)	κL product of a single laser section	
	Low κ wafer ($\kappa = 40 \text{ cm}^{-1}$)	High κ wafer ($\kappa = 70 \text{ cm}^{-1}$)
600	1.2	2.1
800	1.6	2.8
1000	2.0	3.5

Table 5-1. Coverage of κL products

5.3.3 Device Yield

Using the systematic variations of the device design, we have fabricated multi-section DFB lasers. As described in previous section, two fabricated wafers contain 24 device types ($2 \times 3 \times 4 = 24$, two wafers with different κ , three variable cavity lengths and four different waveguide shapes). All the devices fabricated are identified by their own chip ID for a quick and efficient device testing. The fabricated devices have been tested for single-mode yield first. The single-mode test has been performed by observing SMSR as well as threshold current and optical power. Most of the devices show uniform performance in terms of a low threshold current and high optical power ($> 5 \text{ mW}$ at $3 \cdot I_{th}$).

A stable single-mode operation with high SMSR is found to be challenging because of multi-section effects and high κL product. In multi-section bent waveguide lasers, the effect of the quarter-wavelength shift is sometimes cancelled out or becomes unpredictable due to the unwanted coupling between laser sections. Figure 5-5 shows single-mode yield for the 24 device types. A total 728 devices have been tested. As shown in Figure 5-5, straight waveguide lasers with two sections (type D) from high κ wafer exhibit the highest single-mode yield of 98 %. Summary of the device characterization is shown in Table 5-2. As shown in Figure 5-5 and Table 5-2, devices with bent waveguide exhibit low single-mode yield. Straight waveguide lasers from low κ wafer show self-pulsation in the GHz range due to a weak grating, such that the independent lasing or mutual locking can not be achieved. The devices with straight waveguide and high κL product are the best candidates to enable high single-mode yield and monolithic injection locking.

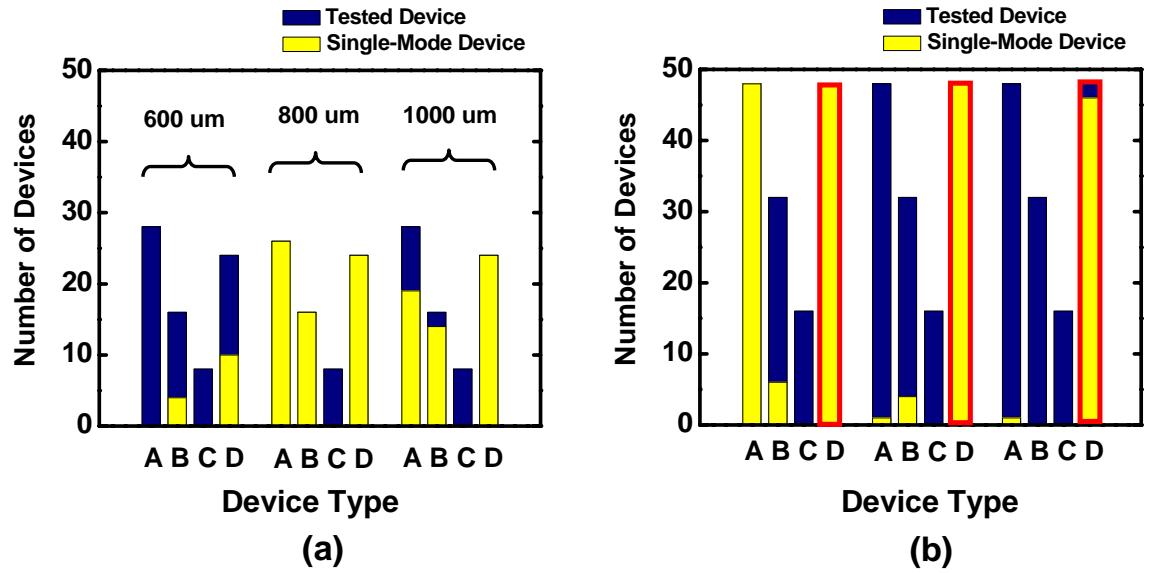


Figure 5-5. Single-mode yield for (a) low κ wafer (b) high κ wafer.

Device Type	Waveguide structure	Total Cavity Length (μm)	Low κ wafer	High κ wafer
A	Straight-bending	600	Low single-mode yield Multi-mode lasing	
		800		
		1000		
B	All bending	600		
		800		
		1000		
C	3-section-bending	600		
		800		
		1000		
D	2-section-straight	600	Self-pulsation	Mutual locking
		800		
		1000		

Table 5-2. Summary of device characterization.

5.4 Experimental Results on Optical Properties

The experimental setup used to measure the optical spectrum, modulation response, and nonlinear distortion of the monolithic injection-locked DFB laser with two gain sections is shown in Figure 5-6.

This setup is more compact than injection locking setups using an external light source since polarization controllers, optical circulators (or isolators), and fiber-to-laser couplers are not required. An external cavity laser is used as a stable wavelength reference for measuring the wavelength dependence on the current tuning of each section. DC current and RF modulation signals are applied to the section 1 through a bias tee, while another DC current is applied to the other laser section. The main difference between this optical injection locking system and the external injection locking system is that both lasers share a common waveguide and there is no optical isolation between them. The modulated output taken from the section 1 is coupled into a high-speed photodetector (34 GHz). The detected signal is amplified by low noise RF amplifier with 20 dB gain and then observed by an RF spectrum analyzer.

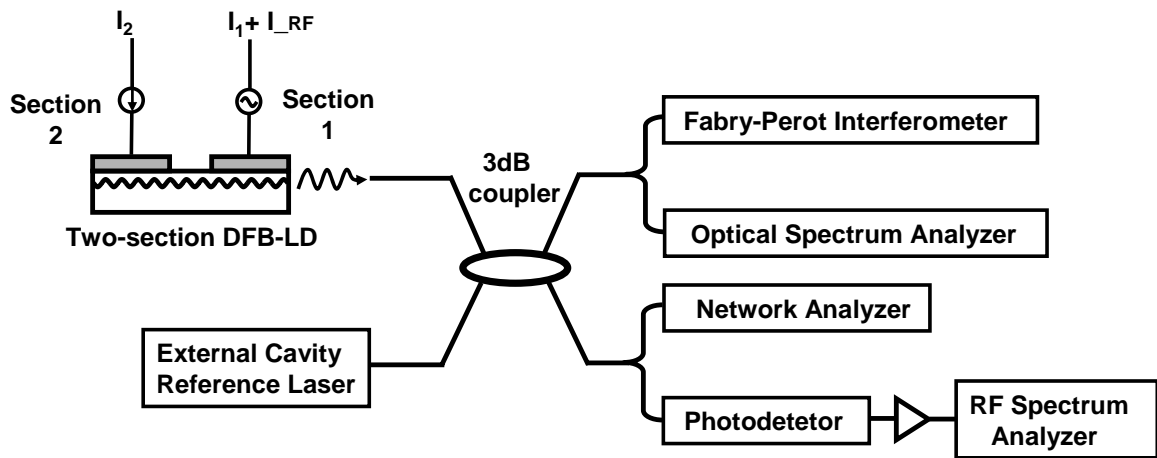


Figure 5-6. Experimental setup.

Figure 5-7 shows the high resolution optical spectra of the two-section laser in (a) mutually-locked and (b) unlocked states measured by a scanning Fabry-Perot (F-P) interferometer. In the mutually-locked state, a single locked mode is observed at +9 GHz (compared to the reference laser) and no other frequency components are observed. In the unlocked state, the two sections lase at two distinct wavelengths that are approximately 28 GHz apart.

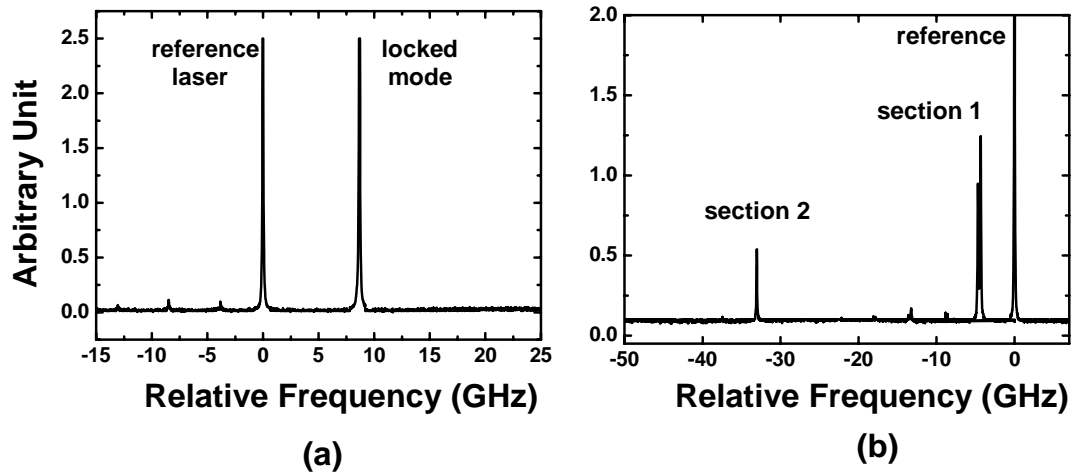


Figure 5-7. Measured optical spectrum. (a) Mutually-locked ($I_1 = 45.2$ mA, $I_2 = 50$ mA) and (b) Unlocked ($I_1 = 45.2$ mA, $I_2 = 61$ mA)

Figure 5-8 represents the relative frequency between the modes from two sections versus the current of the section 2 ($= I_2$). The section 1 is DC-biased at a fixed value of 45.2 mA. As I_2 increases, both the modes from the section 1 and the section 2 move towards shorter frequencies (=longer wavelengths) due to thermal tuning effect. The tuning rate from section 2 is noticeably larger than that from section 1. Consequently, when I_2 decreases, the frequency difference from each section gradually reduces and eventually the mode from section 1 enters the mutually-locked state to the mode from

section 2. The monolithic optical injection locking scheme is very robust. There is only one tuning parameter, namely the current bias on each section. Unlike externally injection-locked lasers, the monolithically-locked laser is much less sensitive to ambient temperature since the frequencies of both laser sections drift in the same direction.

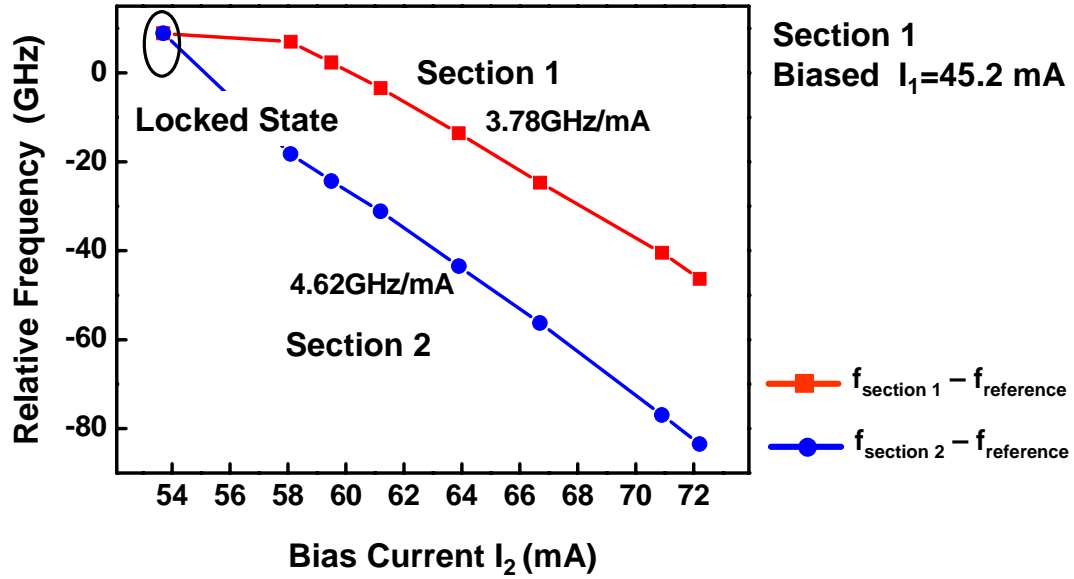


Figure 5-8. Measured tuning characteristic for each mode when the bias current of section 2 ($= I_2$) is varied and section 1 ($= I_1$) is biased at a fixed value of 45.2 mA.

To confirm the independent lasing and mutual locking, optical spectra have been measured at both facets. For this measurement, a different device from the previous measurement has been used, but most of the characteristics are very similar. As shown in Figure 5-9(a), the mode from section 1 exhibits much higher power than the mode from section 2 because the output power is coupled from the facet facing section 1. On the other hand, when the output facet is switched to section 2 under the same bias condition, the peak power from section 1 decreases while the peak power from section 2 increases as shown in Figure 5-9(b). Consequently, we can conclude that the mode on the shorter

wavelength side is lasing from section 1 and the mode on the longer wavelength side is from section 2.

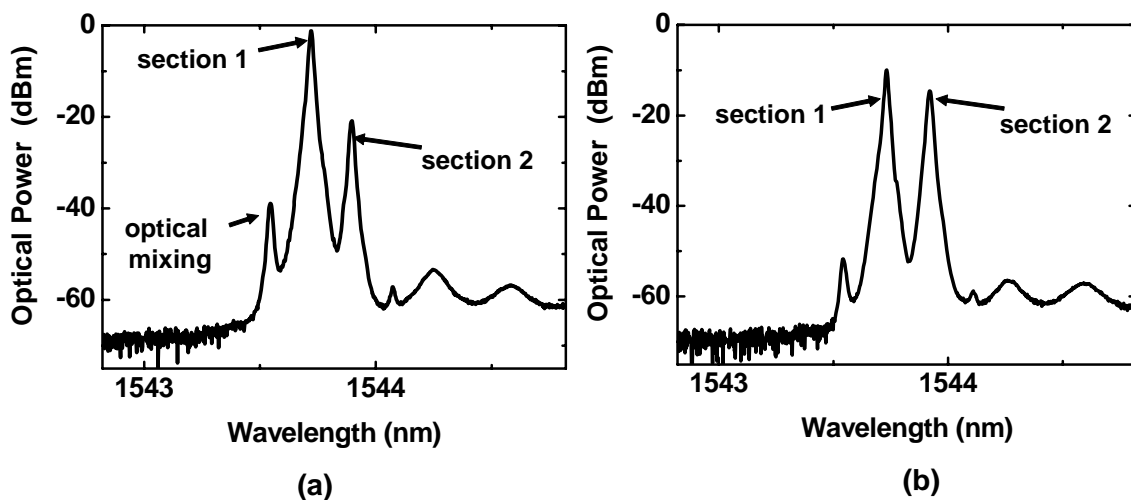


Figure 5-9. Optical spectra measure at the facet facing at (a) section 1 and (b) section 2. Bias current is $I_1 = 30$ mA and $I_2 = 21$ mA.

5.5 Modulation Responses and Nonlinear Distortion Reduction

The modulation frequency response for the device used for Figure 5-7 is shown in Figure 5-10. The relaxation oscillation peak of the free-running state ($I_1 = 45.2$ mA, $I_2 = 0$ mA) is 11 GHz. In the mutually-locked state, the resonance peak is increased to 23 GHz. In the unlocked state, the beating of the two modes generates a very sharp and noisy spike at the difference frequency of ~ 25 GHz in the frequency response. The Lorentzian peak is superimposed on the free-running modulation response.

It is known that the nonlinear distortion becomes more severe as the modulating frequency approaches the relaxation oscillation frequency due to the nonlinear coupling between electrons and photons [58]. Hence, if the resonance frequency of the laser is increased, the nonlinear distortions can be reduced while the modulation bandwidth is increased.

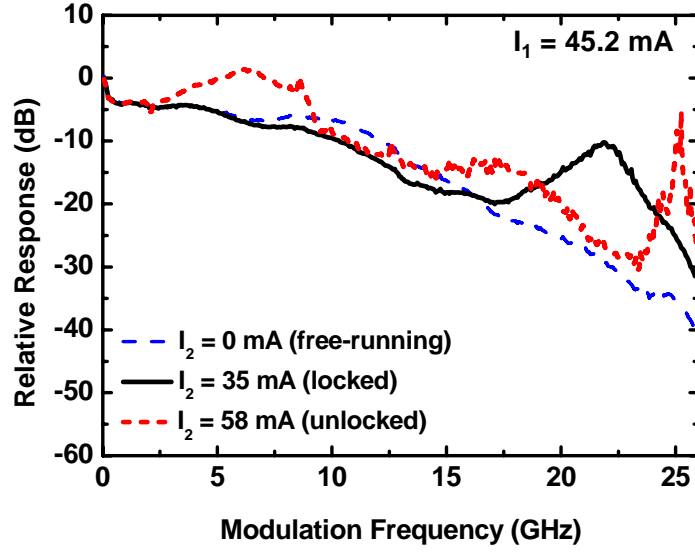


Figure 5-10. Measured frequency responses for various DC bias values on section 2. Section 1 is DC biased at a fixed value of at 45.2 mA and RF-modulated.

To measure the second-harmonic distortion (2HD), laser section 1 is modulated by a single tone RF signal ($f = 9$ GHz). The second harmonic product is measured at 18 GHz. To investigate the 2HD in both locked and unlocked states, I_1 is fixed at 45.2 mA and the I_2 is varied from 0 mA to 65 mA. Mutual locking is observed between 14 mA to 53 mA through optical spectra measurement. The measured 2HD versus I_2 is shown in Figure 5-11. At the mutually-locked state, the second harmonic product is reduced by more than 15 dB compared with the free-running and unlocked state and the bias current range of mutual locking regime agrees well with the range observed in optical spectra measurement. Figure 5-12 shows the suppression of third harmonic distortion. The slave section of the monolithic injection-locked DFB laser is modulated by a 6-GHz RF signal. As shown in this figure, the third harmonic distortion is suppressed by 22.1 dB.

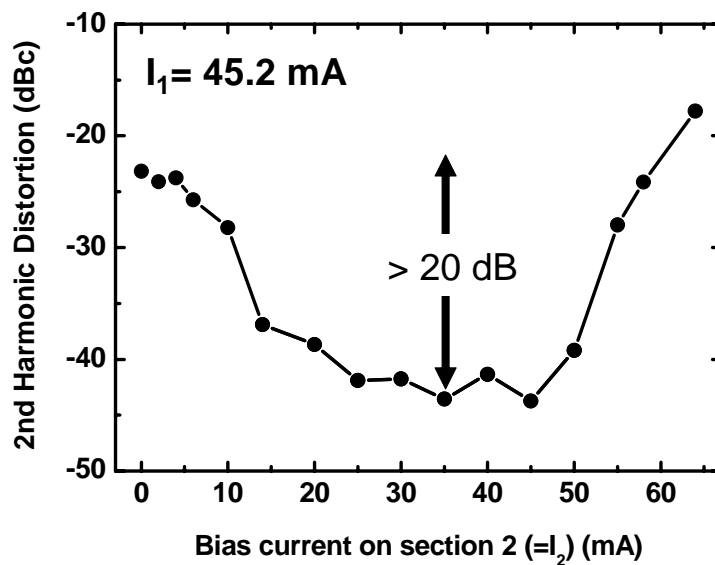


Figure 5-11. Measured second harmonic distortion versus I_2 . Section 1 is biased at 45.2 mA and modulated by a 9-GHz RF signal.

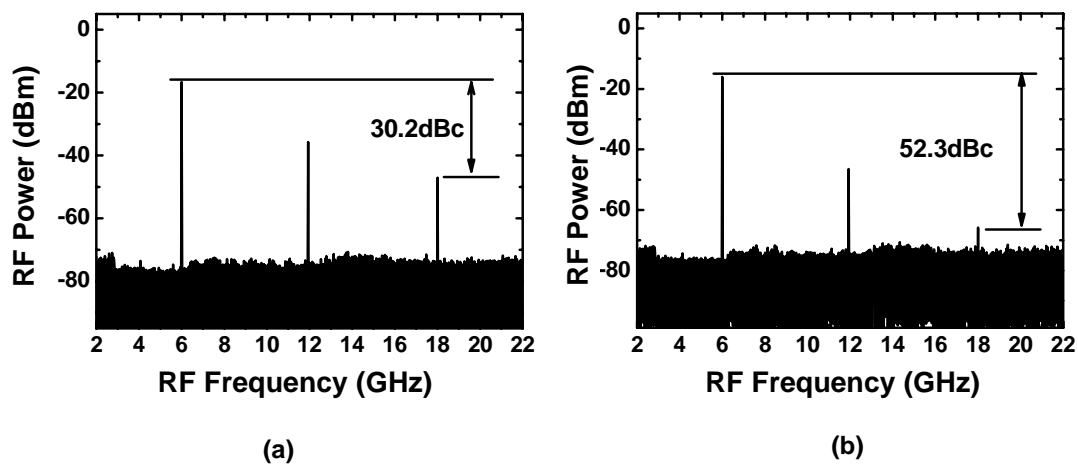


Figure 5-12. . Measured RF spectra when section 1 is modulated by a 6-GHz RF signal: (a) free-running ($I_1 = 45.2$ mA, $I_2 = 0$ mA); (b) mutually-locked ($I_1 = 45.2$ mA, $I_2 = 35$ mA).

Figure 5-13 shows the received RF powers of the fundamental and third-order intermodulation products (IMP3) versus the input RF power for both the free-running and the injection-locked state. The measured noise floor is -140 dBm/Hz. Under the monolithic injection-locked state, the spurious-free dynamic range (SFDR) is increased by 2.9 dB, from $95 \text{ dB}\cdot\text{Hz}^{2/3}$ to $97.9 \text{ dB}\cdot\text{Hz}^{2/3}$. In addition to the suppression of nonlinear distortion, the two-section DFB laser exhibits improved RF performances in higher modulation frequency when it operates in the mutually-locked regime.

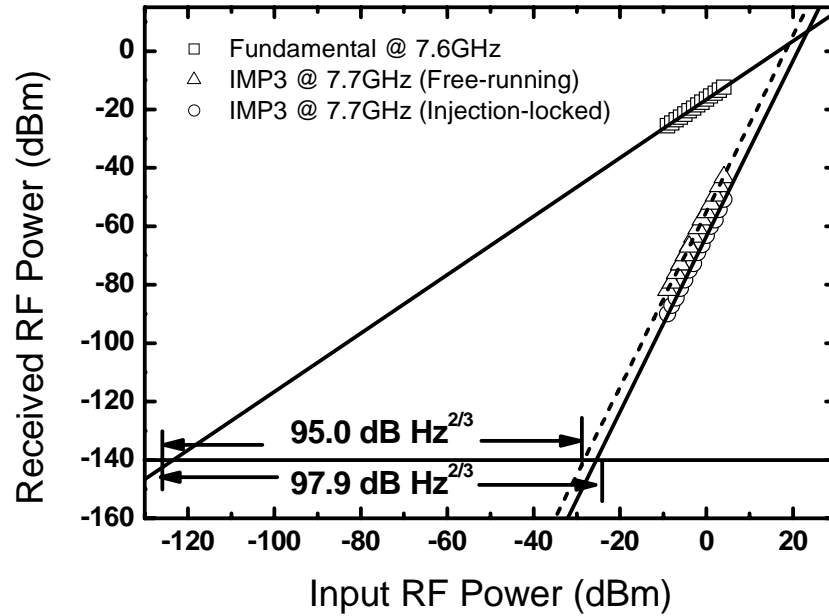


Figure 5-13. The SFDR of the link with directly-modulated two-section DFB laser at $f_1 = 7.5 \text{ GHz}$ and $f_2 = 7.6 \text{ GHz}$.

The improved response to the RF signal at 20 GHz is shown in Figure 5-14 by observing the waveform from photodetector in an oscilloscope. Monolithic injection-locked lasers respond very well to a 20-GHz RF signal, whereas the free-running laser can not respond. The SFDR in the high frequency range (18 GHz) is also measured to

verify nonlinear distortion characteristics when the laser is directly-modulated near the new resonance frequency of 23 GHz. Figure 5-15 is the measured SFDR at 18-GHz range. The SFDR for the mutually-locked state is measured at $87 \text{ dB}\cdot\text{Hz}^{2/3}$ while the free-running laser can not respond to such a high-frequency signal. The measured SFDR is smaller than that at 7-GHz range (Figure 5-13) due to the increased noise floor and distortion products. Figure 5-16 shows the photographs of the packaged chip and module. The laser has been packaged by our collaborator at Multiplex, Inc.



Figure 5-14. Waveforms measured by an oscilloscope at a 20-GHz RF modulation for free-running and injection-locked states.

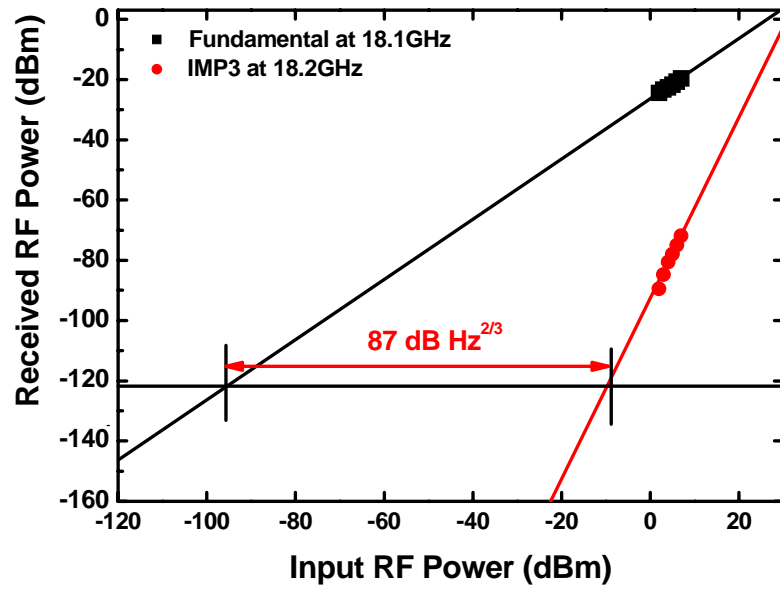


Figure 5-15. Measured SFDR at 18.1 GHz. The laser is modulated by a two-tone signal ($f_1 = 18.0$ GHz, $f_2 = 18.1$ GHz) under mutually-locked state.

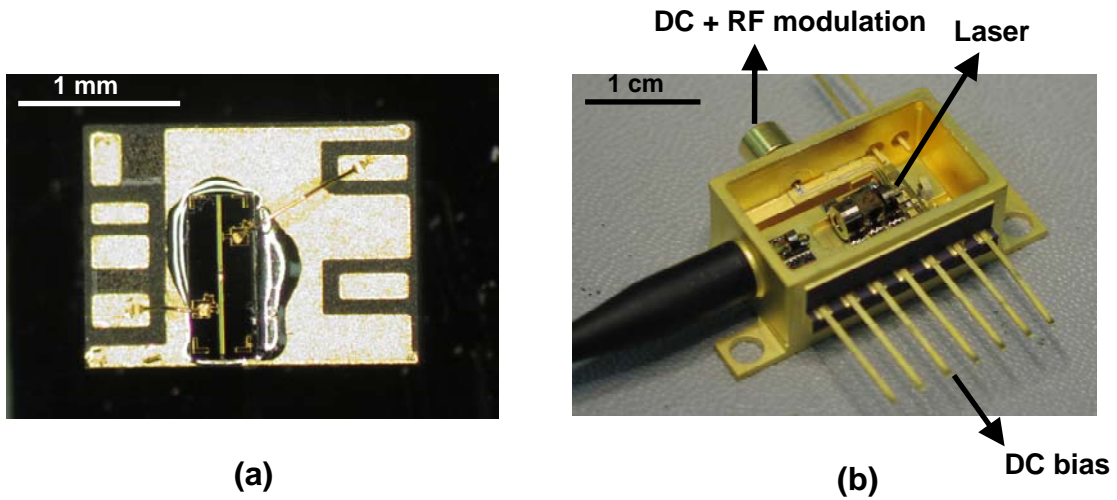


Figure 5-16. Fabricated device and fully packaged injection-locked DFB laser module. (a) Integrated master-slave laser on submount with 25- Ω termination for direct modulation (b) Fully packaged module with output fiber, optical isolator, master laser power monitor, TEC control, and GPO connector for RF input.

5.6 Chirp Reduction and BER Performances

As discussed in Section 2.1, chirp of directly-modulated lasers can be significantly reduced by injection locking [4-7, 9]. In this section, we demonstrate the reduction of laser chirp and improved bit-error-rate (BER) performance in mutually locked lasers.

Figure 5-17 shows experimental setup. One of the laser sections is DC biased and modulated by non-return-to-zero (NRZ) data stream from bit-error-rate tester (BERT). The other section is DC biased only. The optical signal from the laser is coupled into the fiber and transmitted over negative dispersion fiber (Corning MetroCor, $D = -8$ ps/km/nm). The optical power of the received signal is controlled by an optical attenuator before BER measurement. The waveform is observed by an oscilloscope.

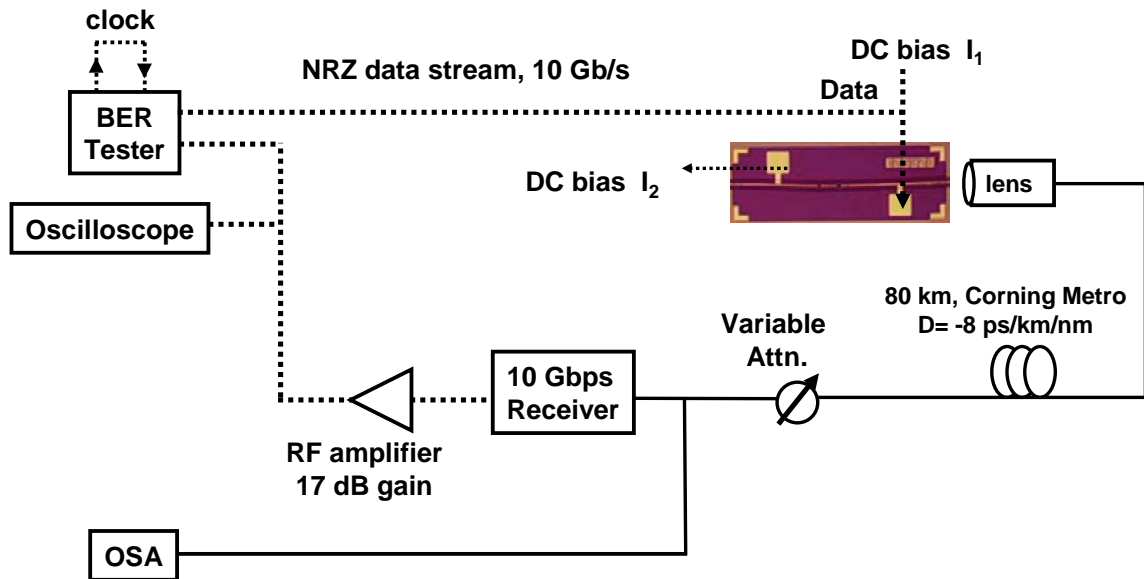


Figure 5-17. Experimental setup for measuring BER performance of the two-section DFB lasers. (variable attn.: optical variable attenuator; OSA: optical spectrum analyzer)

The optical spectra without fiber transmission are shown Figure 5-18(a) and (b) for single section bias ($I_1 = 90$ mA, $I_2 = 0$ mA) and two-section bias ($I_1 = 90$ mA, $I_2 = 30$ mA), respectively. When the modulation signal is applied to the laser, the 3-dB spectral width of the single-section laser is broadened from 0.14 to 0.44 nm due to the laser chirp. On the other hand, spectral width of the mutually locked laser is broaden from 0.14 to 0.21 nm, exhibiting 0.23 nm reduction compared with the single-section bias case.

Figure 5-19(a)-(d) show the measured eye diagrams of the free-running and the mutually injection-locked lasers with and without fiber transmission. Both lasers exhibit similar waveforms for back-to-back transmission as shown in Figure 5-19(a) and (b). However, when the signal is transmitted through an 80-km fiber, the eye opening for the mutually locked laser (Figure 5-19(d)) is much wider than the free-running laser (Figure 5-19(c)).

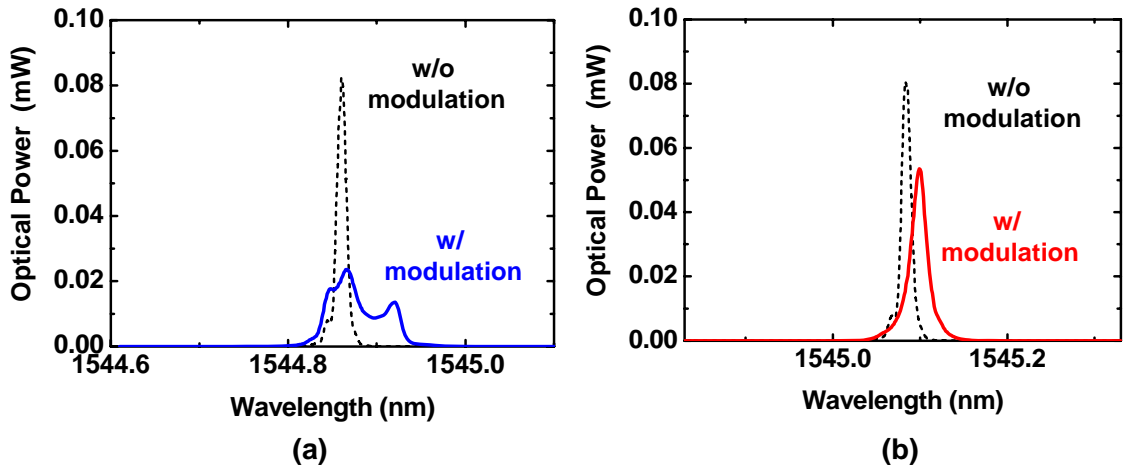
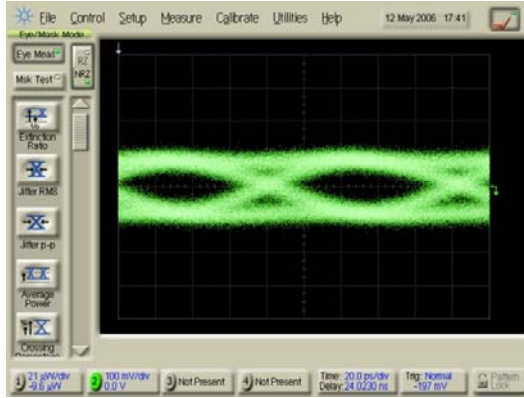
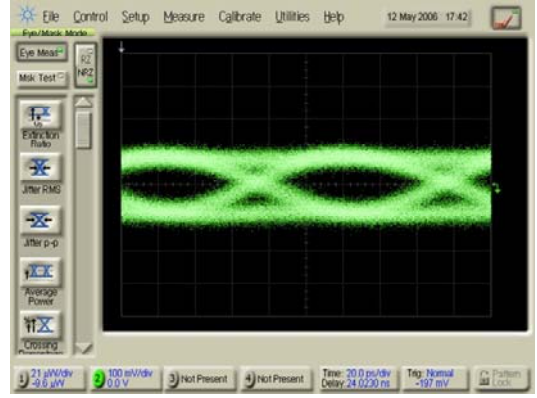


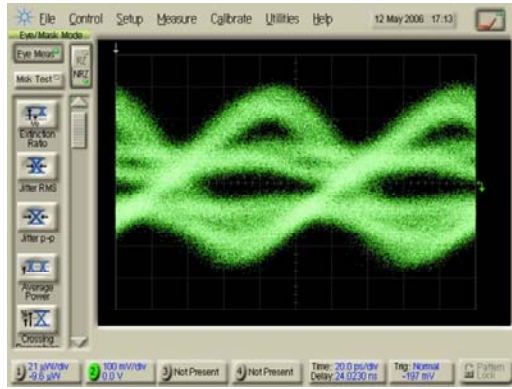
Figure 5-18. Measured optical spectra of the two-section DFB lasers under direct modulation with 10-Gb/s NRZ data: (a) $I_1 = 90$ mA, $I_2 = 0$ mA; (b) $I_1 = 90$ mA, $I_2 = 30$ mA. The optical power is measured in linear scale. The optical spectra without data modulation are depicted as dotted lines.



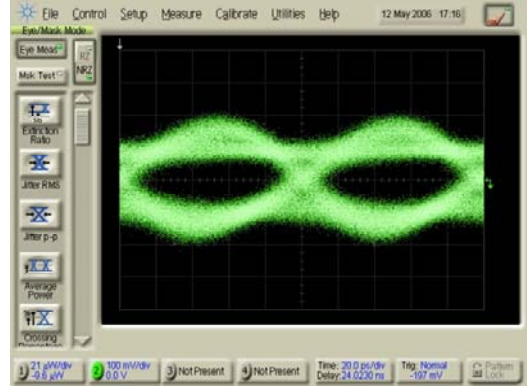
(a)



(b)



(c)



(d)

Figure 5-19. Measured eye diagram for (a) $I_1 = 90$ mA, $I_2 = 0$ mA, back-to-back; (b) $I_1 = 90$ mA, $I_2 = 30$ mA, back-to-back; (c) $I_1 = 90$ mA, $I_2 = 0$ mA after 80-km fiber transmission; (d) $I_1 = 90$ mA, $I_2 = 30$ mA after 80-km fiber transmission.

Figure 5-20 shows the measured BER performances. For the back-to-back measurements, both lasers show almost identical BER performance with on 0.5-dB difference in sensitivity at BER of 10^{-9} . However, the mutually locked laser exhibits > 2.5-dB improvement after 80-km fiber transmission due to the reduced chirp.

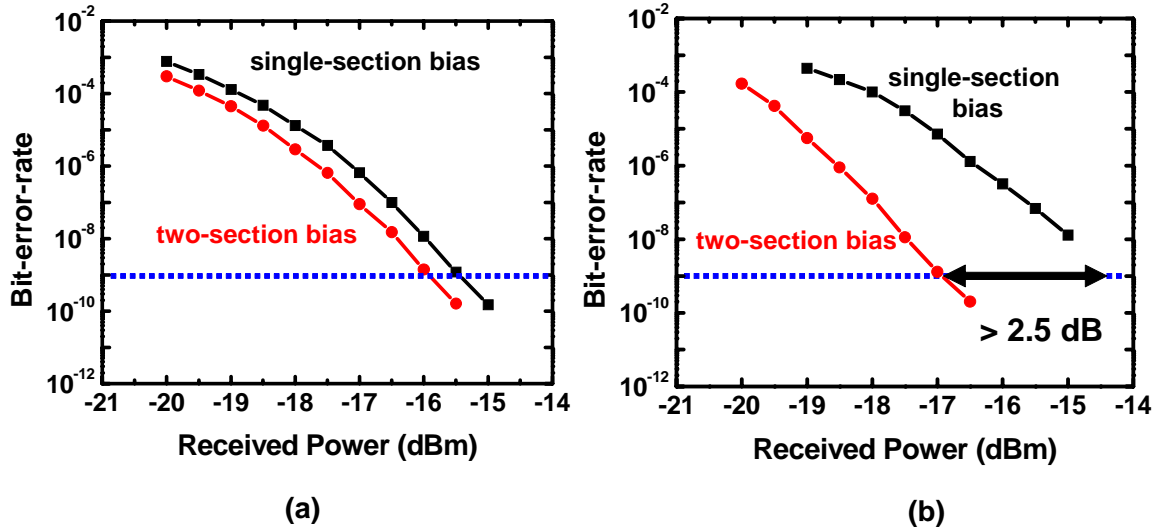


Figure 5-20. Measured BER performances: (a) back-to-back measurement; (b) 80-km fiber transmission.

5.7 Summary

We have fabricated various types of multi-section DFB lasers to achieve monolithic optical injection locking. We have systematically investigated the device parameters, and found that a strong grating is required to attain independent lasing of the two laser sections. By properly controlling the bias currents on both sections, mutual injection locking is achieved. The resonance frequency of the laser was increased from 11 GHz to 23 GHz. The 2HD at 9 GHz range is suppressed by 15 dB due to the increased resonance frequency. A 3-dB improvement of SFDR at 7-GHz has been achieved. In addition to the

suppression of nonlinear distortions and increase of the SFDR, the two-section DFB laser exhibits enhanced modulation response at 20 GHz due to the increased resonance frequency. Chirp reduction is also demonstrated by the two-section DFB lasers. An improvement of more than 2.5 dB in receiver sensitivity has been demonstrated at a data rate of 10 Gb/s after 80-km of fiber transmission. The monolithic mutually injection-locked lasers can be mounted in standard laser packages, and can be employed to improve the performance of directly modulated links.

Chapter 6 Applications of Multi-Section Distributed Feedback (DFB) Lasers

In this chapter, we discuss two applications of the multi-section DFB lasers. The first is large-signal analog modulation with high optical extinction ratio. The multi-section lasers operating in monolithic injection locking regime enable a large optical extinction ratio (> 12 dB) with DC to 2-GHz bandwidth. The optical extinction ratio is 6 dB higher than that of the free-running laser. The second application is optical generation of millimeter-waves using harmonic injection locking in multi-section DFB lasers. We demonstrate the generation of 30-GHz millimeter-waves with a phase noise of -103.8 dBc/Hz at 100-kHz offset.

6.1 Optical Extinction Ratio Improvement Using Directly-Modulated Two-Section DFB Lasers

Large-signal analog modulations with high extinction ratio and GHz bandwidth are needed for active Laser Radar (LADAR) sensors, and infrared (IR) / radio-frequency (RF) scene generations, and analog or multi-level digital optical communication systems. Though a semiconductor laser can easily achieve an extinction ratio of 20 ~ 30 dB, its bandwidth is small at low output power. The relaxation oscillation frequency of a free-running laser is [99]

$$\omega_{R0} = \sqrt{\frac{AP_0}{\tau_p}} = \sqrt{\frac{1 + A\tau_p\Gamma_a N_{tr}}{\tau_n\tau_p} \left(\frac{I_0}{I_{th}} - 1\right)} \propto \sqrt{\left(\frac{I_0}{I_{th}} - 1\right)} \quad (6.1)$$

where A is differential gain, P_0 is photon density inside laser cavity, τ_p is photon lifetime, τ_n is carrier lifetime, Γ_a is the confinement factor, N_{tr} is the transparency carrier concentration, I_0 is the bias current, and I_{th} is the threshold current. Typical semiconductor lasers have a bandwidth of several GHz under normal bias condition (several times of threshold current). However, the modulation bandwidth and relaxation oscillation frequency become very low (\ll GHz) when it is biased near threshold to achieve high optical extinction ratio. Therefore it is not possible to achieve wide bandwidth (DC to ~ 2 GHz) and high extinction ratio simultaneously by direct modulation of semiconductor lasers.

As mentioned earlier, strong optical injection locking has significantly improved the dynamic response of directly modulated semiconductor lasers, including enhancing the resonance frequencies [36, 39-42], suppressing nonlinear distortions [12, 43] and relative intensity noise [10, 48], and reducing chirp [5-7, 9]. Monolithic injection locking is an attractive approach to realize large-signal analog modulation. We have described the small-signal response of monolithic injection locked DFB lasers in Chapter 5. Here, we discuss the large-signal analog modulation of multi-section DFB lasers. Experimentally, we show that the large-signal analog extinction ratio at 2 GHz is improved from 6.8 dB to 12 dB by using a monolithic injection-locked DFB laser.

6.1.1 Link Requirements: Digital versus Analog Link

Large-signal modulation is usually used in digital optical links. Most RF and analog optical links employ small signal modulations. Some applications, such as LADAR and

IR/RF scene generation, do require large-signal analog modulation with very large extinction ratio (~ 60 dB) at GHz bandwidth. Their requirements are different from those of digital optical links, which need extinction ratios of approximately 20 dB but do not require high fidelity in their waveforms. Figure 6-1(a) and (b) illustrate the difference in digital and analog optical links.

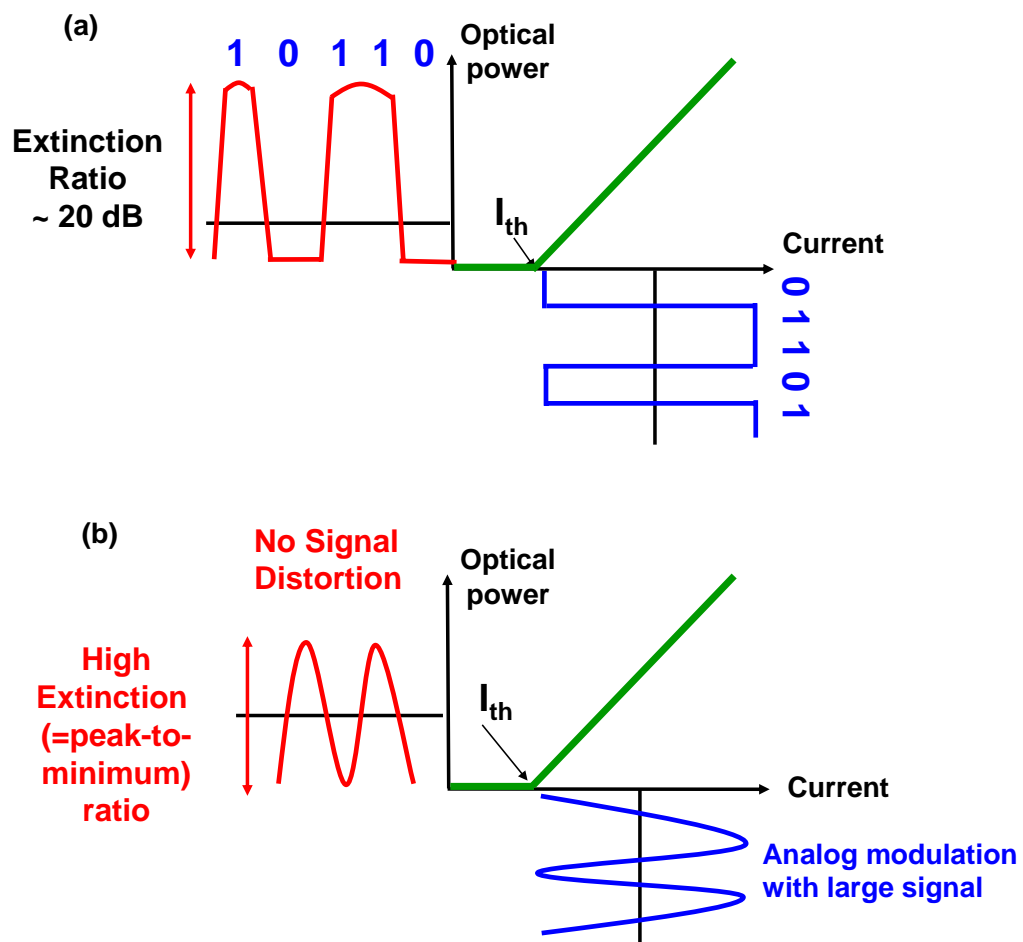


Figure 6-1. Schematic illustrating large-signal modulations with (a) digital and (b) analog signals.

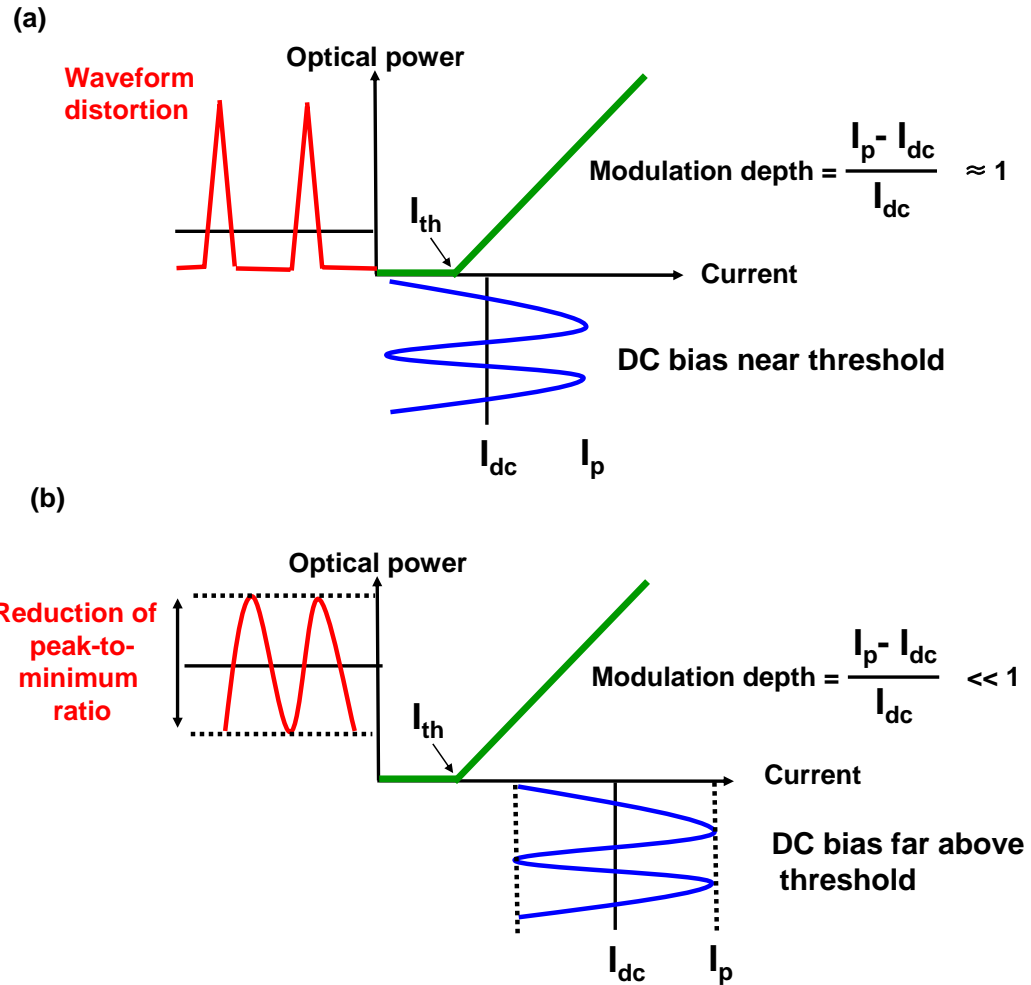


Figure 6-2. Challenges in directly-modulated lasers for analog signal transmission when the lasers are (a) DC-biased at low level and (b) DC-biased at high level.

Direct modulation of semiconductor lasers is desirable for these large-signal analog applications. However, there are some technical challenges, as illustrated in Figure 6-2. To achieve high extinction ratio, it is necessary to reduce the low light level. Biasing the laser around threshold, however, causes the laser to gain switch (Figure 6-2(a)), producing short optical pulses rather than analog waveforms with high fidelity. Biasing

the laser high above threshold, on the other hand, suffers from low extinction ratio, though analog waveforms could be better preserved (Figure 6-2(b)). In this section, we will present a solution by employing optical injection locking.

6.1.2 Measured Large-Signal Response of Directly-Modulated Lasers

Figure 6-3(a) and (b) show the temporal responses of a free-running laser under a large-signal sinusoidal modulation (RF power = 15 dBm) at 2 GHz when the laser is biased at 8.5 mA and 34.3 mA, respectively. At low bias (8.5 mA = $1.1 \cdot I_{th}$), the measured waveform shows a non-sinusoidal, gain-switched waveform because the large signal swings the laser below threshold and turn-on transients manifest as the laser attempts to swing above threshold. The frequency response below threshold is dramatically reduced due to a lack of photons within the slave laser. Though the extinction ratio is greater than 20 dB, the optical waveform is significantly distorted.

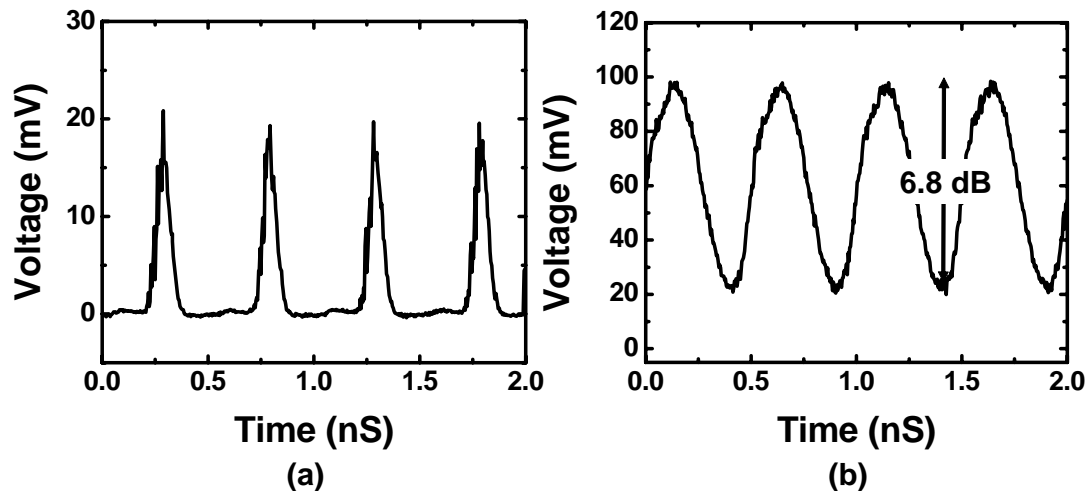


Figure 6-3. Temporal responses of a free-running laser. The laser is modulated by a large-sinusoidal signal at 2 GHz. The DC bias of the laser is (a) 8.5 mA and (b) 34.3 mA.

To achieve a more linear response at high frequencies, the bias current on the slave section is increased to 34.3 mA so that the laser is always above threshold. The measured waveform is shown in Figure 6-3(b). It shows an increase of DC value due to the higher DC current bias. The maximum extinction ratio measured for the free-running case is 6.8 dB. In injection-locked lasers, the turn-on transient of the directly-modulated lasers is significantly reduced because the injection from the master laser suppresses the spontaneous emission of the slave laser as well as increases its modulation bandwidth. Optical extinction ratio of 11.2 dB (Figure 6-4(b)) has been achieved, which is 4.4 dB better than the free-running case (Figure 6-3(b)).

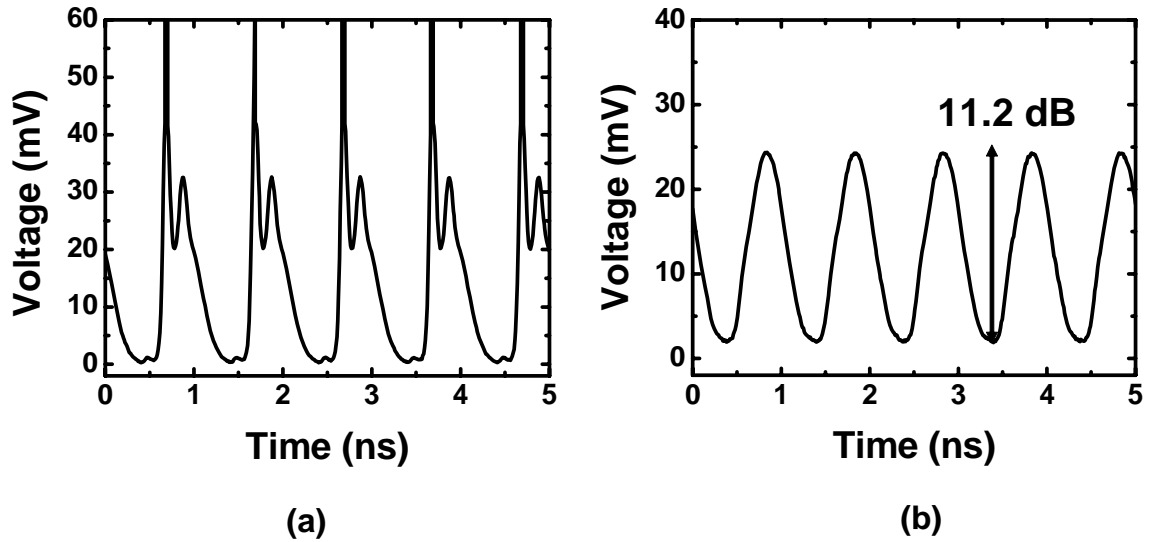


Figure 6-4. Temporal responses of (a) a free-running laser, and (b) an externally injection-locked laser with an injection ratio of -11 dB. The slave laser is DC-biased at $I = 1.5 \cdot I_{th}$ and modulated by a large- sinusoidal signal at 1 GHz.

6.1.3 Optical Extinction Ratio Improvement

To improve the large-signal analog response of the laser, we employ monolithic optical injection-locked DFB lasers with bent waveguides. The schematic of the three-section DFB laser with bent waveguide is shown in Figure 6-5. The three-section laser offers mutual injection locking between laser sections and on-chip control of frequency detuning. A strong DFB grating is employed to confine the photons locally in individual lasers. The κL product is approximately 4 for a cavity length of 500 μm . Since the two lasers are mutually locked, there is no clear distinction on which laser is master or slave. Here, the section with RF modulation will be called the slave laser (i.e., laser section 1, current biased at I_1), whereas the laser with DC bias called master laser (i.e., laser section 2, current biased at I_2). The master laser is further partitioned into two sections so we can tune its waveguide by differential biasing (I_2 and I_3).

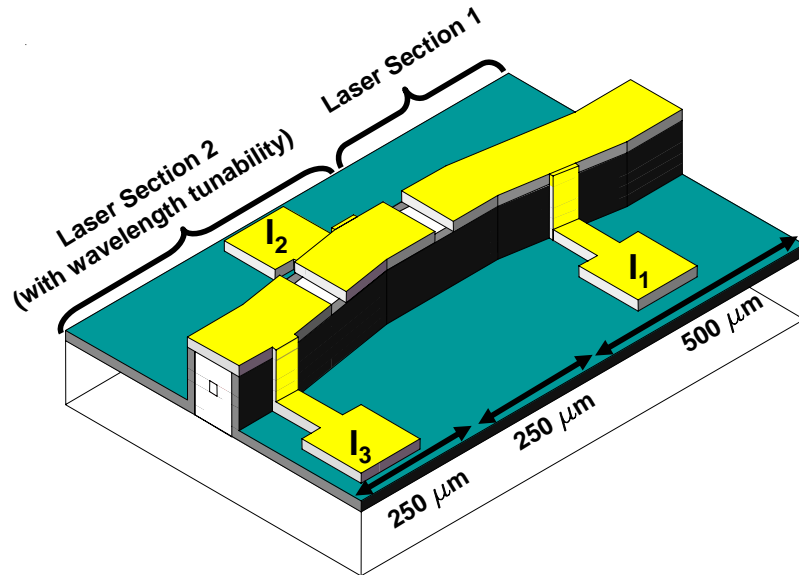


Figure 6-5. Three-section DFB laser for large-signal modulation with high extinction ratio.

The fabrication process of the three-section DFB lasers with bent waveguide is similar to that described in Section 5.2. Capped-mesa buried heterostructure (CMBH) is employed for the laser. It is grown by a three-step metal-organic chemical vapor deposition (MOCVD) growth. Another mesa ($\sim 10\text{-}\mu\text{m}$ wide) is patterned around the active strip to reduce the parasitic capacitance. Typical lithography and waveguide etching processes are followed by an electrical isolation etch of $0.2\text{-}\mu\text{m}$ depth between sections. The top metal contact is split into multiple sections. After etching the p^{++} layer between the sections, over $4\text{ k}\Omega$ of electrical isolation is achieved. In the device, each section operates as an independent laser because of the distributed feedback nature. By adjusting current bias on each section, it is possible to mutually lock two DFB lasers without an isolator between them. However, to achieve an optimum injection locking condition, it is necessary to adjust both the amplitude and detuning frequency of the injected signal. A tunable master laser with split contact is employed to control the detuning frequency.

Figure 6-6 shows measured optical spectrum of the mutually injection locked laser. An anti-reflection (AR) coating with a reflectivity of less than 0.1% is deposited on both facets to suppress the Fabry-Perot modes of the cavity. The output power is collected from the facet near the slave laser. When the bias current of the master section is set at $I_2 = 50\text{ mA}$ ($\sim 6 \cdot I_{th}$), the slave section current I_1 and wavelength tuning section current I_3 are set at 0 mA , the output power measured at the slave section is attenuated by the unbiased section closest to the output facet.

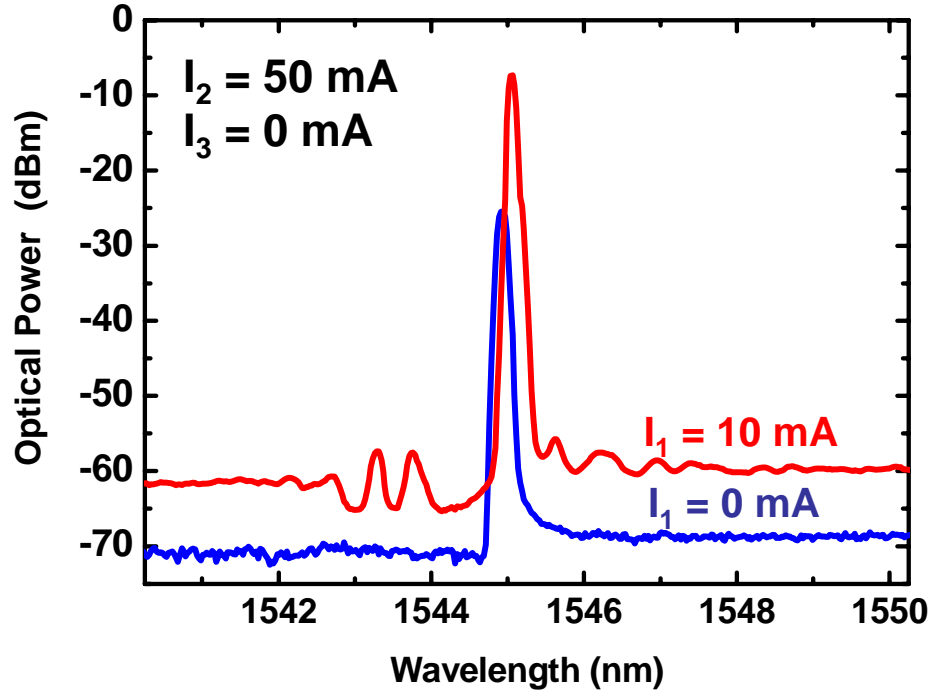


Figure 6-6. Measured optical spectrum from the facet near the slave section (= section 1).

When the slave section is biased slightly above threshold ($\sim 1.3 \cdot I_{th}$) at 10 mA with the same current for section 2 ($I_2 = 50$ mA), the output power increases by 17 dB due to the current injection in the slave section. However, the optical spectrum still shows single-mode lasing because the mode from the slave section is locked to the output of the master section. The lasing wavelength changes slightly towards longer wavelengths due to thermal effect.

Figure 6-7 shows the measured light-versus-current (L-I) curve when the bias current of the master section is maintained at 50 mA. The output power of the slave section varies linearly from the bias current from 1 to 16 mA. As shown in the DC L-I curve, up to 17-dB extinction ratio can be obtained by modulating the current of the slave

section. The abrupt power changing at $I_1 = 17$ mA is due to multimode lasing. The intensity contour plot is also measured for various I_1 and I_2 , and shown Figure 6-8. Greater than 20-dB extinction ratio can be obtained when I_1 is varied from 3 mA to 20 mA while I_2 is kept constant at 20 mA.

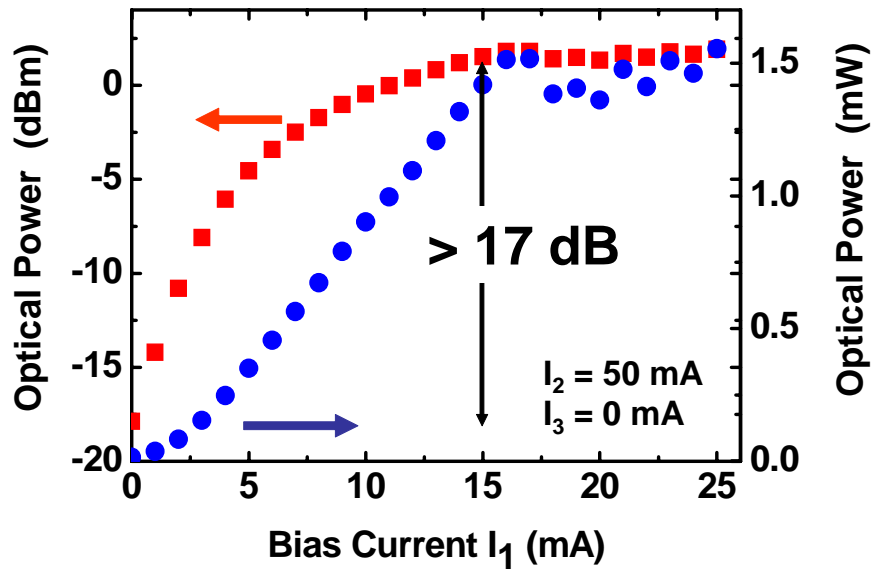


Figure 6-7. Measured light-versus-current curve of the monolithic optical injection-locked DFB laser with bent waveguide. The optical power is shown in both logarithmic (left) and linear (right) scales. The master section current, I_2 , is maintained at 50 mA and tuning section current, $I_3 = 0$ mA.

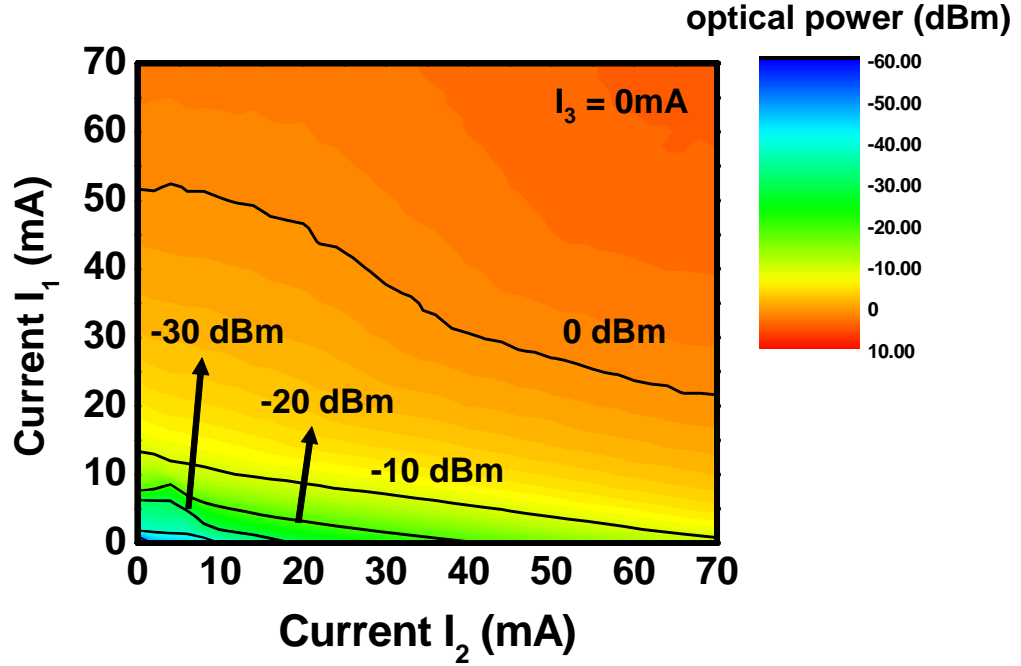


Figure 6-8. Intensity contour plot as a function of bias currents I_1 and I_2 . Current bias for wavelength tuning is fixed at 0 mA. ($I_3 = 0$ mA)

Figure 6-9(a) shows the measured small-signal modulation responses of the free-running laser. The current bias on the section 2 ($= I_2$) is set at 0 mA while the current bias on section 1 ($= I_1$) is varied. Because the threshold current is ~ 9 mA, the laser can respond when the bias level is above threshold. When $I_2 = 50$ mA, the modulation bandwidth is increased dramatically. Figure 6-9 (b) shows the frequency responses for various slave currents from 0 to 10 mA. When the slave laser is below threshold (2 mA), it is essentially an LED and its bandwidth is very small. As soon as the slave laser is biased slightly above threshold (5 mA), the bandwidth is greater than 2 GHz. At higher bias (> 10 mA), the bandwidth is higher than 5 GHz. Therefore, the extinction ratio for wide frequency operation (kHz to 2 GHz) for this monolithic injection locked laser is about 14 dB (for slave laser current from 3 to 15 mA).

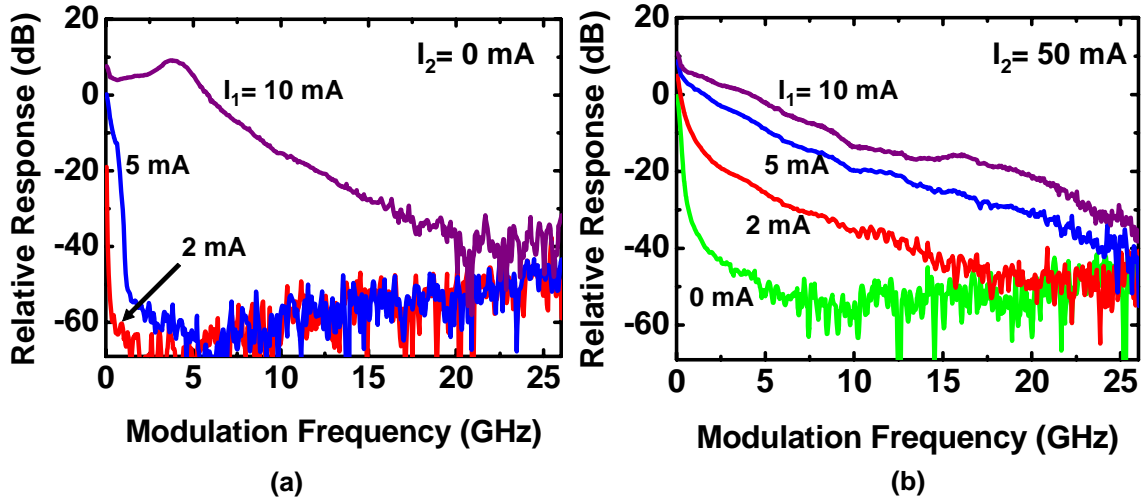


Figure 6-9. Measured small-signal frequency responses for various I_1 . I_2 is fixed at (a) 0 mA, and (b) 50 mA.

The dynamic response of the mutually injection-locked laser under large signal modulation is shown in Figure 6-10. The master section is biased at 50 mA and the slave section is biased at 8.5 mA with the same RF-modulation power (15 dBm) and frequency (2 GHz). The measured extinction ratio of the output waveform is increased to 12 dB, with improved linearity and noise. It should be noted that the free-running laser used for the measurement in Figure 6-3 is actually the slave laser with the master sections unbiased so the waveform in Figure 6-10 can be directly compared with those in Figure 6-3. The increased extinction ratio is achieved because the injected master section light provides a reservoir of photons to the slave section, allowing it to be modulated below its free-running threshold. Therefore, in the injection-locked state, the DC output can be reduced to achieve large extinction ratio while maintaining linearity and modulation bandwidth.

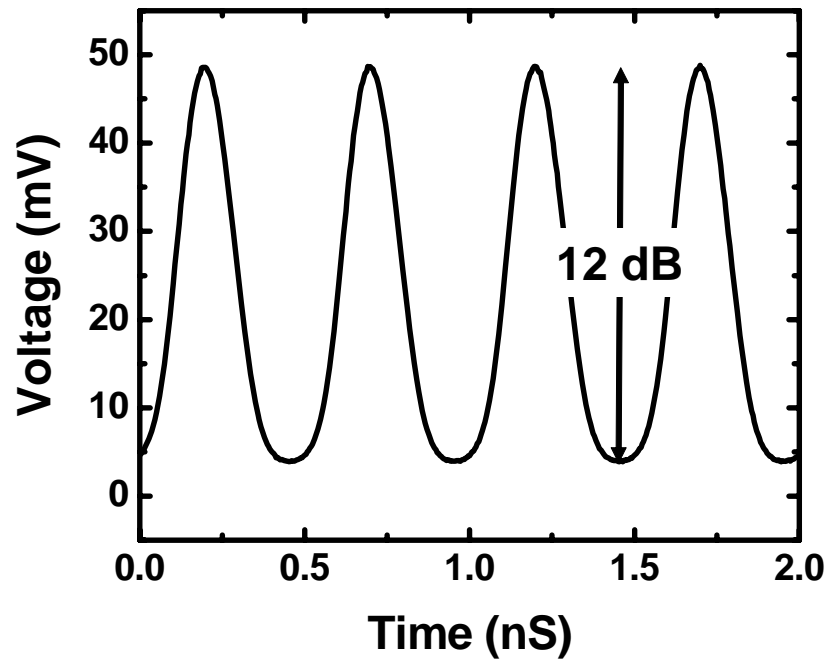


Figure 6-10. Measured time domain waveform of the mutually injection-locked laser. $I_1 = 8.5$ mA, $I_2 = 50$ mA and $I_3 = 0$ mA. The laser is modulated by an RF source with 15-dBm output power at 2 GHz.

6.2 Optical Generation of a Millimeter-Wave Signal Using Sideband Injection Locking in a Two-Section DFB Laser

Optical generation of millimeter-wave has attracted much attention because of its flexibility and applicability in broadband mobile communication systems and optical beam forming [17, 62, 63]. Specifically, sideband injection locking technique using a master and a slave laser is promising for generating millimeter-wave, since it is simple to implement and has high tunability. It often requires two or more light sources - a master laser and a slave laser, or a master laser and two slave lasers [17, 18, 60-63]. Recently, sub-harmonic locking for millimeter-wave generation has been extended to injection locking of passively mode-locked DBR lasers [64] and two-section DFB lasers [65, 66]. In this section, we experimentally investigate the optical millimeter wave generation using two-section DFB lasers introduced in Section 5.2. By using the two-section DFB lasers, we have successfully achieved the optical generation of millimeter wave with high power and signal purity, exhibiting a phase noise of -103.8 dBc/Hz at 100-kHz offset from 30 GHz.

6.2.1 Principles of Optical Millimeter-Wave Generation

Figure 6-11 shows the schematic of optical millimeter-wave generation using injection locking. The lasers are used in this scheme: one master and two slave lasers. The wavelengths of the two slave lasers are spaced near the target frequency, $(m+k)f_{\text{RF}}$, which is an integral multiple of the RF modulation frequency of the master laser. Coherence between the slave lasers is required to generate a low phase noise signal.

Goldberg *et al.* [61] achieved the coherence by injecting modulation sidebands from a master laser into the slave lasers. Since all modulation sidebands from the master laser are coherent, coherence between the slave modes are accomplished when each slave laser is locked to one of the modulation sidebands.

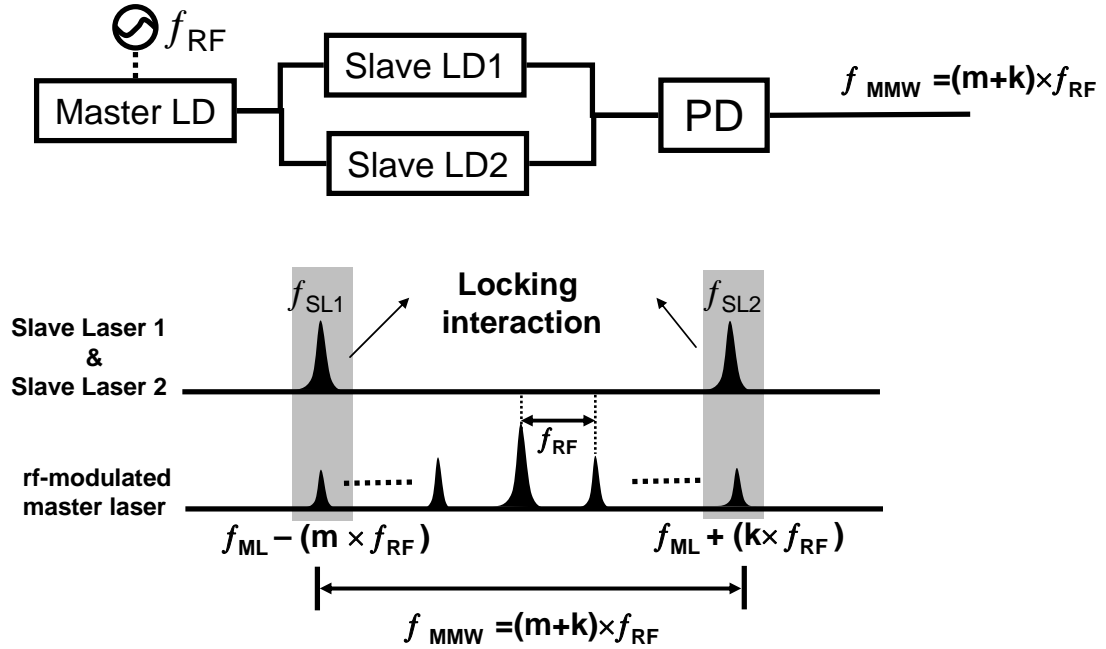


Figure 6-11. Schematic of optical injection locking for millimeter-wave generation.

Because of the strong gratings in our two-section DFB lasers described in Chapter 5, individual section lases on its own, resulting in two distinctive wavelengths similar to those of the two slave lasers in Figure 6-11. Figure 6-12(a) and (b) shows the conceptual diagram on sideband locking in two-section DFB lasers. Here, the section with RF modulation will be referred to the slave laser, and laser section with DC bias the master laser.

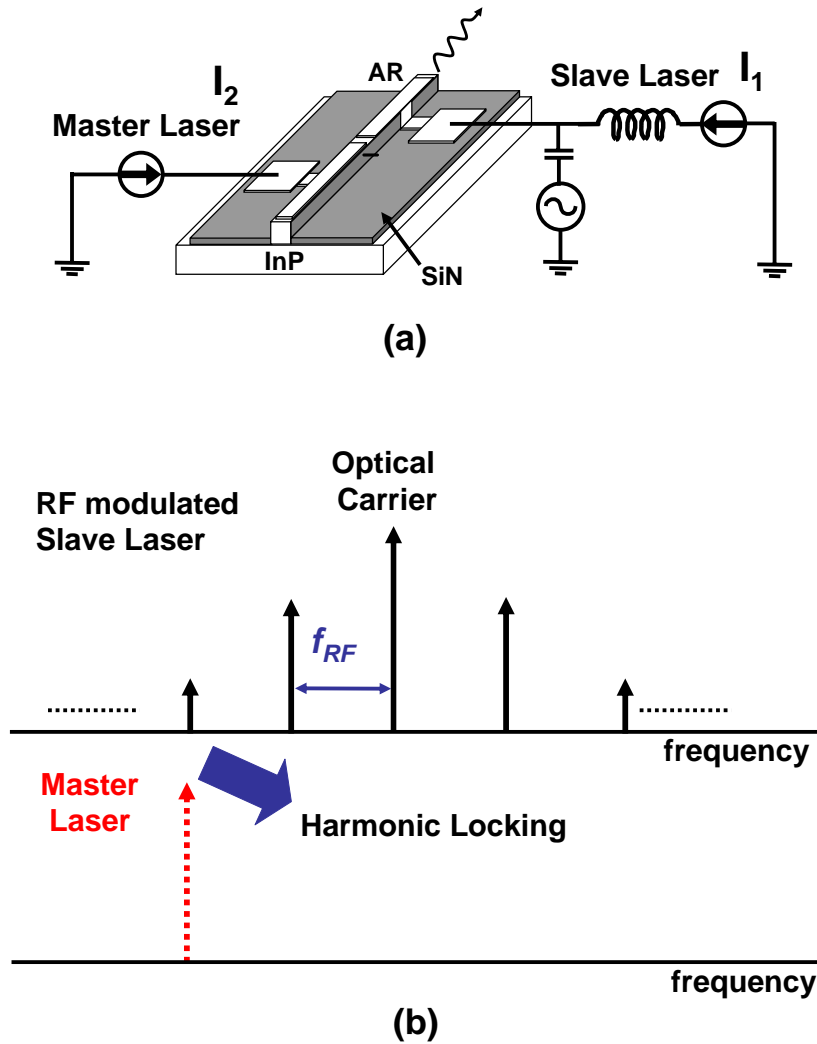


Figure 6-12. (a) Two-section DFB laser used for millimeter-wave generation. (b) Concept of optical millimeter-wave generation by sideband locking in a monolithic laser.

6.2.2 Experimental Results

The optical spectrum of the two-section DFB laser is shown in Figure 6-13 measured by a scanning F-P etalon. A stable laser is used as a reference for the scanning F-P etalon. It is not involved in injection locking. The slave section is biased at 65 mA and master section is bias at 25 mA. The relative frequency of the master section and slave section is

-17.6 GHz and 7.6 GHz, respectively. The beating generates an RF frequency at 25.2 GHz. Other RF frequencies are generated from the beating between the reference laser and the slave laser/master lasers. We change the current bias on the master section while fixing the bias at the slave section. The frequencies of both sections vary continuously, as shown in Figure 6-14.

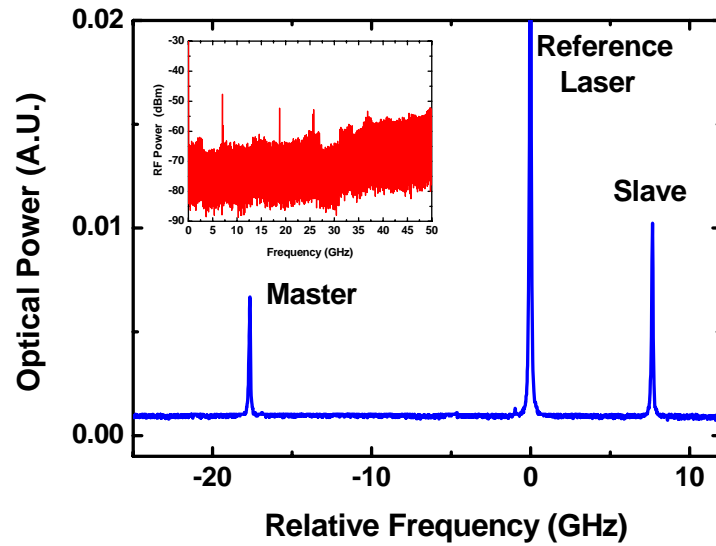


Figure 6-13. Measured optical spectrum. Inset is a measured RF spectrum.

The RF spectrum in Figure 6-15(a) shows a broad peak at ~ 36 GHz resulting from the beating between the master and the slave wavelengths. The slave section is biased at 45.2 mA and the master at 69 mA. The beat signal appears noisy because each section operates independently from each other with random phase difference. To generate a pure 36-GHz microwave signal with high power, the slave laser section is modulated by a 12-GHz RF signal. The third sideband of the modulated slave laser is locked to the master laser. This establishes the phase coherence between the primary modes of the master and slave laser. The beating of these two main modes generates a stable 36-GHz signal as

shown in Figure 6-15(b). In Figure 6-16, a 30-GHz millimeter-wave signal is generated by tuning the master current and modulating slave section by 15-GHz RF signal ($I_1 = 45.2$ mA, $I_2 = 64$ mA). Under the fixed bias condition on both sections ($I_1 = 45.2$ mA, $I_2 = 64$ mA), optically generated millimeter-wave signal can be tuned by varying the RF modulation frequency.

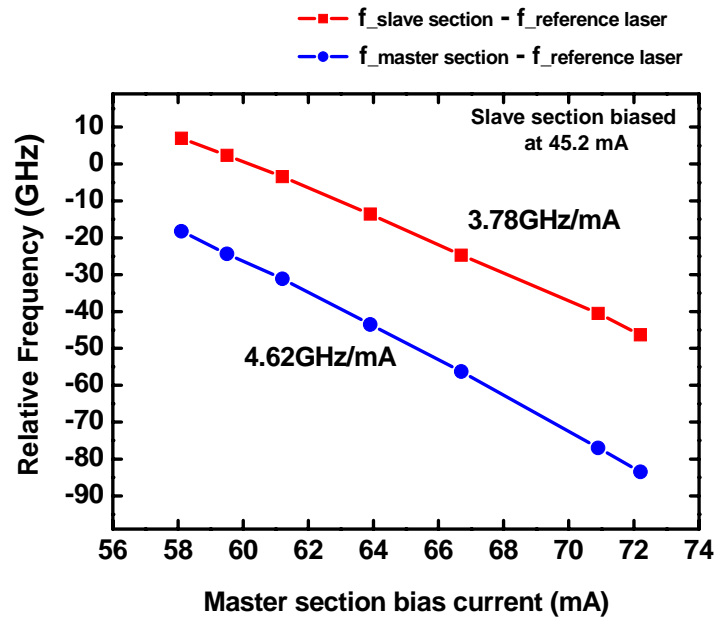


Figure 6-14. Measured relative frequencies of the master and slave sections when the master current is tuned from 58 to 72 mA.

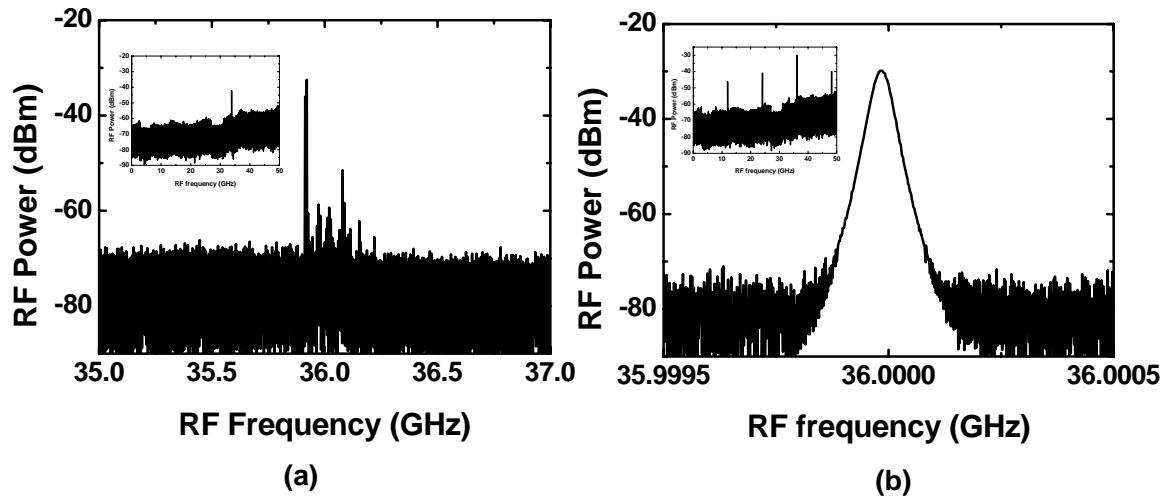


Figure 6-15. Optically generated millimeter-waves (a) without and (b) with a 12-GHz modulation on the slave section. ($I_1 = 45.2$ mA and $I_2 = 69$ mA). Insets are RF spectra measured in 50-GHz span.

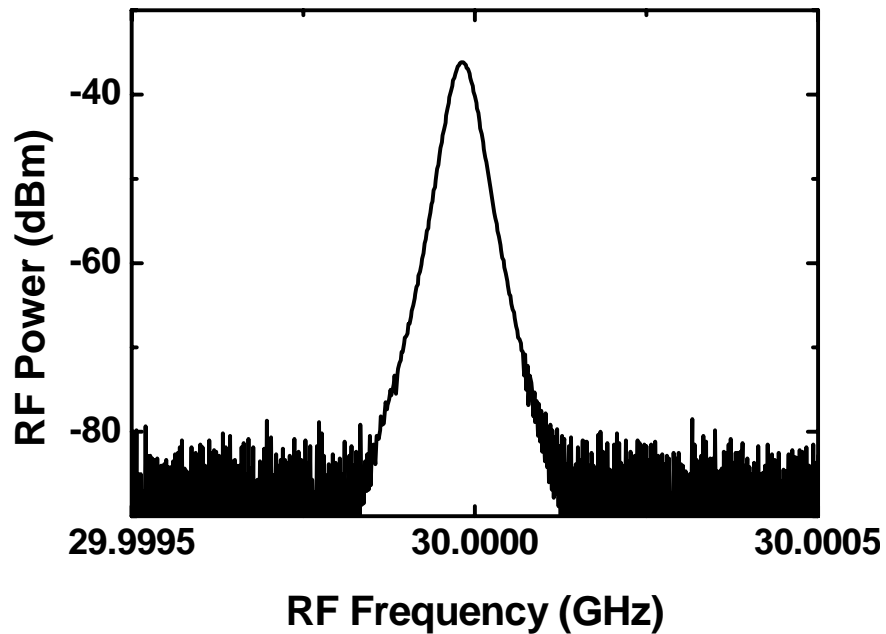


Figure 6-16. Optically generated millimeter-wave signal at 30 GHz by tuning the bias current on the master section ($I_1 = 45.2$ mA, $I_2 = 64$ mA). The modulation frequency on the slave laser is 15 GHz.

As shown in Figure 6-17(a), a millimeter-wave signal is generated at 31.2 GHz by 15.6-GHz RF modulation. However, when the RF modulation is changed to 15.8 GHz, sideband locking is no longer sustained, so that the incoherent beating is observed at ~ 30 GHz.

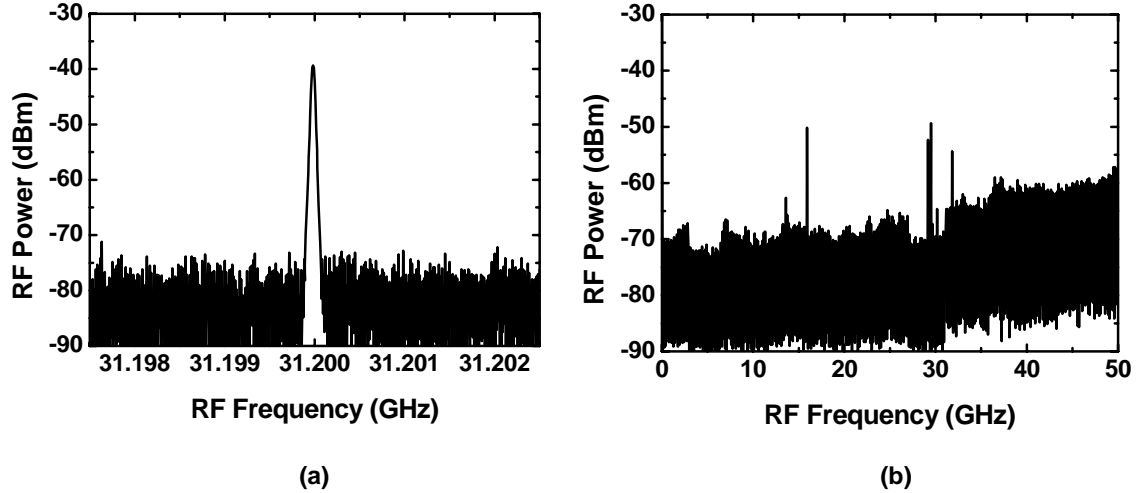


Figure 6-17. RF spectra showing the tunability by changing RF modulation frequency. (a) 15.6-GHz RF modulation (b) 15.8-GHz RF modulation. Bias conditions are same as in Figure 6-16. ($I_1 = 45.2$ mA, $I_2 = 64$ mA)

The phase noise of the generated millimeter-wave has been measured as shown in Figure 6-18. High frequency beat signals of 30 GHz are observed with a low phase noise of -103.8 dBc/Hz at 100-kHz frequency offset. The optically generated millimeter-wave exhibits a slight degradation of a phase noise by 5 ~ 10 dB compared with the RF source used for the RF modulation.

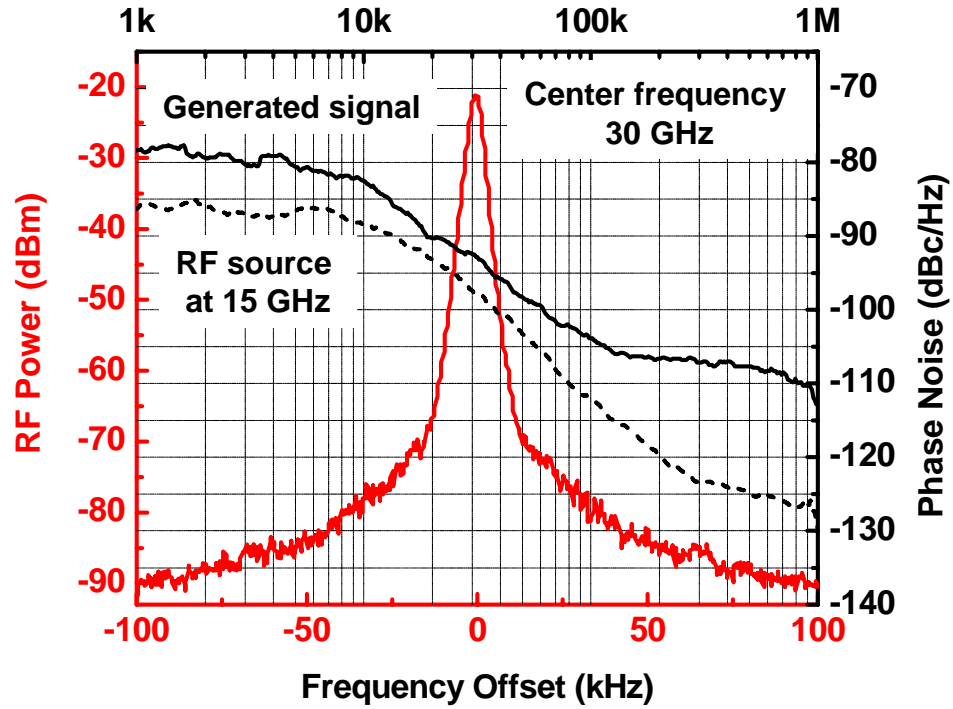


Figure 6-18. Measured phase noise at a 30-GHz millimeter-wave signal.

6.2.3 Summary

Optical generation of millimeter-wave is demonstrated by a simple device and modulation scheme. The fabricated two-section DFB lasers for mutual locking are used for optical sources under independent lasing condition. Coherence between the two independent wavelengths is achieved by RF-modulating one of gain sections. By adjusting the bias currents of each laser section and varying the RF modulation frequency, we realized a simple and environmentally robust millimeter-wave generation system.

Chapter 7 Future Directions and Conclusions

7.1 Futures Directions

7.1.1 Opto-Electronic Oscillators Using Strong Optical Injection locking

Opto-electronic oscillators (OEOs) are capable of generating RF signals with very low phase noise [100, 101]. The low phase noise is achieved through an optical delay in a low-loss optical fiber loop, resulting in a high quality factor (Q). Figure 7-1(a) shows the schematic of a standard OEO. It consists of a light source, an optical modulator, an RF amplifier, and an electric filter. Phase noises lower than best electronic oscillators have been demonstrated at 10 GHz. However, scaling to higher frequencies (> 50 GHz) is limited by the bandwidth of optical modulators and electrical amplifier.

To overcome the limitations, the electro-optic modulator in the OEO can be replaced by a strong optical injection-locked laser, as shown in Figure 7-1(b). Efficient modulation can be achieved at the enhanced resonance frequency. This may eliminate the need for high-frequency RF amplifiers and optical modulators in the standard OEO loop. Low phase noise can be achieved through fiber loop as in the standard OEO. With strong optical injection locking (injection ratio ~ 10 to 20 dB), we believe it is possible to achieve oscillation at 60-90 GHz, or even beyond 100 GHz.

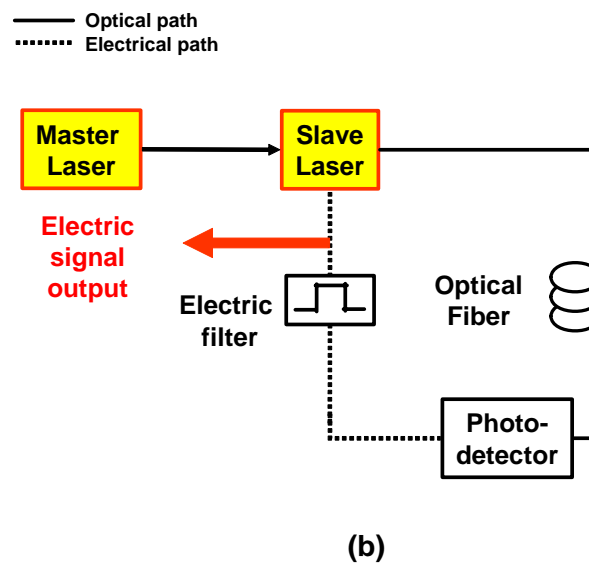
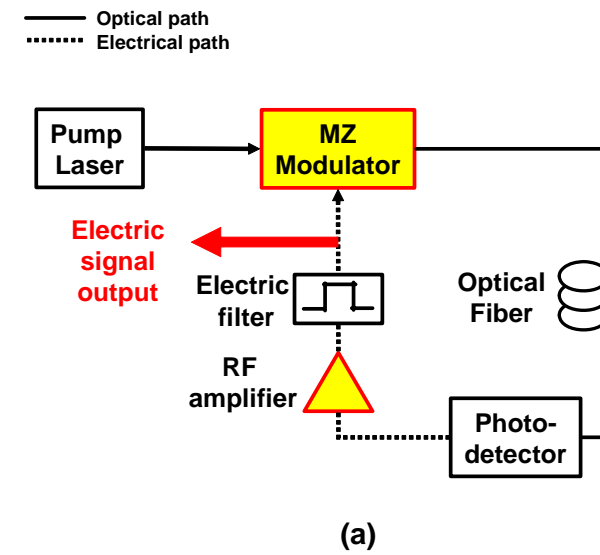


Figure 7-1. Schematic of (a) standard OEO and (b) OEO using ultra-strong injection-locked lasers.

7.1.2 Two-Section Laser Array Integrated with Electroabsorption Modulator

To achieve high optical extinction ratio (65 dB) needed for Laser Radar (LADAR) sensors, and infrared (IR) / radio-frequency (RF) scene generation applications (Section 6.1.3), we can integrate the mutually-locked DFB lasers with electroabsorption modulators (EAMs). These devices can potentially be monolithically integrated to form an analog optical source array, as shown in Figure 7-2.

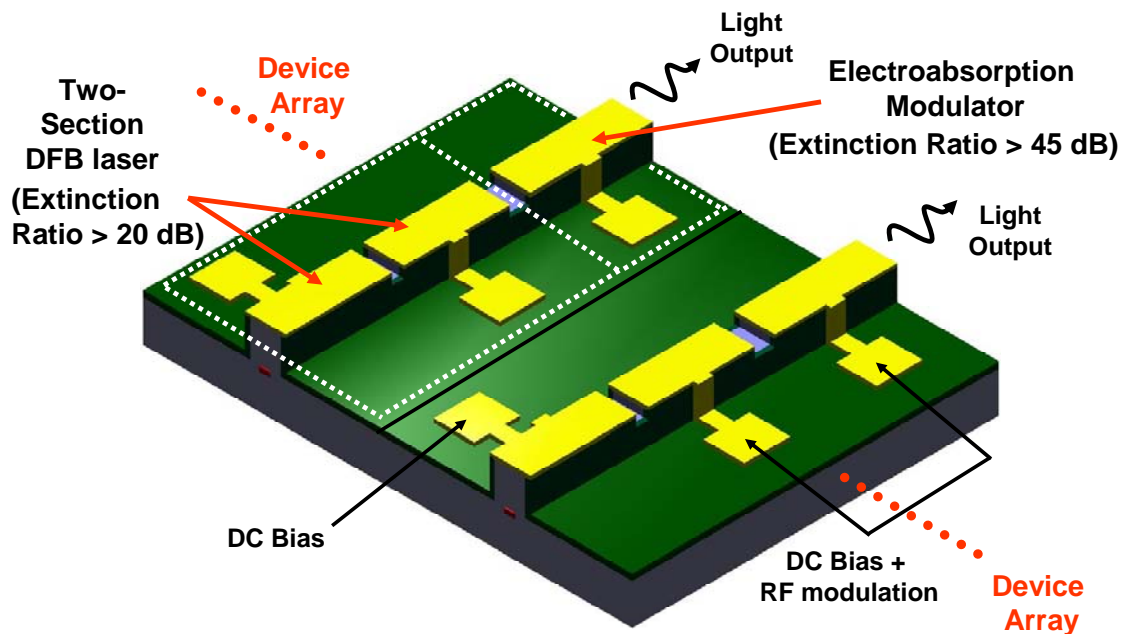


Figure 7-2. Schematic of monolithic analog optical source array comprising two-section DFB lasers and electroabsorption modulators.

The IR/RF scene generator requires a large number of analog optical sources (e.g., 1000x1000), so monolithic integration of sub-array would be indispensable. Typical EAMs used in digital links have extinction ratios of 20 dB. By employing longer length and other optimization for reducing leakage of amplified spontaneous emission from the integrated laser, it is possible to achieve 45-dB extinction ratio. Together with the 20 dB from the mutually injection locked DFB lasers, the overall extinction ratio of the integrated source array could satisfy the required 65 dB.

7.2 Conclusions

In this dissertation, the physical properties, performances, and applications of strong injection-locked distributed feedback (DFB) lasers with various injection locking configurations have been presented. In the first part of the dissertation, strong injection locking with an external master laser is investigated. The measured frequency responses under ultra-strong optical injection locking ($R \sim 10$ dB) exhibit three distinctive modulation characteristics, controllable by the frequency detuning between the master and the free-running lasers. This is confirmed both experimentally and theoretically. By increasing injection ratio and optimizing the frequency detuning, we have experimentally achieved a broad 3-dB bandwidth of 33 GHz and a high-resonance frequency of 31 GHz with a narrowband RF efficiency enhancement of 13 dB.

Under strong injection locking, we have found that the directly-modulated slave laser exhibits asymmetric modulation sidebands. The asymmetry originates from the resonant amplification of the modulation sideband on the longer wavelength side, coinciding with the shifted cavity mode of the slave laser. Taking advantage of this asymmetry, optical single sideband modulation with > 10 -dB asymmetry has been

achieved by direct modulation. The dispersion-limited RF bandwidth has been greatly increased to over 20 GHz after transmission through 80-km fibers.

Optical injection locking technique has been combined with gain-lever modulation in distributed Bragg reflector (DBR) lasers to further improve the RF performance. Experimentally, we have achieved 10-dB enhancement of the AM modulation efficiency, 3x increase of the modulation bandwidth, and 15-dB suppression of the third-order inter-modulation distortion.

Although optical injection-locked lasers exhibit superior performances over free-running lasers, two separate lasers are required. We have attempted to integrate both the master and the slave lasers on the same substrate using multi-section DFB lasers. Mutual injection locking has been successfully demonstrated experimentally. When biased at proper current ranges, the laser operates at a single wavelength and exhibits properties similar to injection locking with external master lasers. These include enhanced resonance frequency (22 GHz), improved SFDR (3 dB), and reduced chirp.

Potential applications of the mutually injection-locked DFB laser include LADAR and IR/RF scene generation. We have successfully demonstrated large-signal analog modulation with an optical extinction ratio of 15 dB and a modulation bandwidth of 2 GHz. Another application is optical generation of millimeter-wave. Using monolithic optical sideband injection locking, tunable millimeter-waves with low phase noise have been successfully generated.

The superior properties of optical injection-locked lasers, particularly those with large injection ratio (~ 20 dB), enable several new applications that were considered impossible by direct modulation. One such application is optoelectronic oscillators with

frequency greater than 50 GHz. Another is LADAR or IR/RF scene generation. Integration of mutual injection-locked lasers with electroabsorption modulators could satisfy the large optical extinction ratio (65 dB) requirement of these large-signal analog optical sources.

References

- [1] C. Henry, "Theory of the linewidth of semiconductor lasers," *IEEE J. Quantum Electron.*, vol. 18, no. 2, pp. 259-264, Feb. 1982.
- [2] P. Gallion, H. Nakajima, G. Debarge, and C. Chabran, "Contribution of spontaneous emission to the linewidth of an injection-locked semiconductor laser," *Electron. Lett.*, vol. 21, no. 14, pp. 626-628, Jul. 1985.
- [3] F. Mogensen, H. Olesen, and G. Jacobsen, "FM noise suppression and linewidth reduction in an injection-locked semiconductor laser," *Electronics Letters*, vol. 21, no. 16, pp. 696-697, Aug. 1985.
- [4] K. Iwashita and K. Nakagawa, "Suppression of mode partition noise by laser diode light injection," *IEEE Trans. Microw. Theory Tech.*, vol. 30, no. 10, pp. 1657-1662, Oct. 1982.
- [5] C. Lin and F. Mengel, "Reduction of frequency chirping and dynamic linewidth in high-speed directly modulated semiconductor lasers by injection locking," *Electron. Lett.*, vol. 20, no. 25-26, pp. 1073-1075, Dec. 1984.
- [6] C. Lin, J. K. Andersen, and F. Mengel, "Frequency chirp reduction in a 2.2 Gbit/s directly modulated InGaAsP semiconductor laser by CW injection," *Electron. Lett.*, vol. 21, no. 2, pp. 80-81, Jan. 1985.
- [7] N. Olsson, H. Temkin, R. Logan, L. Johnson, G. Dolan, J. van der Ziel, and J. Campbell, "Chirp-free transmission over 82.5 km of single mode fibers at 2 Gbit/s with injection locked DFB semiconductor lasers," *J. Lightw. Technol.*, vol. 3, no. 1, pp. 63-67, Feb. 1985.
- [8] S. Saito, F. Mogensen, and H. Olesen, "Effective bandwidth for FM noise suppression in an injection-locked semiconductor laser," *Electron. Lett.*, vol. 21, no. 24, pp. 1173-1175, Nov. 1985.
- [9] S. Mohrdiek, H. Burkhard, and H. Walter, "Chirp reduction of directly modulated semiconductor lasers at 10 Gb/s by strong CW light injection," *J. Lightw. Technol.*, vol. 12, no. 3, pp. 418-424, Mar. 1994.
- [10] T. B. Simpson, J. M. Liu, and A. Gavrielides, "Bandwidth enhancement and broadband noise reduction in injection-locked semiconductor lasers," *IEEE Photon. Technol. Lett.*, vol. 7, no. 7, pp. 709-711, Jul. 1995.
- [11] T. B. Simpson and J. M. Liu, "Modulation characteristics of injection-locked laser diodes," *Proceedings of the SPIE - The International Society for Optical Engineering* vol. 2844, pp. 72-83, 1996.
- [12] X. J. Meng, T. Chau, D. T. K. Tong, and M. C. Wu, "Suppression of second harmonic

- distortion in directly modulated distributed feedback lasers by external light injection," *Electron. Lett.*, vol. 34, no. 21, pp. 2040-2041, Oct. 1998.
- [13] X. J. Meng, D. T. K. Tong, C. Tai, and M. C. Wu, "Demonstration of an analog fiber-optic link employing a directly modulated semiconductor laser with external light injection," *IEEE Photon. Technol. Lett.*, vol. 10, no. 11, pp. 1620-1622, Nov. 1998.
 - [14] H. L. T. Lee, R. J. Ram, O. Kjebon, and R. Schatz, "Bandwidth enhancement and chirp reduction in DBR lasers by strong optical injection," *Conference on Lasers and Electro-Optics (CLEO 2000)*, pp. 99-100, May 2000.
 - [15] C.-H. Chang, L. Chrostowski, and C. J. Chang-Hasnain, "Injection locking of VCSELs," *IEEE J. Sel. Topics Quantum Electron.*, vol. 9, no. 5, pp. 1386-93, Sep./Oct. 2003.
 - [16] V. Annovazzi-Lodi, S. Donati, and M. Manna, "Chaos and locking in a semiconductor laser due to external injection," *IEEE J. Quantum Electron.*, vol. 30, no. 7, pp. 1537-1541, Jul. 1994.
 - [17] R. P. Braun, G. Grosskopf, R. Meschenmoser, D. Rohde, F. Schmidt, and G. Villino, "Microwave generation for bidirectional broadband mobile communications using optical sideband injection locking," *Electron. Lett.*, vol. 33, no. 16, pp. 1395-1396, Jul. 1997.
 - [18] L. Goldberg, H. F. Taylor, and J. F. Weller, "FM sideband injection locking of diode lasers," *Electron. Lett.*, vol. 18, no. 23, pp. 1019-20, Nov. 1982.
 - [19] K. Inoue and M. Yoshino, "Bistability and waveform reshaping in a DFB-LD with side-mode light injection," *IEEE Photon. Technol. Lett.*, vol. 7, no. 2, pp. 164-166, Feb. 1995.
 - [20] S. Kobayashi and T. Kimura, "Optical phase modulation in an injection locked AlGaAs semiconductor laser," *IEEE Trans. Microw. Theory Tech.*, vol. 82, no. 10, pp. 1650-1657, Oct. 1982.
 - [21] S. Kobayashi and T. Kimura, "Optical FM signal amplification by injection locked and resonant type semiconductor laser amplifiers," *IEEE J. Quantum Electron.*, vol. 18, no. 4, pp. 575-581, Apr. 1982.
 - [22] X. Lixin, W. H. Chung, L. Y. Chan, L. F. K. Lui, P. K. A. Wai, and H. Y. Tam, "Simultaneous all-optical waveform reshaping of two 10-Gb/s signals using a single injection-locked Fabry-Perot laser diode," *IEEE Photon. Technol. Lett.*, vol. 16, no. 6, pp. 1537-1539, Jun. 2004.
 - [23] Y. Onishi and F. Koyama, "Analysis of all-optical regeneration using an injection locked two-mode surface-emitting laser," *The 5th Pacific Rim Conference on Lasers and Electro-Optics (CLEO/Pacific Rim)*, vol. 1, pp. 85, 2003.
 - [24] T. B. Simpson and F. Doft, "Double-locked laser diode for microwave photonics applications," *IEEE Photon. Technol. Lett.*, vol. 11, no. 11, pp. 1476-1478, Nov. 1999.
 - [25] T. B. Simpson, J. M. Liu, A. Gavrielides, V. Kovanis, and P. M. Alsing, "Period-doubling

- route to chaos in a semiconductor laser subject to optical injection," *Appl. Phys. Lett.*, vol. 64, no. 26, pp. 3539-3541, Jun. 1994.
- [26] T. B. Simpson, J. M. Liu, A. Gavrielides, V. Kovanis, and P. M. Alsing, "Period-doubling cascades and chaos in a semiconductor laser with optical injection," *Phys. Rev. A*, vol. 51, no. 5, pp. 4181-4185, May 1995.
 - [27] R. Adler, "A study of locking phenomena in oscillators," *Proc. IRE*, vol. 34, pp. 351-357, 1946.
 - [28] H. L. Stover and W. H. Steier, "Locking of laser oscillators by light injection," *Appl. Phys. Lett.*, vol. 8, no. 4, pp. 91-93, Feb. 1966.
 - [29] S. Kobayashi and T. Kimura, "Injection locking characteristics of an AlGaAs semiconductor laser," *IEEE J. Quantum Electron.*, vol. 16, no. 9, pp. 915-917, Sep. 1980.
 - [30] H. Toba, Y. Kobayashi, K. Yanagimoto, H. Nagai, and M. Nakahara, "Injection-locking technique applied to a 170 km transmission experiment at 445.8 Mbit/s," *Electron. Lett.*, vol. 20, no. 9, pp. 370-371, Apr. 1984.
 - [31] J. Wang, M. K. Haldar, L. Li, and F. V. C. Mendis, "Enhancement of modulation bandwidth of laser diodes by injection locking," *IEEE Photon. Technol. Lett.*, vol. 8, no. 1, pp. 34-36, Jan. 1996.
 - [32] G. Yabre, "Effect of relatively strong light injection on the chirp-to-power ratio and the 3 dB bandwidth of directly modulated semiconductor lasers," *J. Lightw. Technol.*, vol. 14, no. 10, pp. 2367-2373, Oct. 1996.
 - [33] J. M. Liu, H. F. Chen, X. J. Meng, and T. B. Simpson, "Modulation bandwidth, noise, and stability of a semiconductor laser subject to strong injection locking," *IEEE Photon. Technol. Lett.*, vol. 9, no. 10, pp. 1325-1327, Oct. 1997.
 - [34] T. B. Simpson and J. M. Liu, "Enhanced modulation bandwidth in injection-locked semiconductor lasers," *IEEE Photon. Technol. Lett.*, vol. 9, no. 10, pp. 1322-1324, Oct. 1997.
 - [35] X. J. Meng, C. Tai, and M. C. Wu, "Experimental demonstration of modulation bandwidth enhancement in distributed feedback lasers with external light injection," *Electron. Lett.*, vol. 34, no. 21, pp. 2031-2032, Oct. 1998.
 - [36] A. Murakami, K. Kawashima, and K. Atsuki, "Cavity resonance shift and bandwidth enhancement in semiconductor lasers with strong light injection," *IEEE J. Quantum Electron.*, vol. 39, no. 10, pp. 1196-1204, Oct. 2003.
 - [37] S. K. Hwang, J. M. Liu, and J. K. White, "35-GHz intrinsic bandwidth for direct modulation in 1.3- μ m semiconductor lasers subject to strong injection locking," *IEEE Photon. Technol. Lett.*, vol. 16, no. 4, pp. 972-974, Apr. 2004.
 - [38] H.-K. Sung, T. Jung, M. C. Wu, D. Tishinin, K. Y. Liou, and W. T. Tsang, "Optical Injection-

- Locked Gain-Lever Distributed Bragg Reflector Lasers with Enhanced RF Performance," *International Topical Meeting on Microwave Photonics (MWP)*, pp. 225-228, 2004.
- [39] E. K. Lau, H. K. Sung, and M. C. Wu, "Ultra-High, 72 GHz Resonance Frequency and 44 GHz Bandwidth of Injection-Locked 1.55- μ m DFB Lasers,," *Optical Fiber Communication Conference (OFC)*, Mar. 2006.
- [40] C. H. Henry, N. A. Olsson, and N. K. Dutta, "Locking range and stability of injection locked 1.54 μ m InGaAsP semiconductor lasers," *IEEE J. Quantum Electron.*, vol. 21, no. 8, pp. 1152-1156, Aug. 1985.
- [41] T. B. Simpson, J. M. Liu, K. F. Huang, K. Tai, C. M. Clayton, A. Gavrielides, and V. Kovanis, "Cavity enhancement of resonant frequencies in semiconductor lasers subject to optical injection," *Phys. Rev. A*, vol. 52, no. 6, pp. R4348-51, Dec. 1995.
- [42] L. Chrostowski, X. Zhao, C. J. Chang-Hasnain, R. Shau, M. Ortsiefer, and M. C. Amann, "50-GHz Optically Injection-Locked 1.55- μ m VCSELs," *IEEE Photon. Technol. Lett.*, vol. 18, no. 2, pp. 367-369, Jan. 2006.
- [43] X. J. Meng, T. Chau, and M. C. Wu, "Improved intrinsic dynamic distortions in directly modulated semiconductor lasers by optical injection locking," *IEEE Trans. Microw. Theory Tech.*, vol. 47, no. 7, pp. 1172-1176, Jul. 1999.
- [44] L. Chrostowski, X. Zhao, and C. J. Chang-Hasnain, "Microwave Performance of Optically Injection-Locked VCSELs," *IEEE Trans. Microw. Theory Tech.*, vol. 54, no. 2, pp. 788-796, Feb. 2006.
- [45] N. Schunk and K. Petermann, "Noise analysis of injection-locked semiconductor injection lasers," *IEEE J. Quantum Electron.*, vol. 22, no. 5, pp. 642-650, May 1986.
- [46] P. Spano, S. Piazzolla, and M. Tamburrini, "Frequency and intensity noise in injection-locked semiconductor lasers: Theory and experiments," *IEEE J. Quantum Electron.*, vol. 22, no. 3, pp. 427-435, Mar. 1986.
- [47] T. B. Simpson and J. M. Liu, "Spontaneous emission, nonlinear optical coupling, and noise in laser diodes," *Opt. Commun.*, vol. 112, no. 1-2, pp. 43-47, Nov. 1994.
- [48] L. Chrostowski, C. H. Chang, and C. Chang-Hasnain, "Reduction of relative intensity noise and improvement of spur-free dynamic range of an injection locked VCSEL," *16th Annu. Meeting IEEE Lasers and Electro-Optic Society (LEOS)*, vol. 2, pp. 706-707, Oct. 2003.
- [49] X. J. Meng, T. Jung, C. Tai, and M. C. Wu, "Gain and bandwidth enhancement of directly modulated analog fiber optic links using injection-locked gain-coupled DFB lasers," *International Topical Meeting on Microwave Photonics (MWP)*, pp. 141-144, Nov. 1999.
- [50] S. Weisser, E. C. Larkins, K. Czotscher, W. Benz, J. Daleiden, I. Esquivias, J. Fleissner, J. D. Ralston, B. Romero, R. E. Sah, A. Schonfelder, and J. Rosenzweig, "Damping-limited modulation bandwidths up to 40 GHz in undoped short-cavity In_{0.35}Ga_{0.65}As-GaAs multiple-

- quantum-well lasers," *IEEE Photon. Technol. Lett.*, vol. 8, no. 5, pp. 608-610, May 1996.
- [51] O. Kjebon, R. Schatz, S. Lourdudoss, S. Nilsson, B. Stalnacke, and L. Backbom, "30 GHz direct modulation bandwidth in detuned loaded InGaAsP DBR lasers at 1.55 μm wavelength," *Electron. Lett.*, vol. 33, no. 6, pp. 488-489, Mar. 1997.
 - [52] W. Kaiser, L. Bach, J. P. Reithmaier, and A. Forchel, "High-speed coupled-cavity injection grating lasers with tailored modulation transfer functions," *IEEE Photon. Technol. Lett.*, vol. 16, no. 9, pp. 1997-1999, Sep. 2004.
 - [53] S. K. Hwang, J. M. Liu, and J. K. White, "35-GHz modulation bandwidth in injection-locked semiconductor lasers," *16th Annu. Meeting IEEE Lasers and Electro-Optic Society (LEOS)*, pp. 710-711, 2003.
 - [54] L. Chrostowski, X. Zhao, C. J. Chang-Hasnain, R. Shau, M. Ortsiefer, and M. Amann, "50 GHz directly-modulated injection-locked 1.55- μm VCSELs," *Optical Fiber Communication Conference (OFC)*, vol. 4, pp. 338-340, Mar. 2005.
 - [55] C. Cox, III, E. Ackerman, R. Helkey, and G. E. Betts, "Direct-detection analog optical links," *IEEE Trans. Microw. Theory Tech.*, vol. 45, no. 8, pp. 1375-1383, Aug. 1997.
 - [56] C. H. Cox, III, E. I. Ackerman, G. E. Betts, and J. L. Prince, "Limits on the performance of RF-over-fiber links and their impact on device design," *IEEE Trans. Microw. Theory Tech.*, vol. 54, no. 2, pp. 906-920, Feb. 2006.
 - [57] T. E. Darcie, R. S. Tucker, and G. J. Sullivan, "Intermodulation and harmonic distortion in InGaAsP lasers," *Electron. Lett.*, vol. 21, no. 16, pp. 665-666, Aug. 1985.
 - [58] K. Y. Lau and A. Yariv, "Intermodulation distortion in a directly modulated semiconductor injection laser," *Appl. Phys. Lett.*, vol. 45, no. 10, pp. 1034-1036, Nov. 1984.
 - [59] L. Chrostowski, C. Chih-Hao, and C. J. Chang-Hasnain, "Enhancement of dynamic range in 1.55- μm VCSELs using injection locking," *IEEE Photon. Technol. Lett.*, vol. 15, no. 4, pp. 498-500, Apr. 2003.
 - [60] L. Goldberg, H. F. Taylor, J. F. Weller, and D. M. Bloom, "Microwave signal generation with injection-locked laser diodes," *Electron. Lett.*, vol. 19, no. 13, pp. 491-493, Jun. 1983.
 - [61] L. Goldberg, A. M. Yurek, H. F. Taylor, and J. F. Weller, "35 GHz microwave signal generation with an injection-locked laser diode," *Electron. Lett.*, vol. 21, no. 18, pp. 814-815, Aug. 1985.
 - [62] R. P. Braun, G. Grosskopf, D. Rohde, and F. Schmidt, "Low-phase-noise millimeter-wave generation at 64 GHz and data transmission using optical sideband injection locking," *IEEE Photon. Technol. Lett.*, vol. 10, no. 5, pp. 728-730, May 1998.
 - [63] L. Noel, D. Marcenac, and D. Wake, "Optical millimetre-wave generation technique with high efficiency, purity and stability," *Electron. Lett.*, vol. 32, no. 21, pp. 1997-1998, Oct. 1996.

- [64] Z. Ahmed, H. F. Liu, D. Novak, Y. Ogawa, M. D. Pelusi, and D. Y. Kim, "Locking characteristics of a passively mode-locked monolithic DBR laser stabilized by optical injection," *IEEE Photon. Technol. Lett.*, vol. 8, no. 1, pp. 37-39, Jan. 1996.
- [65] H. Jin and H. Rongqing, "Tunable millimeter-wave generation with subharmonic injection locking in two-section strongly gain-coupled DFB lasers," *IEEE Photon. Technol. Lett.*, vol. 12, no. 5, pp. 543-545, May 2000.
- [66] H.-K. Sung, T. Jung, M. C. Wu, D. Tishinin, K. Y. Liou, and W. T. Tsang, "Optical generation of millimeter-waves using monolithic sideband injection locking of a two-section DFB laser," *16th Annu. Meeting IEEE Lasers and Electro-Optic Society (LEOS)*, vol. 2, pp. 1005-1006, 2003.
- [67] J. M. Kahn, "1 Gbit/s PSK homodyne transmission system using phase-locked semiconductor lasers," *IEEE Photon. Technol. Lett.*, vol. 1, no. 10, pp. 340-342, Oct. 1989.
- [68] S. Kobayashi and T. Kimura, "Coherence on injection phase-locked AlGaAs semiconductor laser," *Electron. Lett.*, vol. 16, no. 7, pp. 668-670, Aug. 1980.
- [69] A. C. Bordonalli, C. Walton, and A. J. Seeds, "High-performance phase locking of wide linewidth semiconductor lasers by combined use of optical injection locking and optical phase-lock loop," *J. Lightw. Technol.*, vol. 17, no. 2, pp. 328-342, Feb. 1999.
- [70] T. Jung, S. Ji-Lin, D. T. K. Tong, S. Murthy, M. C. Wu, T. Tanbun-Ek, W. Wenshen, R. Lodenkamper, R. Davis, L. J. Lembo, and J. C. Brock, "CW injection locking of a mode-locked semiconductor laser as a local oscillator comb for channelizing broad-band RF signals," *IEEE Trans. Microw. Theory Tech.*, vol. 47, no. 7, pp. 1225, Jul. 1999.
- [71] W. Lee and P. J. Delfyett, Jr., "Optical heterodyne detection based on dual-mode injection locking of modelocked semiconductor lasers," *17th Annu. Meeting IEEE Lasers and Electro-Optic Society (LEOS)*, pp. 1005-1006, 2004.
- [72] W. Lee and P. J. Delfyett, "Dual-mode injection locking of two independent modelocked semiconductor lasers," *Electronics Letters*, vol. 40, no. 19, pp. 1182-1183, 2004.
- [73] W. Lee, M. Mielke, S. Etemad, and P. J. Delfyett, "Subgigahertz channel filtering by optical heterodyne detection using a single axial mode from an injection-locked passively mode-locked semiconductor laser," *IEEE Photon. Technol. Lett.*, vol. 16, no. 8, pp. 1945-1947, Aug. 2004.
- [74] B. K. Mathason and P. J. Delfyett, "Pulsed injection locking dynamics of passively mode-locked external-cavity semiconductor laser systems for all-optical clock recovery," *J. Lightw. Technol.*, vol. 18, no. 8, pp. 1111-1120, Aug. 2000.
- [75] S. Yamashita and D. Matsumoto, "Waveform reshaping based on injection locking of a distributed-feedback semiconductor laser," *IEEE Photon. Technol. Lett.*, vol. 12, no. 10, pp. 1388-1390, Oct. 2000.

- [76] A. Kuramoto and S. Yamashita, "All-optical regeneration using a side-mode injection-locked semiconductor laser," *IEEE J. Sel. Topics Quantum Electron.*, vol. 9, no. 5, pp. 1283-1287, Sep./Oct. 2003.
- [77] S. Yamashita and J. Suzuki, "All-optical 2R regeneration using a two-mode injection-locked Fabry-Perot laser diode," *IEEE Photon. Technol. Lett.*, vol. 16, no. 4, pp. 1176-1178, Apr. 2004.
- [78] Y. Onishi, F. Koyama, N. Nishiyama, C. Caneau, and C. E. Zah, "Dynamic behavior of 1.55- μ m vertical-cavity surface-emitting laser with external light injection," *Conference on Lasers and Electro-Optics (CLEO)* vol. 1, pp. 2, May 2004.
- [79] H. Kawaguchi, Y. Yamayoshi, and K. Tamura, "All-optical format conversion using an ultrafast polarization bistable vertical-cavity surface-emitting laser," *Conference on Lasers and Electro-Optics (CLEO)* pp. 379-380, May 2000.
- [80] K. Hasebe, Y. Onishi, and F. Koyama, "Novel polarization controller based on injection-locked vertical-cavity surface-emitting laser," *Pacific Rim Conference on Lasers and Electro-Optics (CLEO/Pacific Rim)* pp. 164-165, Aug. 2005.
- [81] E. Wong, Z. Xiaoxue, and C. Chang-Hasnain, "Uncooled, optical injection-locked 1.55- μ m VCSELs for upstream transmitter in WDM-PONs," *Optical Fiber Communication Conference (OFC)*, pp. 1-3, Mar. 2006.
- [82] H.-K. Sung, E. K. L. Lau, and M. C. Wu, "Near-Single Sideband Modulation in Strong Optical Injection-Locked Semiconductor Lasers," *Optical Fiber Communication Conference (OFC)*, Mar. 2006.
- [83] K. Sato, S. Kuwahara, Y. Miyamoto, and N. Shimizu, "40 Gbit/s direct modulation of distributed feedback laser for very-short-reach optical links," *Electron. Lett.*, vol. 38, no. 15, pp. 816-817, Jul. 2002.
- [84] A. J. Seeds, "Microwave photonics," *IEEE Trans. Microw. Theory Tech.*, vol. 50, no. 3, pp. 877-887, Mar. 2002.
- [85] R. Lang, "Injection locking properties of a semiconductor laser," *IEEE J. Quantum Electron.*, vol. QE-18, no. 6, pp. 976-983, Jun. 1982.
- [86] F. Mogensen, H. Olesen, and G. Jacobsen, "Locking conditions and stability properties for a semiconductor laser with external light injection," *IEEE J. Quantum Electron.*, vol. 21, no. 7, pp. 784-793, Jul. 1985.
- [87] G. Meslener, "Chromatic dispersion induced distortion of modulated monochromatic light employing direct detection," *IEEE J. Quantum Electron.*, vol. 20, no. 10, pp. 1208-1216, Oct. 1984.
- [88] G. H. Smith, D. Novak, and Z. Ahmed, "Overcoming chromatic-dispersion effects in fiber-wireless systems incorporating external modulators," *IEEE Trans. Microw. Theory Tech.*,

- vol. 45, no. 8, pp. 1410-1415, Aug. 1997.
- [89] B. Christensen, J. Mark, G. Jacobsen, and E. Bodtker, "Simple dispersion measurement technique with high resolution," *Electron. Lett.*, vol. 29, no. 1, pp. 132, Jan. 1993.
 - [90] M. Matt, P. Eva, P. Dan, W. K. Marshall, and Y. Amnon, "Improved laser modulation response by frequency modulation to amplitude modulation conversion in transmission through a fiber grating," *Appl. Phys. Lett.*, vol. 71, no. 7, pp. 879-881, Aug 1997.
 - [91] N. Moore and K. Y. Lau, "Ultrahigh efficiency microwave signal transmission using tandem-contact single quantum well GaAlAs lasers," *Appl. Phys. Lett.*, vol. 55, no. 10, pp. 936-938, Sep. 1989.
 - [92] K. J. Vahala and M. A. Newkirk, "The optical gain lever: A novel gain mechanism in the direct modulation of quantum well semiconductor lasers," *Appl. Phys. Lett.*, vol. 54, no. 25, pp. 2506-2508, Jun. 1989.
 - [93] C. P. Seltzer, L. D. Westbrook, and H. J. Wickes, "The "gain-lever" effect in InGaAsP/InP multiple quantum well lasers," *J. Lightw. Technol.*, vol. 13, no. 2, pp. 283-289, Feb. 1995.
 - [94] C. H. Cox, III, H. V. Roussel, R. J. Ram, and R. J. Helkey, "Broadband, directly modulated analog fiber link with positive intrinsic gain and reduced noise figure," *International Topical Meeting on Microwave Photonics (MWP)*, pp. 157-160, Oct. 1998.
 - [95] R. J. Ram, F. Rana, and P. Mayer, "Cascade semiconductor lasers for telecommunications," *The 15th Annu. Meeting IEEE Lasers and Electro-Optic Society (LEOS)*, vol. 2, pp. 538-539, Nov. 2002.
 - [96] J. T. Getty, L. A. Johansson, E. J. Skogen, and L. A. Coldren, "1.55- μm bipolar cascade segmented ridge lasers," *IEEE J. Sel. Topics Quantum Electron.*, vol. 9, no. 5, pp. 1138-1145, Sep./Oct. 2003.
 - [97] L. Chrostowski, X. Zhao, C. J. Chang-Hasnain, R. Shau, M. Ortsiefer, and M. C. Amann, "Very high resonance frequency (>40 GHz) optical injection-locked 1.55- μm VCSELs," *International Topical Meeting on Microwave Photonics (MWP)*, pp. 255-258, Oct. 2004.
 - [98] T. Tanbun-Ek, R. People, T. Fullowan, C. Bethea, A. M. Sergent, P. W. Wisk, P. F. Sciortino, Jr., S. N. G. Chu, and W. T. Tsang, "Tunable electroabsorption modulated laser integrated with a bent waveguide distributed-feedback laser," *IEEE Photon. Technol. Lett.*, vol. 9, no. 5, pp. 563-565, May 1997.
 - [99] A. Yariv, *Optical Electronics in Modern Communications.*, 5th ed: Oxford University Press, 1997, pp. 586.
 - [100] X. S. Yao and L. Maleki, "Optoelectronic microwave oscillator," *J. Opt. Soc. Amer. B*, vol. 13 no. 8, pp. 1725-1735, Aug. 1996.
 - [101] X. S. Yao and L. Maleki, "Optoelectronic oscillator for photonic systems," *IEEE J. Quantum Electron.*, vol. 32, no. 7, pp. 1141-1149, Jul. 1996.